Instituto Tecnológico y de Estudios Superiores de Monterrey

Campus México city

School of Engineering and Sciences

"Passive Decentralized Island Mode Detection and Optimization-based Design of Passive Filters for Disconnection Events in Microgrid Systems"

A thesis presented by

Juan Roberto López Gutiérrez

Submitted to the
School of Engineering and Sciences
in partial fulfillment of the requirements for the degree of

Doctor of Philosophy

in

Engineering Sciences

Principal Advisor: Dr. Pedro Ponce Cruz
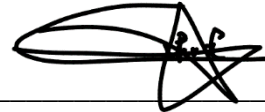Co-advisors: Dr. Luis Miguel Ibarra Moyers

México city, Dec, 2021

Instituto Tecnológico y de Estudios Superiores de Monterrey
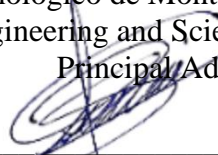
Campus México city

School of Engineering and Sciences

The committee members, hereby, certify that have read the dissertation presented by Juan Roberto López Gutiérrez and that it is fully adequate in scope and quality as a partial requirement for the degree of Doctor of Philosophy in Science in **Engineering Sciences**

Dr. Pedro Ponce Cruz
Tecnológico de Monterrey
School of Engineering and Sciences
Principal Advisor

Dr. Luis Miguel Ibarra Moyers
Tecnológico de Monterrey
Co-advisor

Dr. David Christopher Balderas Silva
Tecnológico de Monterrey
Committee Member

Dr. Alfredo Reyes Rosario
Tecnológico de Monterrey
Committee Member

Dr. Luis Arturo Soriano Avedaño
Universidad Autónoma de Chapingo
Committee Member

Dr. Rubén Morales Menéndez
Dean of Graduate Studies
School of Engineering and Sciences

Mexico City, December 06th, 2021

Declaration of Authorship

I, Juan Roberto López Gutiérrez, declare that this thesis titled, ""Passive Decentralized Island Mode Detection and Optimization-based Design of Passive Filters for Disconnection Events in Microgrid Systems"" and the work presented in it are my own. I confirm that:

- This work was done wholly or mainly while in candidature for a research degree at this University.

- Where any part of this thesis has previously been submitted for a degree or any other qualification at this University or any other institution, this has been clearly stated.

- Where I have consulted the published work of others, this is always clearly attributed.

- Where I have quoted from the work of others, the source is always given. With the exception of such quotations, this dissertation is entirely my own work.

- I have acknowledged all main sources of help.

- Where the thesis is based on work done by myself jointly with others, I have made clear exactly what was done by others and what I have contributed myself.

<div style="text-align:right">

Juan Roberto López Gutiérrez
México city, Dec, 2021

</div>

Dedication

Thanks to the family and friends I have made along this journey. Special thanks to my sister and mother for supporting me and encourage me to keep pushing myself. To all my friends that are now my second family, they not only motivated me through the processes but kept bringing joy on daily basis, to all Elias, Brenda, Inti, Sonia, Alejandra, and Andrea L. that have helped me along the way in special moments seeking advice and comfort.

Acknowledgements

Abstract

In recent years, the electrical network has been evolving towards becoming a more sustainable system, the present environmental concerns regarding the greenhouse gas emission by the energy sector have pushed forward the integration of alternative generation units that promote the decarbonization of the energy production sector. Over the past decades the integration of these "cleaner" energy generation systems has been done in an On-grid and an Off-grid fashion, however, this integration strategy encountered some problems regarding key areas such as control and management, just to mention a few. The microgrid concept is then created to overcome these issues, allowing a seamless integration to the electrical network of the growing alternative generation assets, improving how these "cleaner" energy production alternatives are managed into more sustainable systems.

In Microgrids with a high penetration of renewable energy sources, power converters are used to regulate the produced energy to a single voltage and frequency reference value across the microgrid. Adequate incorporation of an LC filter at the output of power electronic devices allows the attenuation of harmful harmonics that can be introduced to the microgrid's energy bus. By traditional methods, LC filter values can be calculated by means of the power rating, switching frequency, cutoff frequency, and using the bode frequency domain. It is important to consider that, a microgrid including distributed generators can operate connected to the main electrical network or in an isolated manner, referred to as *island operation*. The transition between both states can occur voluntarily, but a disconnection can also happen unexpectedly. The associated transients can be harmful to the grid, and compensating actions must be triggered to avoid service interruption, preserve power quality, and minimize the possibility of faults.

It is important to consider that in transition from a connected to an autonomous microgrid operation, the calculated LC filter can lead to high harmonic injection. As a result, a tuning methodology capable of obtaining the right set of parameters for the LC filter for such transition events can improve the performance of the microgrid. Alternately, such transition events must be detected to enable compensating action; *island detection methods* are essential to this end. Such techniques typically depend on communication networks or on the introduction of minor electrical disturbances to identify and broadcast unexpected islanding events. However, local energy resources are distributed, variable, and are expected to be integrated in a plug-and-play manner; then, conventional island detection strategies can be ineffective as they rely on specific infrastructure.

To overcome those problems, this work proposes to improve the islanding phenomenon in two main contributions. To tackle the issues in regards to the introduction of harmful transients by traditional LC filters, this work optimizes the LC output parameters with respect to the size of the filter components, the *IEEE Std 519-2014*, and bandwidth of the filter, within a bounded region of values subjected to performance conditions such as voltage output, and the produced total harmonic distortion measurements during the transition from a connected

to an autonomous operation. In a case study, genetic algorithm optimization is used to obtain the LC filter parameters and compared to a conventional arithmetic methodology to obtain the values of the filter. The optimization results in a set of values that lead to a higher harmonic attenuation after the transition rather than a conventional method using the switching frequency as the main design factor.

In the other end of the islanding phenomenon, where islanding events must be detected while avoiding traditional infrastructure setbacks, a straightforward, distributed island detection technique is proposed, this technique relies only on local electrical measurements, available at the output of each generating unit. The proposed method is based on the estimated power-frequency ratio, associated with the stiffness of the grid. A "stiffness change" effectively reveals island operating conditions, discards heavy load variations, and enables independent (distributed) operation. The proposal was validated through digital simulations and an experimental test-bed. Such test-bed consists of a Real-Time HIL implementation, the proposed *island detection algorithm* is programmed to run in an embedded format while connected to a Real-Time simulator running a microgrid equivalent model in the form of a three-phase parallel RLC load as recommended by the IEEE Std. 929 and IEEE Std. 1547 for islanding detection. Results showed that the proposed technique can effectively detect island operation at each generating unit interacting in the microgrid. Moreover, it was about three times faster than other reported techniques.

List of Figures

5

List of Tables

Contents

Chapter 1

Introduction

1.1 Preamble

1.1.1 Towards Smart cities

When looking to the past, cities have always looked for innovative solutions to social, economic, transportation, logistic, and energetic paradigms. With the accelerated growth of the technological sector, these solutions have been slowly adapting to the available technological resources. In today's technological panorama, where data availability is one of the principal resources for the development of new and tailored technologies, several proposals have been developed around data analysis techniques that seek a better understanding of the acquired data. This is to provide made-to-measure solutions to the many challenges surrounding developing cities [1]. This would mean that the extraction, analysis, and interpretation of the acquired data can lead to smart and innovative solutions tailored to specific problems.

Data can be acquired through a vast network of sensors, cameras, and the monitoring of device-to-device communications. This data can represent specific behaviors of a given social or industrial sector and can be directed to the optimization of key processes. The availability of these "smart" solutions through the acquisition and analysis of data has led to the concept of *Smart Cities*. This concept is created to merge critical points in the development of cities and an established *data acquisition network* (DAN) into a holistic system that seeks global objectives with political and environmental interests. These key areas of interest are shown in figure 1.1 according to Lavalle et al [2].

It is important to mention that the development of certain areas in the *smart city* context is heavily dependent on the city and governmental policies that can hinder or endorse the application of certain technologies. In this context, the United Nations have developed the 2030 agenda for Sustainable Development Goals, which is an urgent call for action by all countries in regards to 17 sustainability paradigms concerning today's society [3]. This statement

by the United Nations motivates governments to promote research and industry efforts to attain the challenges of natural resources management and environmental areas within the key aspects concerning the development of *Smart cities* [2]. Although there is not an official definition for *Smart cities*, these can be comprehended as systems that seek the most efficient and effective solutions to the many social, environmental, and logistic problems of cities by digitalizing the behavior of its residents through the collection and interpretation of data captured by a DAN.
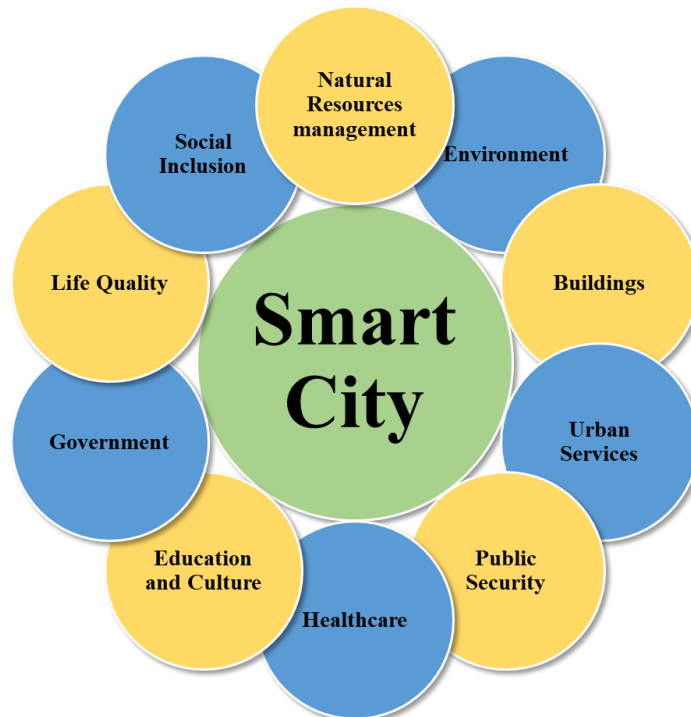
Fig. 1.1: Areas of interest in future Smart Cities

For example, authors in [4] expose how the analysis of parking behavior data (obtained thanks to a sensor-based DAN) of populated sectors in a city can help in the creation of solutions that can alleviate traffic congestion due to the lack of parking spaces during peak hours. In another scenario, current environmental challenges that target the sustainability aspect behind the production, management, and consumption of electrical energy have been pushing "smart" projects around the globe to tackle the global energy paradigm.

The "smart" solutions for energy sustainability and management challenges have been presented at different stages of the electrical network, from generation and distribution stages to the residential sector and single households. In all these stages, the presence of "smart" metering devices enables the possibility of acquiring data that represents these entities, thus, tailored energy management solutions can be developed for every stage in the conventional

electrical network scheme. Since cities are a collection of single entities (households and buildings), it only makes sense that in order to better manage such big systems, the management of small entities is required. Therefore, *smart cities* can be divided into scaled-down systems as a strategy to dive into the present problem, more specifically, the energetic challenges can be dived in what is known as nanogrids, microgrids, and smartgrids. These divisions are illustrated in figure 1.2.
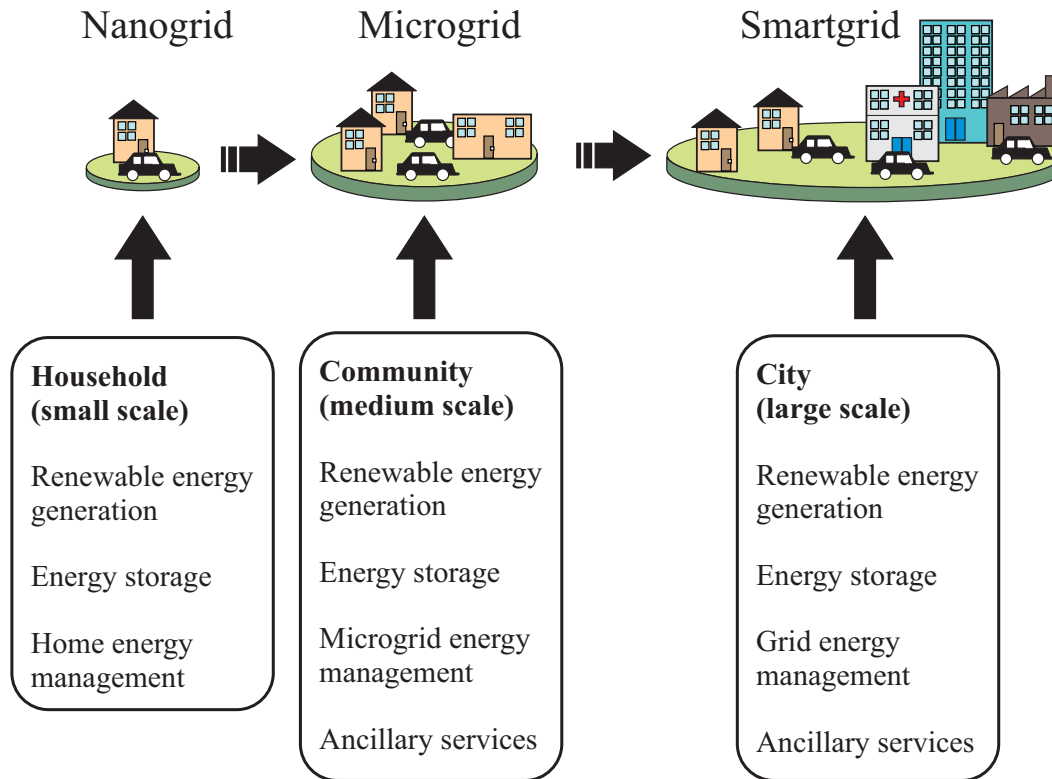
Fig. 1.2: Scaled-down energy system in the development of smart cities

Nanogrids are the more considered a small scale system, these are commonly formed by a single household with energy generation, storage, and management capabilities, the latter are commonly driven by the acquired data from "smart" devices and the local metering system. Subsequently, microgrid and smartgrid are the medium and large scale systems respectively, as shown in figure 1.2, these systems have not much difference except for their implementation scale. Since the size of implementation is a main factor behind the investment cost, microgrids have been a subject of study for the development of smartgrid, essentially becoming a building block in the future of the electrical network [5]. Certainly, this motivates research efforts to tackle present issues in the development of microgrid systems. To better understand the motivation to develop such a system, the following section dives deeper into the paradigms of the current electrical network, and how these are also a factor behind the interest in microgrids.

1.1.2 Paradigms of the electrical network

The ongoing growth in electrical power production due to rapid urbanization has ratified the need to expand the current electrical network generation capacity. The increasing power demand has also introduced environmental, economical, and infrastructure management challenges that can not be overlooked in the future planning of electrical networks [6]. According to a study generated by the U.S Environmental Protection Agency, the global electrical power generation market imposes a significant share of greenhouse gas production. In more detail, the power generation sector in the U.S was responsible for having a 27% share of the total greenhouse gas production in 2018 [7]. According to another report by the U.S Energy Information Administration, the electricity consumption in the U.S is expected to increase by 2.2% in 2021 when compared to the previous year [8]. Implying that the greenhouse gas production by the energy production sector is expected to grow during 2021.

In other reports presented by two different organizations show the global generation shared by various technologies. The first statistics report is published by the United Nations in 2018 [9] while the latter is issued by the Global Wind Energy Council in 2021 [10]. In contrast, the first report states that in the year 2015 the global energy generation sector produced a total of $23,672$ Terawatt hour [TWh] while the second study shows a 14% increment by the year 2019, reporting a total production of energy equal to $26,942$ [TWh]. Figure 1.3illustrates how various generation technologies contributed to the total energy production in their corresponding year [9] [10] . The energy generation by renewable assets incremented by a total of 5%, while other conventional generation technologies shrunk in their total contribution.
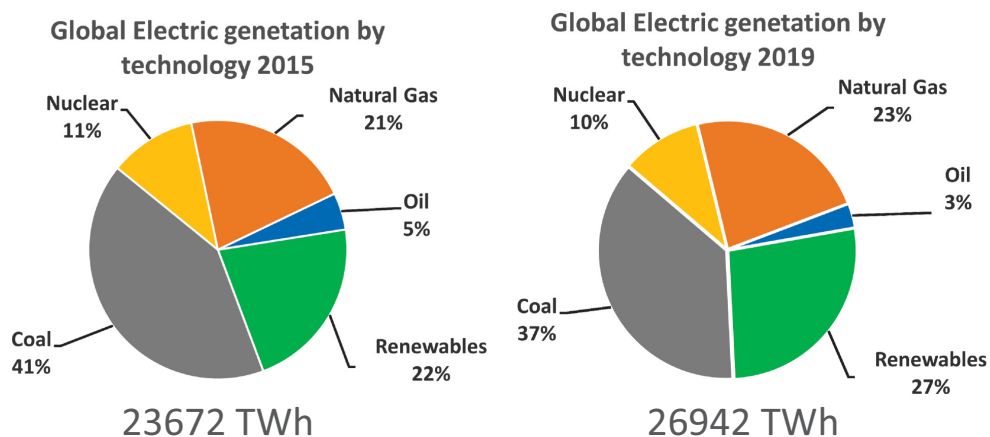
Fig. 1.3: Global energy production share by generation technology - 2015 and 2019

The perceivable growth in the produced electrical energy can be associated with the grid expansion and environmental challenges in the energy production sector, these paradigms have opened a doorway for innovative and alternative solutions that seek the resolution of these

objections. In this sense, small scale distributed electrical networks capable of combining and adopting alternative generation sources with a "cleaner" generation footprint and a proprietary connection point to the power grid are a viable solution to overcome the challenges of reducing the greenhouse gas emissions by the energy production sector while providing flexibility to the expansion intricacy of the current electrical network.

The modern microgrid system is highly upheld by the rapid development of generation technologies that can harness more efficiently the energy produced by renewable assets. A study conducted by the International Renewable Energy Agency in 2021, shows how this *renewable energy sources* (RES) have grown in the global installed capacity in the past decade [11]. Figure 1.4 illustrates the growth of the globally installed renewable energy generation capacity as the growth in specific renewable systems such as photovoltaic, hydro-power, and wind-energy systems [11]. The study concludes that the global generation capacity by renewable sources has grown at a yearly average of 8.6% since 2011. On the other hand, hydropower, wind energy, and photovoltaic systems have grown on a yearly average of 2.6%, 14.4%, and 28.8% respectively.
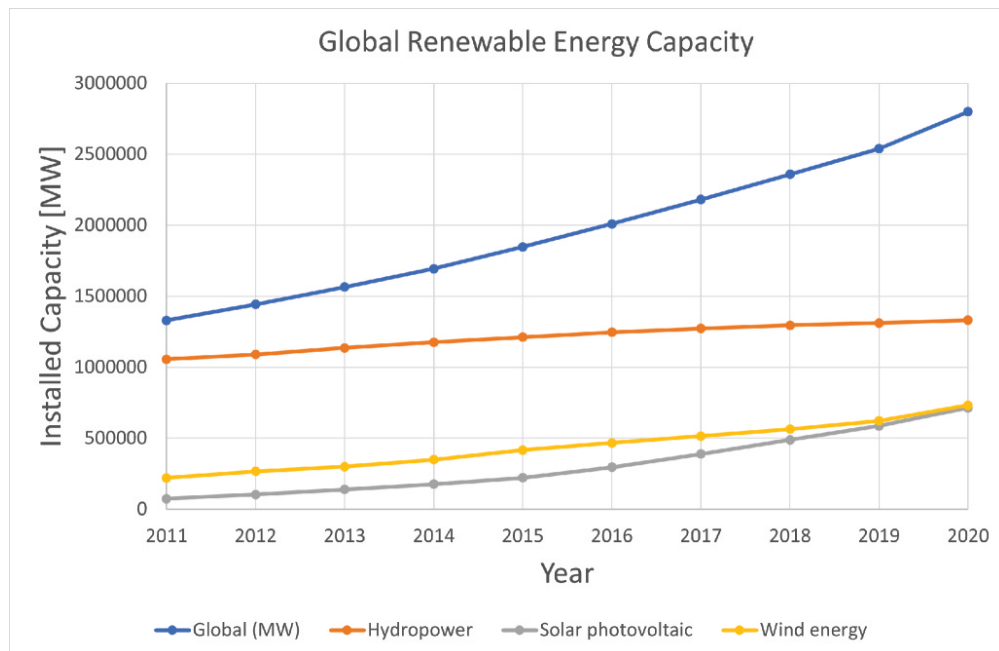
Fig. 1.4: Global installed renewable energy capacity - from 2011 to 2020

In the particular case of Mexico, the total energy production increased in 9% from 2015 to 2020, producing a total of 338740 GWh according to the International Energy Agency [12]. Despite the foreseeable growth in Mexican energy production, the use of cola-based generation sources decreased in a 74% from 2015 to 2020, going from 33803 GWh to only 9079 GWh produced by coal-based sources. The decarbonization of the Mexican energy

market has also impacted other nonrenewable generation sources such as the ones based on oil consumption. Such oil-based sources have decreased in a 64% over the past 20 years, almost 30.3% decrease every 5 years. However, other nonrenewable sources have had an increment in their contribution to the Mexican energy market, such as the case of natural gas. This particular nonrenewable source has had an 61% increment every 5 years, and currently, it is responsible for 64% of the total energy production in Mexico [12].

On the other hand, renewable energy sources have also increased their generation share in the past decades in the Mexican energy market. For instance, renewable sources such as solar photovoltaic and wind energy have had a percentile increment of 5660% and 225% respectively in the past 5 years [12] (see figure 1.5 [12]). Particularly, solar photovoltaic energy has been a strong investment point of the Mexican electrical infrastructure. One big motivator for this noticeable increment in the installed generation capacity of solar photovoltaic (besides the decarbonization of the electrical market) has been the wide number of Mexicans without access to the main electrical network, according to [13], almost 5 million people remain without electricity, where a portion is mostly settled in remote communities outside the coverage area of the national grid system. This has pushed new Off-grid projects that seek the resolution of the energy requirements of such isolated communities. These projects have been mostly presented as Off-grid installations of solar photovoltaic cells, this is dude the great compatibility with the communities landscape and geographical location.

Out of such reasons the "Creation and development of the Mexican center for innovation in smart electrical networks and microgrids" was instituted in 2018 under the mantle of the National Institute of Electricity and Clean Energy or INEEL, by its acronym in Spanish. Such agreement is heavily supported by the solution of microgrids as systems that represent a better integration of alternative generation sources to the national power management system. In such agreement, the section PE-A-21 deals with microgrids for the electrification of isolated communities, to develop and evaluate distributed generation technologies [14]. The main objective of such policy intend to develop a real microgrid test-bed for testing, development of public policies, and analysis of operational and control topologies for better integration to the national power management system. Also, those projects are intended to contribute to the development of a platform for the modeling of microgrids under different schemes. In addition, the project has the objective of installing clean energy sources such as photovoltaic panels and mini-hydraulic plants in remote communities to promote the economic development of such isolated communities.
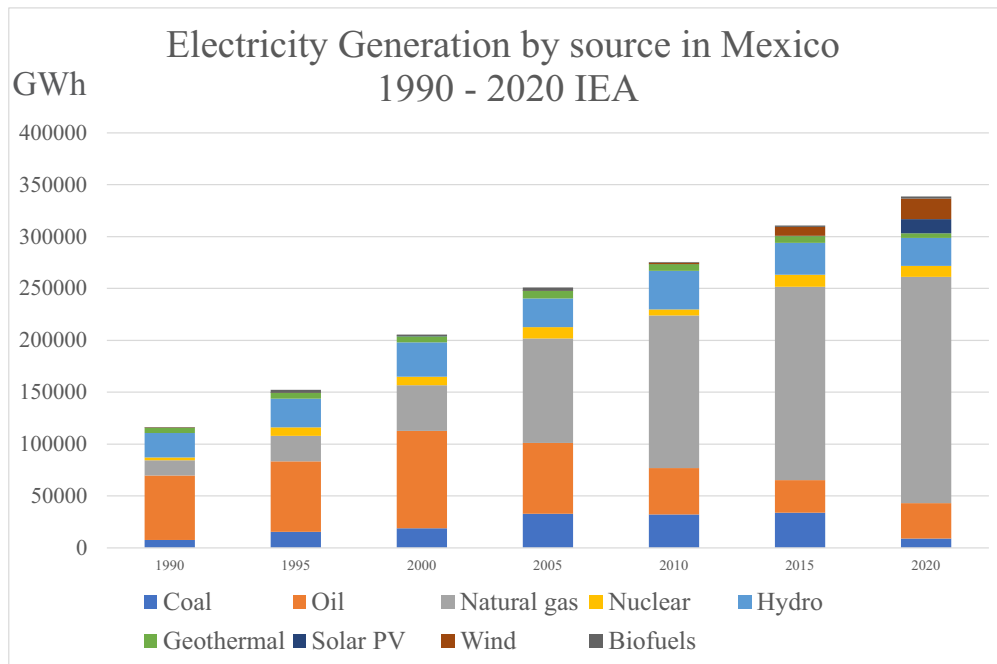
Fig. 1.5: Electricity Generation by source in Mexico 1990 - 2020

The annual average growth of each renewable source is directly related to other economical and geographical motives. Each asset represents a different type of investment, where costs of the manufacturing process, transportation, installation, maintenance, and end-of-life recycling protocols depend highly on the chosen RES. In contrast, other geographical studies are required prior to the installation of any RES. The geographical location is a crucial factor in the performance of each RES, especially in the cases of photovoltaic and wind energy systems. It is important to mention that the provided flexibility to the power grid by renewable assets also depends on the type of the chosen renewable generation system. For instance, hydro-power is restricted to areas that contain rivers and bodies of water with a unidirectional and constant flow of water. Therefore, this is the slowest growing renewable asset with limited addition of flexibility to the power grid with a stranded growth due to limited geographical location factors.

The provided flexibility to the power grid is a clear benefit of distributed generation systems based on RES [15]. Photovoltaic and wind energy generation pose a greater flexibility aspect when compared to hydro-power generation, hence, these generation systems suggest a higher annual average increment as shown in figure 1.4. In recent years photovoltaic generation has gained more popularity in the residential sector as some governmental programs are encouraging users to adopt this form of energy generation by giving tax incentives to reduce the cost of installation [16]. Overall, the growing installation capacity of the photovoltaic system can

be attributed to its high location flexibility, making it ideal for private consumers in residential areas that seek the benefit of a "clean" energy generation at lower installation cost when compared to other RES, pushing forward the development of sustainable communities.

On the other hand, wind energy systems represent the second-fastest-growing RES according to the International Renewable Energy Agency [11], the developing interest in this "clean" energy generation technology can be attributed to its higher efficiency rates when compared to other RES excluding hydro-power generation [17]. Due to its complex and high investment cost, this generation of technology is not ideal for the private consumer. Nonetheless, its applications are more adequate to high scale projects aimed to be part of a grid parity scheme where ancillary services to the power grid are provided [10].

Beyond the recognized motivation of the decarbonization of the energy production sector by adopting "cleaner" energy generation alternatives, the grid expansion paradigms associated with the inclusion of renewables in the power grid is still a complex topic to cover. Aspects such as communication, control, management, storage, and distribution of the many generation and consumption assets need to be taken into consideration [18]. In contrast, a settled power grid is restricted to urbanized areas, where high-power central plants are installed in a centralized fashion, covering for communication, control, and management requirements in a single entity, where, its possible expansion to remote communities can be achieved, however, this option can be economically unfeasible. Additionally, the centralized nature of a settled power grid can compromise the reliability of the whole network since a failure in the generation or transmission system would compromise the quality and overall reliability of electrical power [15].

To overcome the high cost of increasing the reach and reliability levels of a centralized power plant, especially to energy-deprived communities located in remote or difficult access areas, while taking advantage of the high degree of flexibility that most RES possess, Off-grid installations of RES represent a viable solution to the expansion and decarbonization paradigms. However, the mentioned communication, control, management, storage, and distribution of these assets need to be thoroughly studied to output a competent and reliable distributed electrical network. A direct consequence of this need is the creation of a system capable of full-filling the above-mentioned requirements, this system is commonly known in the literature as a microgrid [19, 20, 21], which basic schematic is illustrated in figure 1.6.
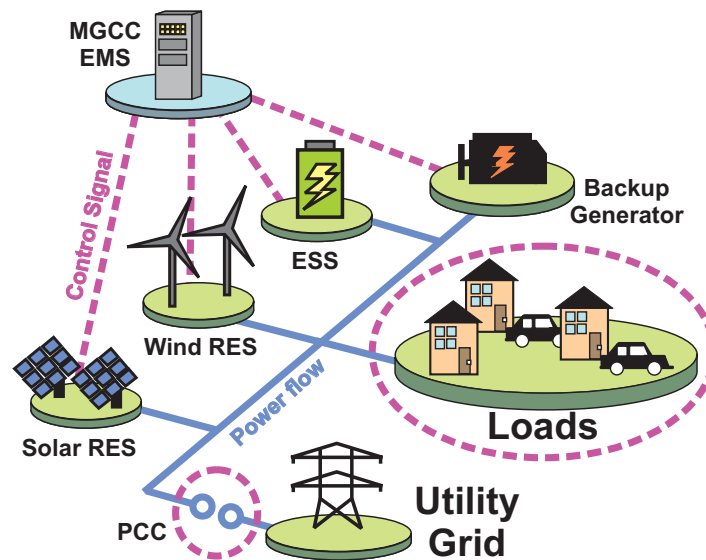
Fig. 1.6: Simple Microgrid schematic

Microgrid systems are expected to aid in regarding the present environmental and limited reach problems that the present electrical network has to face towards the development of sustainable communities. The expected ways in which a microgrid can help in solving the mentioned paradigms are dependant on their geographical planning, arrangement, and size [22]:

- The exploitation of locally available resources that can be used for power generation in a distributed manner, commonly referred to as Distributed Energy Resources.

- The local consumption of the produced energy eliminates the need for transition lines, creating distributed electrical networks that minimize the losses of transmission and distribution lines.

- *Energy Storage Systems* (ESS) can be deployed to save any excess of energy production and supply it back when needed.

- Higher supply reliability and fault isolation.

- Improved power quality thanks to local control and management of generation assets.

- Improved generation flexibility bounded to specific geographical conditions.

- Provide ancillary services to the main electrical grid, contributing to power demand as part of the distribution system.

Despite the type of the installed renewable generation capacity, On-grid vs Off-grid, the previously mentioned concept of a microgrid stands in either configuration. Microgrids are formally described as a small-scale distributed electrical network formed by a cluster of Distributed Generation Units (DGUs) in the form of alternative generation technologies, with control, management, and communication properties that contribute towards the quality of the deliver electrical energy to a local end consumer [23, 20].

Microgrid systems can be designed to operate in either configuration, On-grid or Off-grid, the former is commonly referred to in the literature as a grid-connected operation while the latter is known as an island or stand-alone or island operation [24, 25, 26]. The operation mode of the microgrid is coordinated at a unique point of connection to the grid, commonly referred to as the Point of Common Coupling (PCC) as illustrated in figure 1.6.

Stand-alone microgrids are highly beneficial to energy-deprived communities, by relying only on an Off-grid installation of RES the energy needs can be covered on a daily basis. The Off-grid installation capacity of RES has increased in recent years. Figure 1.7 illustrates the global growing behavior of the Off-grid installed renewable energy capacity from 2011 to 2020, the annual average growth is estimated to be of 9.9% for the global capacity [11]. It's important to notice how photovoltaic energy remains the fastest growing renewable generation technology even on an off-grid scenario with an annual average growth of 27.6% [11].
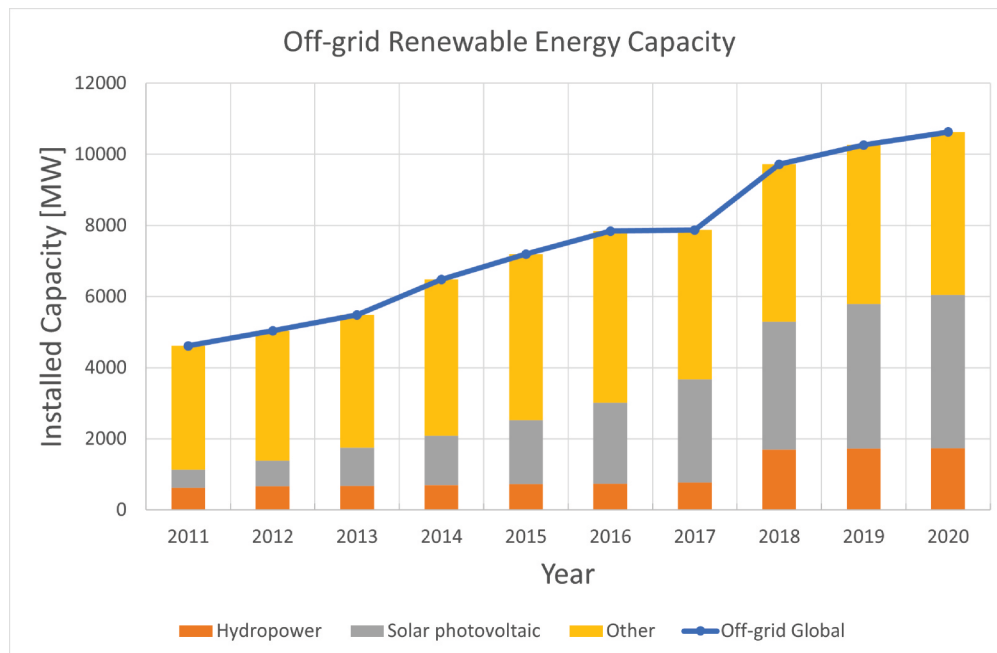
Fig. 1.7: Global installed gigawatts by RES versus the global generated GT of CO_2 from 2012 to 2018

The benefits associated with the environmental and flexible operation of Microgrids that draw the advantages of DGUs will be decisive in the future of the electrical networks. On the other hand, its effect as a system based on low emission sources can be determined by a large number of factors. Thus, there are clear components that regulate the impact of Microgrids as a distributed electrical network, such as:

- The intermittent performance of renewables with decaying efficiency points.

- The geographical location of DGU to maximize the production.

- The growing power demand in isolated communities with a fixed renewable generation capacity.

- A seamless operation with the power grid, minimizing disturbances and contributing to the power demand.

- Protection schemes.

- The microgrid topology

- The control and communication strategies to coordinate generation assets.

- The management and optimization of resources according to historic and prediction models.

- The environmental and economical costs of deployment.

- The seamless transition between *operating modes* to maintain a reliable operation.

The improvement and innovation over the above-mentioned components play an important role in the further modernization of the current electrical network. Certainly microgrid systems are far from a mature stage, thus, their evolution as part of the electrical generation market will continue to adapt to the environmental and economical needs of its users. It is essential to consider that the integration of microgrids is not an automatic environmental benefit, other studies have questioned the viability of microgrids in terms of the greenhouse gas production of its components and planning [17]. However, the decarbonization and decentralization of the electrical market do play an important role in the future of these distributed alternatives. Hence, the administration of renewables via microgrid systems is foreseen as a beneficial and crucial building block towards the future of the electrical network [5].

1.1.3 Microgrid as a system

Transitioning to sustainable energy systems will require that new policies and social strategies be tailored around actions to improve the integration of technologies that allow the reduction in the overall consumed energy while having an increasing proportion of renewable generation [27]. Energy sustainability is a concept that encompasses the technological, socioeconomic, political, and social energy consumption behavior of individuals. Technologically, the sustainability concept is described as the adoption of resource-efficient technologies that minimize the cost of energy production regarding their environmental impact [28]. Nonetheless, other management aspects regarding energy production and consumption need to be carefully revised in order to develop a holistic sustainable system.

As a consequence of having the technological and management requirements for a sustainable system, the energy sector was forced to develop a more efficient and comprehensive way to accomplish such a goal by the incorporation of microgrids into the established power grid. Microgrids are commonly assumed as distributed sustainable systems capable of reducing the environmental impact of the energy production sector [29].

However, this assumption may be erroneous depending mostly on which planning stage is being reviewed of the whole microgrid system. The sustainability aspect of microgrids can be severely questioned regarding the greenhouse gas emission investment of producing, deploying, and recycling most of its components, basically, the life cycle Assessment needs to be thoroughly revised as stated by [17]. On the other hand, microgrids can be comprehended as sustainable from an operational point of view if a combination of renewable generation and energy management techniques is applied during its service stage.

The work presented by Ibarra et [17], highlights how the manufacturing environmental impact of low-level components suppose a high emission rate of greenhouse gases and in some cases the production of harmful waste during the manufacturing process. To avoid falling into this predicament and ensure a beneficial long term deployment of microgrid systems the revision of the following requirements becomes essential:

- Environmental payoff time, the lifespan of individual components needs to be sufficient to cover for their manufacturing environmental footprint.

- Generation efficiency rates, procuring a high generation efficiency by avoiding internal or external factors that can hinder the performance of the installed generation assets.

- High environmental cost of specific components, some components such as batteries used by ESS can be an environmental burden due to their manufacturing and disposal protocols.

Hence, its addition needs to be carefully revised to ensure the sustainability of the system [30, 31].

Indeed, the manufacturing environmental cost of low-level components can significantly hinder the sustainable reputation of RES, hence the microgrid as well. Currently, there is a lack of studies that highlight the environmental impact of early manufacturing stages in microgrid components, mostly, a high-level operation of microgrid management towards a sustainable operation is reported in the literature [32, 33, 34], covering for the operational stage and the benefits of RES. For this reason, microgrids are mostly conceptualized as sustainable systems and a partial or total solution to the environmental challenges of the energy sector. Although the manufacturing stage of RES in microgrids can be questioned regarding their sustainable benefits, there is no doubt that the decarbonization of the energy sector will brighten its environmental panorama through alternative generation sources with a zero-emission rate of greenhouse gases. For that matter, microgrids are not discarded as part of the future of a sustainable electrical network.

It is crucial to consider that the sustainable overview of an operating microgrid depends mostly on its *operating conditions* and operation modes. Microgrids can be planned in different configurations with distinctive objectives. For instance, in a grid-connected configuration, the microgrid can be seen as a dispatchable generation unit that reliefs some strain from the power grid by contributing to the power demand with the possibility to have active participation in the energy market, grid-connected microgrids can be also be configured to operate independently if any faults or disturbances are detected, this disconnection process is commonly known as an islanding event and widely studied due to the heavy transients that may be introduced by an *unintentional disconnection* [35, 36, 37].

Lastly, autonomous or island microgrids capable of supplying the energy demand of a determined set of local loads without a direct connection to the power grid and relying only on available DGUs and *energy management systems* (EMS), this particular type of microgrid plays a major role in the sustainable reputation of the whole microgrid system concept [29].

Commonly, isolated microgrids depend on fossil-fuel-based DGU to properly meet a standard power delivery by dictating the nominal voltage and frequency levels required by the local load [29]. According to [38], in the year 2014, 50% of the installed isolated microgrids in Canada was based on diesel generators, causing a significant share of greenhouse gas emission by the power requirements of isolated communities. Therefore, a growing interest in an off-grid deployment of DGU based on renewable assets.

In this manner, isolated microgrids that typically depend on fossil generation can migrate to "cleaner" generation sources and curtail the greenhouse gas emission share by isolated generation systems, pushing even forward the approval and deployment of these generation

technologies. Nonetheless, other supervisory, intercommunication, and low-level control factors are required to properly explore the sustainable benefit of isolated microgrids, the proper management of resources can have a significant impact on the environmental and economic aspects behind the operation of these off-grid installations.

1.1.4   How have Microgrids been Implemented?

The flexibility behind some of the alternative generation sources based on renewable assets has encouraged different community sectors to adopt this type of energy generation into their current electrical scheme, certainly, the advantages that come with the investment of modernizing the electric energy network outweigh the capital cost in properly planned systems, these advantages of reducing the carbon footprint, improving the operational efficiency while lowering the energy consumption cost with the possibility of monetizing the generated energy through active market participation are attractive attributes behind the rapid popularization of microgrids in different sectors.

In the beginning, microgrids were mainly used for military applications, especially in their island configuration and based on diesel generators. However, other areas such as aviation, residential, academic, utility providers, public services, emergency services, and those within the private sector seek the advantages of the emerging alternative generation sources, figure 1.8 shows the mentioned sector where microgrids tend to have a greater presence. Nonetheless, other applications may surge as the current electrical network is shifting to cover new social and industry needs.

Fig. 1.8: Microgrid fields of application

More often than not, the residential and utility provider sectors are the most popular application areas for microgrid systems, most of the academic work is focused on improving the different control layers for a better integration or independent performance. A clear example is the present electrical circumstances of 200 remote communities in Alaska, as a case study, the northwest state has been dealing with an electric energy shortage in a wide number of communities, forcing the adoption of islanded microgrids based on diesel generation sources. This creates concern about the amount of greenhouse gas emissions and the profitable aspect behind the diesel fuel dependency.

For that matter, the American state has endorsed the deployment of renewable-based microgrids, especially focusing on hydropower, wind energy, and photovoltaic generation to migrate from diesel-based microgrids to RES-based facilities, also, the majority of these new installations will be updated to be able to connect to the main electrical grid whenever the expansion of the electrical network is achieved [39]. By taking this approach, more than 200 communities will be able to contribute to the main network power demand besides having the ability to operate independently in the case of any disruptive events due to the harsh geographical and meteorological conditions.

Besides the in-land microgrid facilities, other microgrid systems based on hydro-power plants play a crucial role in the energy market of the northwestern American state. This RES accounts for the second-largest generation source with a 108 Mwh rating representing 39% of the total capacity [40]. The hydro-powered communities acquire almost 100% of their electrical demand by this generation source, however, the northern part of Alaska is forced to adopt on and off-shore wind generations and photovoltaic systems as the hydropower availability are not optimal in the northern parts of this state.

The Alaska case has quickly developed due to the ongoing necessity of lowering energy generation costs while improving the reliability and environmental impact of island communities. It is expected that island microgrids perform as efficiently as grid-connected systems since there is no other alternative and the current scenario force the island operation as the grid state standard. Currently, island systems operate under a constant power output, leading to immediate consumption of the produced energy or diverting the excess for heat purposes. Nonetheless, communities are slowly incorporating ESS as a way to save energy and manage more efficiently the generation and consumption assets, more sophisticated *energy management systems* are still to be implemented, these would allow greater impact on the social, economic, and environmental aspects behind the independent electrical infrastructure of the northwestern state.

Another robust microgrid case is the one found in a mall village in the south of Sweden, as wind and solar generation is adopted in a microgrid system that supports a *seamless disconnection* from the main electric grid. The microgrid was built upon an established grid where a

model predictive control-based-EMS, ESS, diesel backup, controllable loads, and secondary sub-stations were installed to evolve into a microgrid. The installed *energy management system* (EMS) is programmed to optimize the generation and consumption scheduling, balance the power demand and regulate the system frequency. The microgrid is also built to support *planned island event*, where the various grid-forming units operate under the *droop control* scheme to achieve a *seamless transition* by matching the active and reactive power to zero through the manipulation of the voltage and frequency references[41].

On the other hand, the work presented by [42] restates the economic and social impact of having a resilient and reliable electricity infrastructure in the aviation industry, it is estimated that an electrical fault that results in a partial or complete electric system failure can cause up to a US$150 million loss in revenue. For that matter, 3.3 MW of photovoltaic generation was installed in the San Diego international airport in 2015 to keep the airport operation online despite *sudden disconnections* or disruptive events to avoid any flight cancellations or delays in case of an electric system fault. In parallel with improving the electric system reliability, the 3.3MW installation is estimated to save US$8 million in the energy consumption bill, while reducing the overall carbon footprint by 3.7 Kton of CO_2 per year of operation [42].

Undoubtedly, these advantages can be translated to other areas, for example in the private sector, microgrids are used to reduce the energy consumption bill of corporate building while helping with the green image of certain enterprises. Commercial Building microgrids can be a great case of study on how different energy management strategies affect the performance of a closed system. For instance, the work presented by [43] introduces a gain-scheduled-based algorithm to implement in building microgrids to focus on the resolution of power quality issues. Other approaches include the management of Heating – Ventilation - Air conditioning systems as controllable loads to fall under a demand response management scheme [44], in the same manner, other services can be linked to this management technique to further reduce consumption cost and balance the power demand of the building microgrid, commercial refrigeration, and lighting can also be included into the demand response scheme.

Another great example of microgrid deployment is described in the project held by the University of California San Diego, this is a great lesson on how microgrids can fulfill the requirements of more than one area of application. In this particular case, an On-campus microgrid is installed with the purpose of reducing the carbon footprint of the academic institution at a 92% rate, while providing a case study for further research and development in the different control levels of the microgrid structure.

The On-campus microgrid is equipped with a 42 MW generation capacity and with on and off-grid photovoltaic generation systems, multiple ESS with up to 2.7MW capacity ready to operate under a grid-forming scheme, and a microgrid central controller that monitors

and coordinated the operation while analyzing the reliability constraints of the system. The communication scheme of the On-campus microgrid is established as centralized to improve the coordination of generation and energy storage assets, as the energy market participants speed up the return of the initial investment [45].

Lastly, areas such as emergency and public services are seen more often in hospitals, public lighting, firefighting, and police stations as backup systems in case of any *disconnection events*, although their applications are more towards the dynamics of an uninterruptible power supply based mainly on diesel generators and ESS, their management and operation should be considered with int the microgrid realm. It is important to notice that most of the already implemented systems obey a typical and safe infrastructure, from the communication to the control aspect.

This can be attributed that most of the microgrid deployed projects are to cover the electrical need of isolated or poorly connected communities, therefore a high level of reliability with low risk is required, as in the case of the northern part of Alaska. On the other hand, a heavily integrated system with grid-forming, grid-feeding, and grid-supporting units can also be deployed in communities with lower dependency and risks, as the microgrids are built over an established grid and not built from the ground up, as in the case of the small village in Sweden.

These two examples are a great set point for microgrid planning and deployment, where these systems can be either prepared from scratch or build over the electric grid, the former approach fits a specific and future energy requirements of an isolated community in a project plan that contemplates the geographical condition, energy consumption rates, ideal generation agents, among other crucial factors. The latter approach promotes the installation of household photovoltaic systems among other distributed generation sources to moderate the energy supply by the main grid, slowly modernizing the electrical network. Nonetheless, other challenges remain as the microgrids should be contemplated as building blocks on a future Smartgrid, connectivity, communication, control, and management are regulated factors in today's microgrids infrastructure, but these can fall short in expectations on how the Smartgrid will be developed in a not so distant future.

1.2 Problem statement

As mentioned, the integration of alternative generation sources at the power grid's distribution level has led to new challenges in the electrical network's control, communication, and management areas. Indeed, availing of local resources comes with added complexity and requires coordination mechanisms to ensure their effective integration, such as the microgrid.

Microgrids add flexibility since their operation is not restricted to a permanent connection to the primary power grid; they can act independently in what is known as *island operation*. However, switching between *operating modes* implies varying dynamics and dealing with a "weaker" network when disconnected by the primary power grid.

In recent years multiple microgrid studies have been performed to understand and improve certain areas of interest in the microgrid system. A particular area of interest is the transition between operating modes in the microgrid, research in this area focuses on mitigating possible transients introduced to the microgrid's energy bus due to *transition events*, mainly when shifting from a connected to an autonomous operation [46, 47, 48]. Most of the research dedicated to achieving seamless transition resorts to the development of control techniques for the interfaced power electronic devices in combination with *islanding detection algorithms* [24, 49].

As reviewed from previews microgrid implementations, these systems are mostly planned to operate in a cooperative fashion with the main grid in an independent manner in case of an intentional or *unintentional disconnection*. In either case, microgrid systems that are planned to support both operating modes must have a mechanism that detects such *disconnection events* [50]. However, an unintentional disconnection would force an island operating state, potentially introducing harmful transients and degrading power quality. It is then essential to detect the islanding events within the microgrid to trigger ancillary services and exert compensating actions [51]. Nonetheless, DGUs are *distributed* and the microgrid is expected to integrate DGUs and other electrical agents in a *plug and play* fashion. A changing, variable, and spread microgrid poses severe challenges to a typical communications approach. Therefore, there is a need for distributed *island detection algorithms*.

On the other hand, the performance of these control-based solutions is dependent on the right design or tuning of the controller's gains. In most cases, these tasks are not straightforward, where an erroneous tuning of these controllers gains can lead to a deficiency in the power electronic device's controller performance; this deficiency can be translated to an increment the injected *Total Harmonic Distortion* (THD) to the microgrid's energy bus due to the transition effect over the switching devices within the power electric converter. The harmonic content at the output side of the interfaced power electronic device can be mitigated by implementing LC filters. Therefore, the effect of the transition in the filter performance needs to be analyzed since most of the literature takes for granted the attenuation of harmonics during and after transition events with the originally calculated filter parameters. This causes a clear problem in the selection of the filter parameters for such *transition events*. Hence, the development of a tuning methodology capable of obtaining the right set of parameters for the LC filter for a transition event can improve the performance of the microgrid whenever an *unintentional disconnection* event occurs

1.3 Justification

In the case of island detection algorithms, these can be classified as (i) *remote* detection methods (RDM), (ii) *passive* detection methods (PDM), and (iii) *active* detection methods (ADM) [52]. RDMs are typically based on supervisory control techniques, relying on communication infrastructure. Then, some of their main disadvantages are the communication latency and interference, happening in power-line-based methods [53]. PDMs monitor electrical variables at the PCC [52] to create a tripping signal according to predefined thresholds [54]. As the signal must be shared across the microgrid, PDMs typically imply the need and disadvantages of communication infrastructure. Finally, ADMs operate at individual DGUs introducing minor electrical disturbances to the grid, analyzing the response, and determining its operational state [55]. The main drawback is the degradation of power quality due to the introduced electrical disturbances and the late response depending on the electric disturbance. Also, multiple interacting DGUs may interfere with each other [56].

It is important to mention that PDMs and ADMs are considered as local detection techniques [57] due to the continuous monitoring and analysis of "local" electrical variables such as voltage, frequency, active and reactive power. However, this technique can not operate along with the distributed nature of microgrids, requiring a certain level of communication or by having interfering paradigms in multi-participating DGU under the same ADM. This communication dependency of RDMs and PDMs limits the expandability of the distributed electrical network and can be considered a target for cyber-attacks, adding security concerns to the islanding mechanism, putting at risk the operability of the microgrid during transition events. While the pollutant nature of ADMs degrades the delivered power quality of the grid, especially if a large number of DGU is operating under the same contamination principle. In addition to that, these methods are not fully independent and rely mostly on a near communication link between different contributing agents, usually called neighbor to neighbor communication.

For that matter, a locally driven *islanding detection algorithm* is one of the main contributions of this work. The developed algorithms work on local and available measurements that can be found within the primary controllers of the microgrid. The purpose of a local detection method is to eradicate the shortcomings of communication-based techniques and other invasive and pollutant island detection algorithms.

On the other hand, microgrids with a high penetration number of RES incorporate these alternative generation units through Power Converters (PCs) in the form of DGU [58]. PCs are power electronics switching devices with the objective of regulating the produced energy to a single voltage and frequency reference value. Microgrids that include Photo-voltaic (PV) energy generation and ESS resort to Voltage Source Inverters (VSI) to transform a DC voltage input to a regulated AC voltage output with a nominal frequency [59]. VSIs are power

devices with high energy conversion efficiency. Nonetheless, by cause of the high switching frequencies the voltage and current output may contain harmful harmonics especially during *transition events* when the microgrid switches from a connected to an independent operation [60], resulting in unsafe operating conditions for the connected loads despite the high efficiency of the PCs. A low-pass filter equipped between the output side of the VSI and the loads can attenuate the injection of harmful harmonics caused by the high switching frequencies [61]. Despite that, the equipped low-pass filter can lead to a short time higher harmonic injection during *transition events* if its components are not properly obtained.

In that context, one of the main contributions of this work is the development of a tuning methodology capable of obtaining the right set of parameters for the LC filter for a *transition event*. The outcome of the proposed methodology can improve the performance of the microgrid during such events. This work optimizes the LC output parameters with respect to the size of the filter components, the *IEEE Std 519-2014*, and bandwidth of the filter, within a bounded region of values subjected to performance conditions such as voltage output, and the produced THD measurements during the transition from a connected to an autonomous operation.

1.4 Research question and hypothesis

To drive this research, the following research questions are formulated:

What is the relationship between low-level electrical variables available to particular DGUs and the detection of islanding conditions in a microgrid system?

What is the impact of the output LC filter in the attenuation of the total harmonic injection during a transition event?

To answer the research question, the following hypotheses are defined:

The low-level electrical variables that can be measured locally within the scope of a single DGU can be linked to individual droop characteristics, in a connected state the droop characteristics are understood as "stiff" since their dynamics are driven by the main electrical network. However, the same droop characteristics can morph into a "weak" state due to the same disconnection event. In this sense, by implementing an algorithm capable of monitoring the individual electrical variables to compute the describing droop characteristics it is possible to obtain the global operating status of the microgrid in a local fashion, avoiding the shortcoming of communication-based techniques and invasive methods.

Since a wide range of filter, parameters can be selected or obtained through conventional design procedures, and operational region for different combinations of the LC filter parameters can be obtained, this operational region can be then evaluated against the desired cost function during transition events *to find the optimal value for the interfaced LC filter.*

1.5   Proposed Solution

This work presents a different approach in the task of attenuating the injected THD by a grid-supporting VSI in a microgrid's bus during and after a transition event between connected and an autonomous operation while meeting the *IEEE Std 519-1992* and *IEEE Std 519-2014* standards on harmonic voltage distortion. This approach consists of finding an optimized set of LC filter parameters within a bounded region of values that guarantee the desired performance during and after the transition event. The optimization process is done using genetic algorithms due to its natural selection and classic evolutionary optimization nature, with respect to the size of the filter components, the THD during and after a transition event, and the bandwidth of the filter since this attribute eliminates the lowest order harmonics of the output voltage waveform of the VSI.

The proposed optimization of the LC filter, aids in the delivered quality of the electrical energy by reducing the amount of injected harmonics during and after the transition event, while maintaining the harmonic injection levels to an allowed standard in a connected state of the microgrid. This proposal is referred to as system independent because it uses local data from the primary control layer to obtain the optimal LC filter parameters, this is possible because there is no need for a reconfiguration of the Microgrid Central Controller since there is no linkage between the primary control layer and the Microgrid Central Controller [62]. In other words, the filter performance and the used local data employed during the optimization process are independent of the Microgrid Central Controller. The evaluation of the system is done in a modified version of the *IEEE 13 node test feeder*.

Overall, DGUs are expected to operate independently within a microgrid under a *distributed* approach. Their management is desired to be decentralized, not relying on a communication layer or a central controller. Therefore, a passive detection algorithm is proposed in this work, operating over local DGU variables only. Specifically, the proposed algorithm analyzes the power-frequency ratio deviations at the DGU terminals without inserting disturbances to the grid. Opposed to the reviewed literature, this algorithm does not require a communication network or a secondary verifying system, interacting directly with its associated DGU and acquiring measurements directly from the DGU's outputs. Out of this, the proposal does not imply adding devices but adding a software module to the DGU controller, avoiding increased costs or maintenance.

Such a distributed approach eradicates the need for communicating a tripping signal, as each generating unit would make the same detection independently. In doing so, the cost of new communication lines can be saved, and *plug-and-play* features can be availed in future microgrid implementations. In addition, since the proposed method does not inject any electrical disturbance to the grid, it is possible to have multiple DGUs operating under the same island detection mechanism without major concerns regarding the interference between each other.

1.6   Objectives

Indeed, one of the biggest advantages and attracting factors behind the deployment of microgrids is the possibility of transitioning from a connection to an autonomous operation in a seamless manner. The transition can between operating modes is acknowledged by *islanding detection algorithms*, where their main task is to inform the state of the grid to rapidly adjust any countering measurements to the transition effects. On the other hand, other parts of the generation system, such as the output LC filter, can contribute to attenuating the harmful transients caused by such *disconnection event*.

In such context, the objectives of this work can be listed as follows:

- Develop a distributed *islanding detection algorithm* that locally estimates the droop characteristics of a DGU.

- Detecting *disconnection event* by monitoring the rate of change of the estimated droop characteristics.

- Validate through simulation the proposed distributed *islanding detection algorithm*

- Validate the dynamic consistency of the island detection proposal by having a Real-Time Hardware-in-the-Loop implementation.

- Analyze the region of operation of an interfaced LC filter during transition events in the microgrid model.

- Optimize through the implementation of the genetic algorithm the LC filter parameters for transition events.

1.7   Published Work

1.7.1   Book Chapters

Ibarra, L., Lopez, J. R., Ponce, P., & Molina, A. (2020). Empowering Energy Saving Management and Microgrid Topology to Diminish Climate Challenge (M. Lackner, B. Sajjadi,

&W.-Y. Chen, Eds.). doi:10.1007/978-1-4614-6431-0_127-1.

1.7.2 Journal Articles

Lopez, J. R., Cruz, P. P., & Gutierrez, A. M. (2021). VSI LC filter optimized by a genetic algorithm from connected to island microgrid operation. Energy Systems. doi:10.1007/s12667-021-00432-0.

López Gutiérrez, J. R., Ibarra, L., Ponce, P., & Molina, A. (2021). A decentralized passive islanding detection method based on the variations of estimated droop characteristics. Energies.

López Gutiérrez, J. R., Ponce, P., & Molina, A. (2021). Real-time power electronics laboratory to strengthen distance learning engineering education on smart grids and microgrids. Future Internet, 13(9). doi:10.3390/fi1309023.

1.7.3 Conference Proceedings

Gutiérrez, J. R. L., Cruz, P. P., & Gutiérrez, A. M. (2019). Bounded region optimization of PID gains for grid forming inverters with genetic algorithms. In Advances in soft computing (pp. 277–289). doi:10.1007/978-3-030-33749-0_23.

Mendez-Flores, E., Lopez-Gutierrez, J. R., Macias-Hidalgo, I., Ramirez-Cadena, M. d. J., Vargas-Martinez, A., Lozoya-Santos, J. d. J., . . . Molina-Gutierrez, A. (2019). Design, Implementation and Nonlinear Control Analysis of a Furuta Pendulum System. In 2019 4th International Conference on Control and Robotics Engineering (ICCRE) (pp. 65–69). doi:10.1109/ICCRE.2019.8724376.

Chapter 2

Theoretical framework

2.1 Microgrid Management Architecture

To overcome the control and management problems the microgrid hierarchical control architectures is widely suited [63], this architecture divides the microgrid control and communication objectives in three different levels: (i) primary level, in charge of an even power distribution among the interconnected DGU while regulating the delivered voltage and frequency, its operation is done using only local measurements without a communication link to other control layers; (ii) secondary layer, counters the possible voltage and frequency deviations produced by the primary layer by introducing a secondary control term in the power-sharing controllers, its operation is commonly dictated by the tertiary control layer using global variables of the microgrid system; and (iii) tertiary layer, the management of generation and storage agents, these are regulated to assure an efficient power flow in the microgrid following a desired economical or generation objective-driven mainly by the Microgrid Central Controller (MGCC) and EMS [64]. The aforementioned control layers are illustrated in figure 2.1.

The communication infrastructure also dictates the degree of intelligence of microgrid systems, by choosing an adequate communication technology, the microgrid system can be future-proofed and be integrated more easily in the future electrical network schematic [65]. Communication has become an essential component in the operation of microgrids and electrical systems. As mentioned, the communication requirements of a microgrid are dependent on a specific hierarchical control level. This is attributed to the diverse reaction time requirements of each control layer.
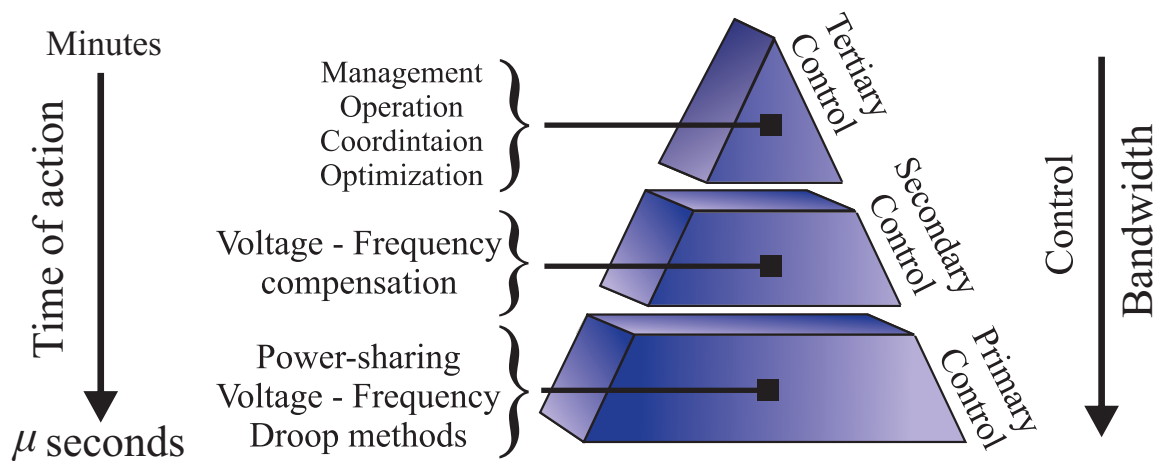
Fig. 2.1: Hierarchical control architecture

In the past, primary controllers had a master-slave configuration, where generation sources were connected in a parallel fashion and transmitting data from the slaves to the master generator to level the power output of each generation source, although this configuration achieved high power-sharing efficiency, it was limited to high-bandwidths, creating flexibility and stability paradigms, especially in microgrid with a high penetration of renewables. For that matter, communication-less or localized power-sharing techniques were developed, eliminating one communication layer dependency, thus, making a more stable, reliable, and flexible system.

Since the primary controllers are embedded within each DGU, its data transfer actions are done locally, meaning that there is no interaction or a direct data exchange with other control layers within the hierarchical architecture. Its localized communication feature facilities its communication requirements where these can be covered by conventional technologies such as optical fiber and twisted-pair cables, however, these technologies are required to be suitable for the fast processes timing required by the voltage and frequency regulation actions. It is required that the chosen communication technology for primary controller applications be fast and reliable as most of the exchanged data in this control layer are essential and critical for a safe and sustainable operation of the microgrid. According to the IEEE 2030.07 standard [66], the response time for immediate actions, protection, and low-level control should stay within the micro-second realm [65].

The secondary controllers are the link between the primary control layer and the tertiary controllers, thus, its communication requirements are the highest of all three layers. One of the major setbacks of communication requirements for the secondary controllers includes the delay introduced by the data exchange among different components across the communication network [67], especially if a low-level variable adjustment is commanded from the tertiary to

the primary level.

Communication delays can degrade the performance of the different control layers and can be caused by a collision between different data sets inside the same communication line, creating waiting time delays and the need for transmission retry mechanisms in the communication protocols. Moreover, simple and multiple data packet transmissions also represent an issue regarding the limit in the data package size and the delay between data sets respectively, causing a partial decision-making process for the controller actions hindering the suitable performance of the microgrid system. The secondary controller communication link goes to all contributing agents, the linkage configuration has been demonstrated to have an important role in the performance of the secondary control actions.

Commonly, secondary controllers are implemented using wired communication technologies, due to the high priority in data transfer fidelity and low latency rates, optical fiber and twisted pairs being the most common technologies for this implementation. However, due to the recent advancement and growth in wireless technologies, wireless networks have been an attractive alternative due to the increased flexibility and low scalability costs [68]. Despite the selected communication infrastructure, the reaction time for secondary control actions such as messaging reference offsets, synchronizing power-sharing capabilities, and control must remain under the sub-second realm according to the IEEE 2030.07 [66].

Lastly, the tertiary controller communication requirements are more flexible in how the data is transmitted and the speed at which it is required. The required action time for the tertiary layer is in the range of a few minutes or even days, depending on the selected management and operation strategies. The slow action time allows the integration of other wired and wireless communication technologies such as Power Line Communication, ZigBee, Bluetooth, Cellular signal, and Long Range communication links. Most of these commutation technologies offer a lower implementation cost while adding flexibility to the communication infrastructure. Nonetheless, other technologies such as Cellular signals are more adequate for urban microgrid implementations rather than isolated applications, this is due to the coverage area restrictions especially in emerging technologies such as 5G cellular networks [65].

Since microgrids are known for having a vast number of internal and external variables that can benefit or impede optimal performance. Appropriate control and operation objectives must be carefully selected according to numerous components that can be found within the microgrid's architecture [69]. The previews statement corroborates that, microgrids can not be enclosed in a single definition, their configuration is unique and specific for every system.

This leads to the idea that obtaining a generic model for all microgrids is an unfeasible task to achieve. However, by having a generic monitoring system capable of acquiring and presenting global information regarding the many operational aspects of the microgrid, including whether the microgrid is operating in an island or grid-connected state, all decision-making actions can be simplified despite the chosen system configuration. This assures a safe and cost-effective operation without major concerns about the model of the microgrid [21].

Current proposals on *islanding detection algorithms* can be located mostly at the tertiary level within the microgrid's hierarchical control architecture. Since RDM bases their operation on having a fixed communication infrastructure and PDM require an internal communication network, it would result advantageous to have the receiving end of the communication link that outputs an islanding signal to a higher control and management level [70]. In this sense, RDMs and PDMs can be allocated within other management strategies of the microgrid.

On the other hand, primary and secondary control layers are in charge of having a standardized voltage and frequency output and an ever power distribution by the multiple alternative generation units found in a microgrid system, these layers summarize the control efforts regarding the quality of the delivered electrical energy. Since the power quality can be managed by these control layers, ADM is placed within these levels of the hierarchical control architecture, by modifying references of electrical signals to introduce minor electrical disturbances to the grid. However, in most cases, the performance of the primary and secondary controllers depends on the model accuracy of the microgrid and/or a specific microgrid configuration. Therefore, ADMs can suffer from a sub-optimal operation depending on the employed microgrid configuration, especially since multiple ADMs can interfere with each other. Therefore, extensive pre-studies contemplating the type of generations and consumption agents that are to be connected to the microgrids main bus need to be taken into consideration to correctly obtain a specific model and assure the correct operation of the many management strategies that depend on the right operation of primary and secondary controllers.

2.1.1 Energy Management Systems

Since microgrids are considered unique for each implementation, there is a requirement for generic management strategies that can cope with the management task regardless of the microgrid's architecture. These generic management strategies can be included in the EMS concept, which represents a collective solution to the operational management paradigm of these systems. EMS is in charge of manipulating the available controllable agents according to recommendations given by a management model that can contemplate consumption and generation forecasts obtained through the study and analysis of energy market fluctuations, time of use tariff profiles, and historical weather information. This allows for a wider view of

the current and future external variables that affect the optimal operation of microgrids. However, these management models also collect information from the consumption, generation, and energy storage through an Advanced Meter Infrastructure, this action updates the modeling process and improves the decision-making action, adapting to the individual nature of the microgrid and optimizing its performance according to desired economic or environmental objectives.

In essence and from a global management perspective, EMS operation objectives as a high-level controller should:

- Optimize the grid's power flow.

- Forecast the operating conditions of RES based on geographical weather data.

- Have a dynamic consumption, and energy exchange plan according to pricing schemes.

- Monitor the State of Charge (SoC) of distributed ESS.

- Create load profiles that model the power demand behavior to manage more efficiently the various assets.

Overall, EMS should seek global benefits contemplating the above-mentioned objectives to ensure long-term sustainability.

Although the global objective of EMS remains similar for every system, different management techniques have been proposed in the literature. For example, the work presented by [71] deals with the optimization of the demand side consummation, this alone falls in a popular management strategy known as Demand Side Management (DSM). DSM strategies have the advantage of controlling the power demand through controllable loads to avoid under and over-generation scenarios that could potentially hinder the delivered voltage and frequency levels by the DGU. These scenarios are illustrated in figure 2.2. DMS can be further categorized according to different objectives such as (i) energy efficiency; (ii) time of use; (iii) Demand Response (DR); and (iv) spinning reserve. Also, DSM can be carried out by active participation of the users, increasing the user awareness over how the electrical energy is being used and the running consumption tariffs.
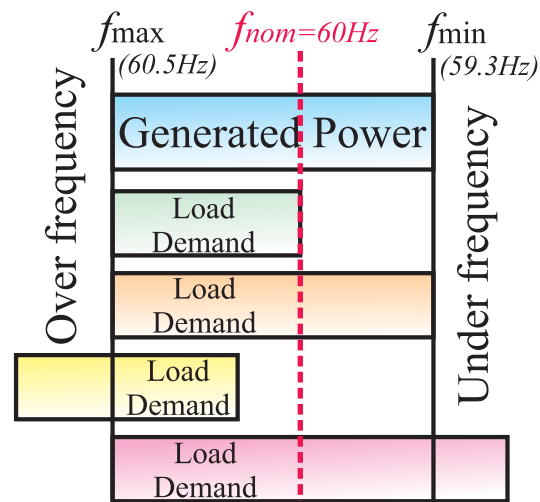
Fig. 2.2: Under and over frequency scenarios

Depending on the applied strategy the consumer can become a crucial factor in the management of the generated and consumed energy, some strategies aim to inform the user about their energy consumption to directly endorse the correction of consumption habits, alternative strategies promote an upgrade on the many house appliances to more energy-efficient systems, while other strategies aim towards the awareness of the energy pricing, the pricing of consumed energy can be fixed or dynamic, the former sticks to a pricing plan where the cost of energy is higher or lower depending on specific periods time along the day, while the latter, changes according to consummations peak hours and available energy, increasing the pricing on a peak demand scenario to motivate the users to cut on their energy consumption, both strategies aim toward educating the consumer in how and when is best to consume energy [72].

Alternatively, strategies based on energy efficiency deal directly with the operational efficiency of electrical devices within houses and buildings, since this strategy compares the performance of new to old devices it helps to create consciousness on the savings that can occur if the outdated devices are switched to more energy-efficient alternatives, i.e, switching from old HVAC system to new one. Also, structural modification can be suggested to the users to improve the thermal efficiency of spaces, as the thermal variable plays a crucial role in the energy efficiency reputation of buildings, especially on seasons with a high use intensity [71].

On the other hand, demand response and spinning reserve strategies act over defined schemes and have little to no interaction with the user. Demand response can act upon pricing rates, emergency, and control signals, resulting in an automated behavior of how electrical energy is consumed. On the other hand, spinning reserve techniques deal with electrical variables

like the active power delivery and frequency levels to regulate the quality of the delivered energy and maintain an adequate level of supply reliability [73], this strategy allows a more autonomous behavior while still pursuing sustainable and economic benefits of autonomous microgrids from the consumer side. In fact, the last two strategies are adequate for island systems as agreed by [74] and [75].

As a result of the DSM strategies, another EMS has been proposed by considering other system variables such as the operational forecast of renewables, the SoC behind dispatchable ESS, the power output limits, generation type, power balance, power flow, operation conditions, and pollutant emissions. These variables are often part of a bigger scheme-driven high-level strategy i.e, fuzzy logic, game theory, scheduling, unit commitment, optimal power flow, and predictive control-based methods can be found in the literature.

Nonetheless, current trends indicate the application of Artificial Intelligence-based Methods (AIbM), the incorporating of these would allow machine learning strategies to be applied in predictive planning and optimization of processes in EMS [76]. As a result, tailored management strategies can be obtained with more precision at an individual and global level in comparison when antique constrained rule-based strategies were the main algorithms formulating its operation [77].

In fact, it is expected that the EMS ecosystem will encounter a bigger integration of AIbM, these would improve the flexibility of current DSM strategies, especially those that rely on the energy consumption habits of the consumers. In a recent case, the project known as Google DeepMind developed by Google in 2019, applies a machine learning-based method to an EMS in charge of Google's energy usage, the results indicate that the AIbM is was able to reduce in 15% its power consumption [78].

With this case in mind, it is clear to see how AI will benefit the electricity system, improving consumption and grid management. AI will play an important role in the future of electrical systems, by changing the way the consumer interacts on daily basis with the power grid, making generation, consumption, and exchange processes more efficient and helping to define the microgrid as a dispatchable generation system and as a building block towards the future electrical network.

Alternatively to global management strategies, EMS also play a crucial role at the electrical level, the purpose of an EMS is to maintain an electrical balance between the generated and the consumed energy, this can be achieved in different ways, by managing the generation levels of the available DGUs, by having controllable loads that can impact the microgrid's power demand, by having ESS capable of reserving or liberating electrical energy on command, and by having active participation with the main grid through power exchange strategies [21].

It is important to notice that in cases where the microgrid is operating without the connection to the main grid, EMS becomes a critical aspect for the right operation. While operating in *island conditions*, EMS is required to deal with the management of low-level controllers, by way of explanation, EMS in autonomous microgrids should [79]:

- Balance the power generation.

- Respond in an agile manner to any disturbances.

- Manage the charging and discharging schedules of distributed ESS.

Overall, the presence of a large number of generation and consumption agents, each with unique dynamic behavior, and the lack of direct connection to the power grid causes an increased sensibility to electrical disturbances. Hence, EMS is a crucial component required to maintain the nominal quality levels of the delivered energy [79]. Therefore, it is crucial to integrate island detection strategies to facilitate the regulating task of EMS in an *island state* of the microgrid.

2.2 Microgrid Operating Modes

As perceived from the different control levels of the microgrid, *island detection algorithms* such as RDMs and PDMs operate with global electrical variables rather than low-level control electrical measurements. Thus, to achieve a *distributed island detection* strategy, it is imperative to understand the operation of basic structures behind primary controllers. The main objective behind the primary controller's implementation is the delivery of nominal voltage and frequency levels. Primary controllers are commonly categorized according to the role of their governed generation unit, and according to the literature, three main primary control operation modes can be found within the microgrid system, these are categorized in:

- Grid-connected mode

- Island mode

- Grid-supporting

2.2.1 Grid-connected

Grid-Feeding control

Grid-connected control is commonly referred to in the literature as a grid-feeding control strategy, where the main objective is to follow the commanded references of voltage and

frequency from the power grid. This control strategy is only used during a grid-connected operation of the microgrid or in cases where stiff voltage and frequency references are found within the microgrid system.

In this configuration, it is crucial to denote that all grid-feeding units should be perfectly synchronized with the dominant ac voltage values to accurately regulate the active and reactive power exchange between the microgrid and the main grid [80]. Additionally, the delivered voltage and frequency by grid-feeding units can be regulated by high-level controllers according to desired power management strategies. Figure 2.4 shows the basic control block behind this operating mode.
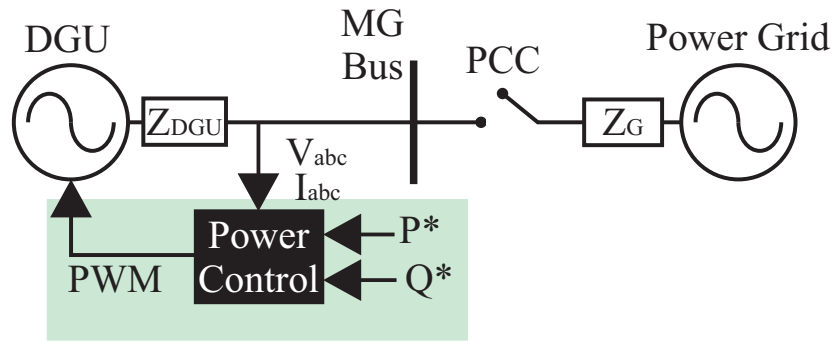
Fig. 2.3: Simple control schematic, Grid-feeding

where the power control block has active and reactive power references as inputs, commonly dictated by a higher controller layer. Then, the reference signals are fed forward to an inner current control loop to regulate the injected current by the governed DGU. In the most basic control structure, the current control loop compares the current reference signals in a synchronous reference frame obtained through equation (2.1).

$$
\begin{aligned}
i_d^* &= \frac{P^*}{V_d} \\
i_q^* &= \frac{Q^*}{V_d}
\end{aligned}
\tag{2.1}
$$

where P^* and Q^* are the active and reactive power references respectively, and i_d^* and i_q^* are the current references for the inner current control loop.

Then, the current references in their dq notations are compared to the measured current values in the output side of the DGU. The difference between such values is then the input of a linear controller. The most common implementation for linear current control is based on the conventional PI or PID controllers, these controllers are set to operate along with a dq reference frame by transforming the three-phase voltage and current signals to their synchronous

reference frame equivalents [80]. The transformation from the natural to the synchronous reference frame is achieved by means of the Park transformation (see Appendix A), these transformations facilitate the control task, thus linear controllers can be implemented [80].

The output of the linear controllers is then inversely transformed from a synchronous reference frame to the natural reference frame, that is from dq to an abc notation. Afterward, the signal is then the input for a pulse-wide modulation technique to generate the gate signals that drive the switching power electronic deceives.

The high-level control of grid-feeding units regulates the programmed active and reactive references, usually managed by power plant controllers or maximum power point tracking strategies. This characteristic makes this control strategy ideal for a parallel operation of multiple grid-feeding units since the power output references can be easily balanced through high-level management systems. Nonetheless, grid-feeding units can not operate in an island scenario without other energy generation agents capable of providing a stiff voltage and frequency reference, therefore, grid-forming units or diesel-based generation units are commonly planned to operate alongside grid-feeding units.

2.2.2 Island mode

When the unique connection point between the microgrid and the power grid is open, the microgrid operation mode changes to an autonomous or island operation. This particular state of the microgrid has many challenges associated with its efficient control and management of resources. Particularly, the loss of a stiff reference of voltage and frequency causes control paradigms around the independent regulation of these crucial variables. Control strategies around the island mode are constructed with the objective of maintaining nominal voltage and frequency levels despite system imperfections such as non-linear loads, unbalanced load systems, and the intermittent nature of RES.

Grid-Forming control

Island-mode strategies control are commonly studied as grid-forming controllers, this type of control is capable of following its given voltage and frequency references since these are lost in an autonomous operation. Specifically, grid-forming control is highly susceptible to parameter variations and low-level electrical disturbances. This generates stability paradigms that could potentially lead to sub-optimal performance of the generation units. Hence, it is crucial to have properly tuned controllers or adopt a control technique capable of minimizing the hindering effect of these undesired scenarios. Figure 2.3 shows the basic control schematic for grid-forming units.
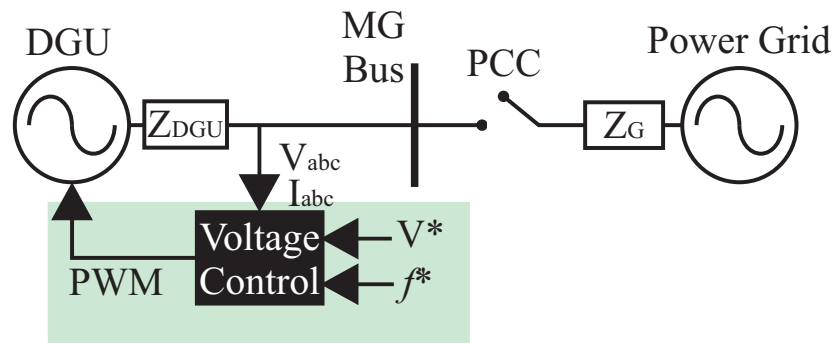
Fig. 2.4: Simple control schematic, Grid-forming

The illustrated voltage control bock is formed by two control loops in a cascade fashion, the first control loop is known as an external voltage control loop, while the latter is mostly reefed as the inner current control loop [80]. The input of an external voltage control block is the voltage and frequency references commonly dictated by the main grid. The measured voltage and current at the end side of the DGU are also an input of the voltage control bock. A reference frame transformation (see Appendix A) is used to obtain the dq components of the voltage reference and the measured voltage and current. The dq components of the voltage references are compared to the measured voltage values in the dq form, the resultant difference is then the input of a linear controller (commonly PI controllers) for each of the synchronous reference frame components, the output of such controllers is labeled as the current references in the dq notation for the inner current control loop. Subsequently, these current references are compared to the measured current values and the resultant difference is then the input of the second liner control layer. Finally, the output of the second control layer is transformed back to an abc notation to function as the input of the modulation technique to drive the power electronic devices.

It is important to mention that the high sensitivity associated with grid-forming units creates a requirement for highly accurate system synchronization to avoid any phase, frequency, or amplitude mismatches. This is particularly crucial in systems with multiple grid-forming units operating under a parallel scheme. This mode of operation is commonly coupled with systems that supply a constant DC voltage output to reduce the uncertainty of having a variable input source such as photovoltaic, and energy storage systems. However, this is not always the best alternative, especially since the performance of photovoltaic arrays is known to be dependent on weather conditions. For that matter, grid-forming units are better paired for energy storage systems where the constant DC output can be guaranteed, this results in a stable delivery of voltage and frequency values. Grid-forming units can also adopt linear controllers such as PI and PID, these controllers can also operate along with the dq reference frame.

Grid-Supporting control

Lastly, the supporting mode configuration falls under the grid-supporting control definition. The objective of grid supporting controllers is to act as an Uninterruptible Power Source (UPS), this is to regulate the voltage and frequency values of the microgrid without major concerns about the operation mode. In this case, grid-supporting controllers are found to be suitable in either configuration of the microgrid, grid-connected, or island operation. In addition to the bi-functionality of grid-supporting units, other advantages surrounding this strategy make it ideal for microgrid applications.

For example, this strategy contemplates the delivered active and reactive power as a function of the voltage and frequency values, meaning that in a parallel operation of multiple grid-supporting units, even power distribution can be achieved without the intervention of a high-level controller, accomplishing "communication-less" primary level power-sharing controllers.

Furthermore, grid-supporting units can be configured to function as current or voltage sources. The latter must be connected through a physical or virtually emulated link impedance, this allows to mimic the dynamics of synchronous generators to properly compensate for the active and reactive power delivery. On the other hand, the former configuration allows the regulation of the delivered voltage and frequency values in either configuration of the microgrid, this is done as a regulatory service to adjust the delivered power by other generation units. Figure 2.5 shows the basic control scheme for a grid-supporting unit acting as a current source, while figure 2.6 shows the basic control scheme for a grid-supporting unit acting as a voltage source.
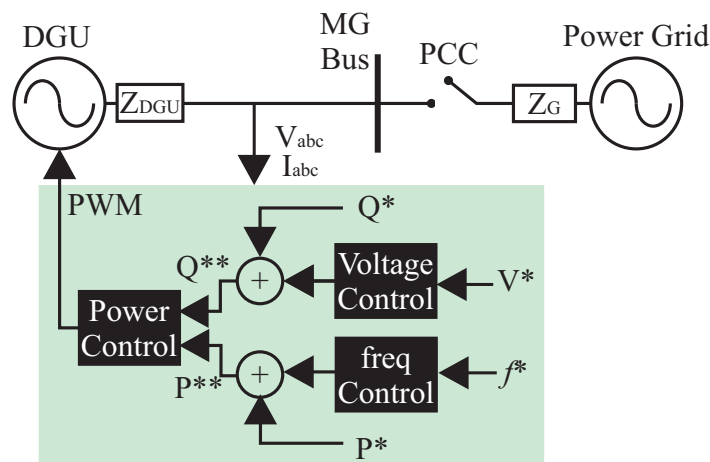
Fig. 2.5: Simple control schematic, Grid-Supporting as a current source
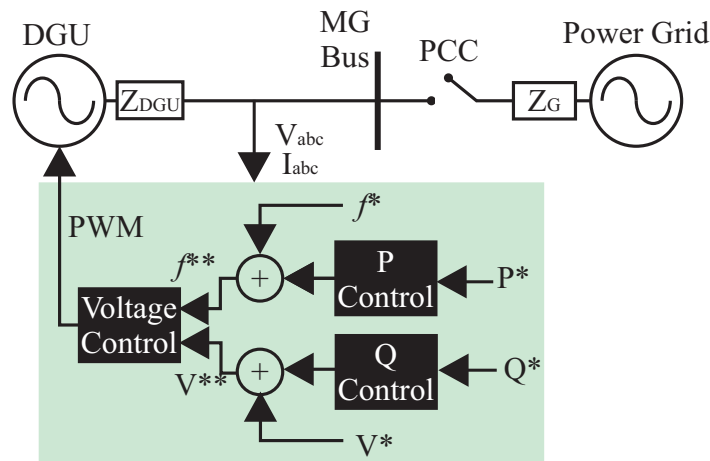
Fig. 2.6: Simple control schematic, Grid-Supporting as a voltage source

These control strategies can be divided into three states. The first sage is the principles of droop control (more details in regards to this control strategy are given in a future section of this Chapter). The second third stages are different for each of the presented strategies, where the former (illustrated in figure 2.5) is formed by the power control and current control loops of a grid-feeding unit, while the latter (illustrated in figure 2.6) is formed by the external voltage control loop and the inner current control loops of the grid-forming strategy. In a sense, what makes a grid-supporting unit is the addition of droop control strategies that output the required active and reactive power references for the former strategy as the voltage and frequency references for the latter case.

Certainly, the advantages of grid-supporting units make this mode of operation attractive for microgrid applications. By being able to operate in both modes of operation, their implementation can soften the harsh effect of *disconnection events* and improve the seamless transitions between modes of operation [80]. For that matter, grid-supporting units are one of the most commonly researched operation modes in the literature as *power controllers*, the provided ancillary and regulatory services are attractive characteristics in the pursuit of more efficient, autonomous, and sustainable microgrids.

2.3   LC Filter

To attenuate the harmonic injection, an LC filter is usually connected between the VSI output and the loads, by this implementation, the reduction of the harmonics generated by the high switching frequencies of the PWM technique and the nonlinear load characteristics is accomplished in the voltage waveform [81, 82]. When compared to a conventional L filter, the LC filter provides better attenuation to high-frequency harmonics [83] and exhibits an

improved dynamic performance. Nevertheless, LCL filters are also a good alternative to L and LC filters, LCL filters have a better overall performance as reviewed in [60].

Nonetheless, LCL filters increase the complexity of the system, resulting in a more convoluted model slowing down the design procedure. Thanks to the literature, the procedure of how to design the filter parameters according to different criteria is well-known [84]. Despite the chosen filter architecture, the IEEE standards on harmonic voltage distortion for electrical systems *IEEE Std 519-1992* and *IEEE Std 519-2014* need to be fulfilled to ensure a proper microgrid operation with a THD limit of 5% and limit of 12% THD over a maximum period of 3 seconds respectively.

Both standards highlight the recommended operation and qualifications for harmonic control in the field of electrical power systems. However, the standard *IEEE Std 519-1992* clarifies the consumers' harmonic voltage distortion limit at the PCC, this being 5% for general systems and 3% for special applications including hospitals and airports. This standard recognizes the obligation of the generations agents to supply the loads with resembling pure sinusoidal voltage waves[85].

On the other hand, a description and border setting in real-life applications is exposed in the standard *IEEE Std 519-2014* [86], it is stated that the maximum allowed THD measurement per day should be less than 1.5 times the THD limit of 8.0%, meaning that a maximum of 12% THD is allowed for periods shorter than 3 seconds. Overall, the latter restates the collaborative obligation involving both consumption and generation agents, to maintain the recommended harmonic limits for voltages and currents within the electrical power systems[85].

2.3.1 LC filter Analysis

When working with VSI one of the main concerns is frequency regulation and pure sinusoidal voltage and current waveform at the output side of the PC. The harmonic distortion of the output voltages of a VSI depends on the parameters of the LC filter. By traditional methods, the attenuation of the VSI switching frequencies depends on the cutoff frequency of the filter, a smaller cutoff frequency results in a greater voltage ripple attenuation. In relation, the bandwidth of the filter has a similar impact on the voltage ripple attenuation. A high LC filter bandwidth can result in lower attenuation. Figure 2.7a shows the effect of different LC filter bandwidths applied to the three-phase voltage output of a VSI, this effect is also studied in [87].
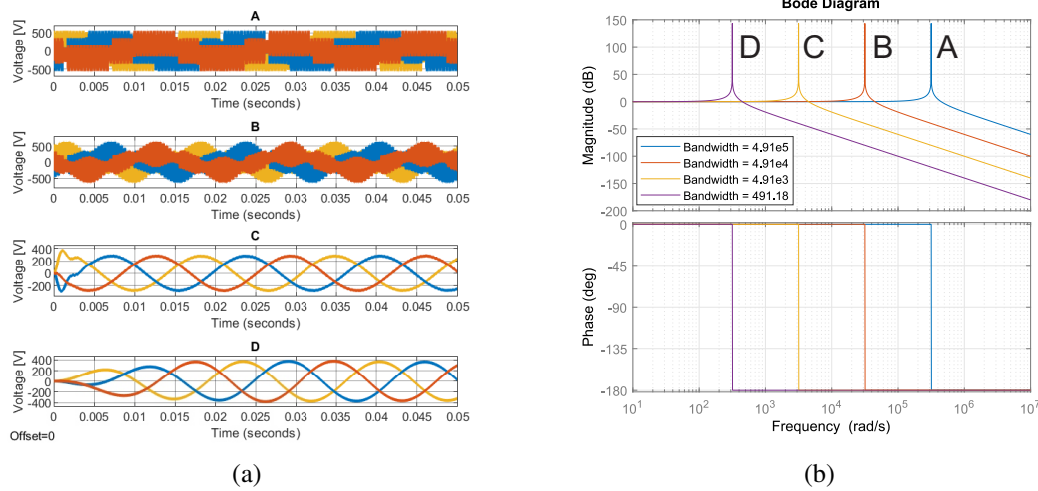
Fig. 2.7: Bandwidth effect over a VSI three-phase voltage output

The Voltage signals in figure 2.7a go through different LC filters with different bandwidths, figure 2.7b illustrates the effect of different filters applied to the voltage signals A, B, C, and D. The smaller bandwidth results in a better attenuation of the voltage ripple. However, a small bandwidth can have negative effects on the overall voltage output signal of the VSI, by over attenuating the voltage signal and causing a slower VSI response to any disturbance.

2.4   Microgrid Power Control

The holistic performance of power-control actions can be divided into two different control layers. The primary and secondary layers as seen in the hierarchical control architecture. In these two layers, each controller has a different level of manipulation of microgrid variables and communication requirements. First, the primary controller's performance depends only on a direct manipulation of electrical variables found at a distribution low-level, i.e., delivered voltage, frequency, active, and reactive power. This layer allows a proper interconnection between the DGUs and the electrical grid, and grants a regulated power exchange between generation sources within an independent microgrid system.

The interconnection is achieved through power electronic devices, typically interfaced along with RES to properly harness and regulate the delivered electrical energy. Where the primary controller assumes the task of guaranteeing the quality of the provided power despite the intermittent nature of the RES, and other electrical disturbances, such as grid disconnections and load variations. Proper implementation of the primary controllers can lead to the reduction of the maintenance cost and frequency of DGUs, augmenting the lifespan of interconnected electrical devices, such as batteries, fuses, and transformers, while ensuring the

stability of the grid.

Since the performance of the primary controller is known to be sensitive to parameter variations the stability of the grid highly depends on a proper controller design for the interfaced DGUs. Thus, an insufficient behavior of the control strategies to counter the effects of power imbalances, parameter variations, transitory, and architectural changes can drive the microgrid to an unstable state [88]. On the other hand, a capable controller in charge of balancing the power contribution of each DGU allows a "seamless" behavior of the microgrid despite possible sudden changes.

As reviewed in the previews section, the control requirements can be divided according to the hierarchical control architecture of the microgrid. The categorization of the control actions is done according to specific low and high-level control objectives, where primary and secondary control layers attain all the control efforts in regards to the regulation of the delivered electrical variables. Indeed, both control layers pursue a stable and regulated power delivery among all the contributing agents by seeking a balanced power output depending on the individual characteristics of each generation unit. Therefore, it is crucial to mention that both control layers operate under the same principle of what is known as *droop control*. This control technique is based on the nature of synchronous generators to emulate the physical dynamics of a generator within a control loop, resulting in a stable power line despite the lack of inertia in the system, therefore, rejecting possible disturbances [89]. The following subsections dive into the basic principles behind synchronous generators to later dive deeper into the droop control strategy.

2.4.1 Synchronous generator for deriving droop characteristic and control

Most of the electrical power demanded in today's electrical network is generated through the implementation of synchronous machines. However, most of the electrical energy produced at the microgrid level comes from renewable sources that are interconnected thanks to power electronics devices, these devices do not have the inherent mechanical inertia of synchronous generators, meaning that during unexpected disturbances, the power electronic devices can not stabilize the whole power system by generating or absorbing power through the inertia properties [90]. For that reason, synchronous machines have excelled over the years in tasks that require the transformation of mechanical input to an electrical output when acting as synchronous generators. Their damping and stabilization capabilities are highly desired in today's energy generation through power electronic devices.

For that matter, it is crucial to know the basic operation behind synchronous generators, to derive control techniques that can emulate such mechanical behavior in the current microgrid

topology. For a basic understanding, when a synchronous machine acts as a generation source a prime mover is required to drive the generator's rotor and produce AC electrical power [89]. The synchronous generator basic schematic is illustrated in figure 2.8.
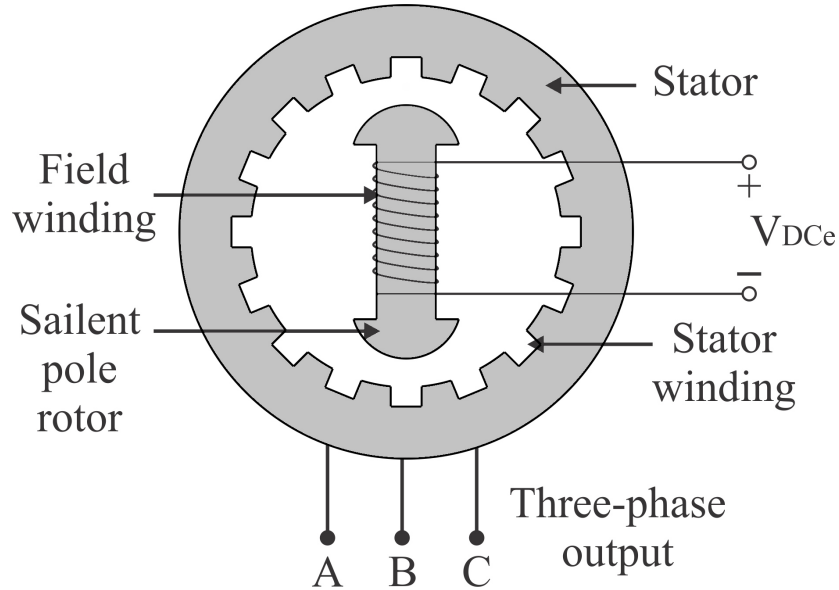
Fig. 2.8: Synchronous Generator Schematic

Synchronous generators can be divided into three main physical components, the rotor, the stator, and the wingdings. The rotor can be described as a permanent magnet when its corresponding winding is fed with a continuous current creating a magnetic field around the rotor, this is achieved by having a DC voltage source to excite the rotor's winding. Rotors can be excited externally or internally by the implantation of a slip ring that allows taking advantage of the prime mover to generate the required DC input. This excitement voltage is represented by the variable V_{DCe} in figure 2.8. A stator can be formed by a P number of poles, this parameter is crucial to determine the frequency (f) and rotational speed (N) of a three-phase synchronous generator, as their relationship is clearly seen in (2.2).

$$f = \frac{PN}{120} \tag{2.2}$$

Once the rotor windings are excited and a magnetic field is created at each pole of the rotor, the rotating action generated by the prime mover creates a rotating magnetic field, this creates a change in flow dispersion, then, this cyclic change generates an alternating voltage signal at the stator's winding terminals.

In the generator form, a constant frequency output is required, from (2.2) it can be deducted that frequency output can be regulated by varying the number of interfaced poles or by chaining the rotational speed. Since in an implemented generator, the number of poles is fixed to

design criteria, the rotational speed is the only remaining factor that can drive the frequency of the system. Therefore, synchronous generators are commonly placed on facilities that can provide a continuous flux of movements such as hydro-power systems or steam turbines, this is done with the objective of having better management capabilities of the rotational speed with added mechanical implementations [89].

Alternatively, if the frequency of the system is disturbed, causing fluctuations in the global value of the frequency, the rotational speed would be affected. However, this is not the case since the inertia of the synchronous machine impedes the larger deviations. This phenomenon can be translated to a relationship between the generated power and frequency rating. Leading to the principles of virtual synchronous machines and droop controllers to maintain nominal levels of the delivered electrical power in systems that lack the inertia characteristics of synchronous machines.

2.4.2 Droop Control Fundamentals

As previously mentioned, the complexity behind the operation of microgrid systems demands that extensive pre-deployment studies contemplating the type of generation agents, type of loads, peak load demand, long-term weather conditions data, operation modes, long-term load demand forecast, and communication needs, be conducted to assertively promote the deployment to these micro distributed generation networks. It is important to mention that microgrid systems with multiple interfaced DGUs with different power ratings and a variable load demand requires the integration of EMS to accurately command and adjust the power references of the interfaced DGUs while maintaining the voltage and frequency values within the nominal range.

The power range variability of DGUs combined with the power demand variations can trigger power imbalances in the microgrid, causing power oscillations and hindering the overall quality of the supplied energy. Typically, the resolution for the power imbalances is seen through control strategies that mirror the dynamic behavior of synchronous generators creating the basic principles of droop control strategies [80].

Typically, the resolution for the power imbalances is seen through control strategies that mirror the dynamic behavior of synchronous generators creating the basic principles of droop control strategies [80]. Synchronous generators rely on their mechanical power to maintain an even power distribution, in the case of an increasing load the generator's speed decreases while the electromagnetic torque of the generator increases, this effect is also related to the frequency of the grid and can be translated to power electronic devices, where changes in the frequency can be related to the delivered power, similarly, the same behavior can be deducted

on the reactive power side with the delivered voltage, therefore, creating these relationships known as P/f and Q/V droop control for non-mechanical generators [91].

These control techniques assure the ideal power-sharing conduct of the interfaced DGUs. However, since power electronic devices lack the physical response of a synchronous generator, droop control techniques are commonly used in combination with control methods that emulate the physical dynamics in a virtual environment, this combination of control methods diminishes the effect of disturbances in a non-mechanical generation system, this second control technique is commonly referred in the literature as Virtual Synchronous Generator Control (VSGC) [92].

Droop methods are used to manage the power-sharing in microgrids by decreasing delivered active and reactive power when the microgrids' frequency and voltage increase respectively [80]. The power demand in a microgrid operating under an autonomous scheme can cause different scenarios in the delivered voltage and frequency values, i.e, figure 2.2 shows the cases for the over and under frequency scenarios, that is, for a finite generation capacity, an overactive power demand would lead to a delivered frequency under the desired nominal rate, on the other hand, a decrease in the based demand could lead to an increase in the delivered frequency.

Droop controllers are widely studied in the literature, several modifications and proposals have been done over the years like VSGC to overcome specific problems including power-frequency, power-voltage, voltage-current, and voltage-based droop controllers [58, 67]. However, conventional droop controllers are still being used and are among the most popular approaches due to their easy implementation and understanding. Conventional droop control can be interpreted as the linear relationship between a correlating set of local electrical variables, the linear relationship is driven by droop characteristics specific to a given DGU. The equations (2.3) and (2.4) represent the conventional droop control strategy, also known as P/f and Q/V droop control.

$$f_{nl} - f_{fl} = -m_p P_{max} \tag{2.3}$$

$$V_{nl} - V_{fl} = -m_q Q_{max} \tag{2.4}$$

Where f_{nl} and V_{nl} represent the frequency and voltage points at a specific point known as the "no-load" point, subsequently, f_{fl} and V_{fl} serve as the "full-load" points of the frequency and voltage, while P_{max} and Q_{max} stand for the active and reactive power rating of the specific DGU. Finally, m_p and m_q are known as the droop characteristics, these represent the slope of the linear relationship between the correlated electrical variables. A graphical representation of these equations is shown in the figure2.9, where f_{op} and V_{op} are the nominal frequency and voltage respectively.
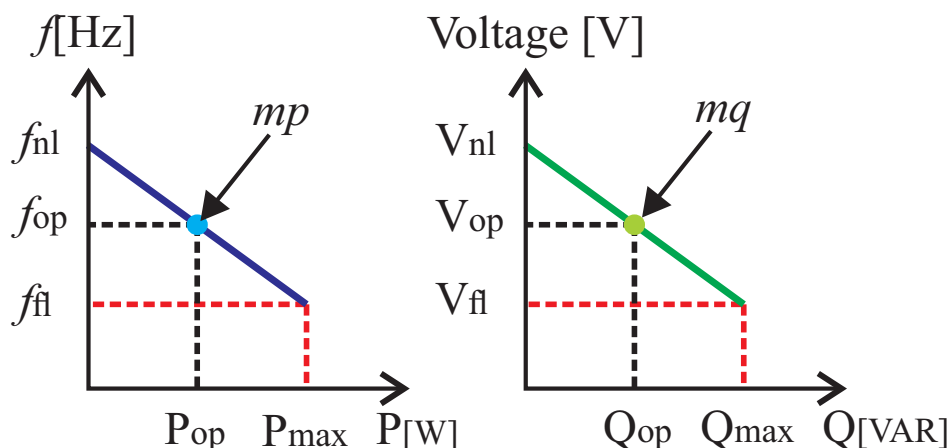
Fig. 2.9: Classic Droop Control

These equations help to establish a "smooth" interaction of multiple DGU connected to the same bus of energy. However, the interconnection of multiple DGUs lights up the power-sharing performance requirements, where the microgrid's demanded power must be covered "evenly" by all the interconnected generators. This "even" power supply is achieved by adopting the above-mentioned droop control strategy in each DGU. It is important to mention that the characteristics of each DGU can be different, meaning that the interfaced generators can possess different "no-load", "full-load", and generation rating points. Particularly, this leads to different droop characteristics for each DGU.

An example of this droop characteristic variety is shown in the figure2.10, where three inter-faced DGU supply a given load. This example shows how the contributing generation can be different between DGUs despite operating under the same frequency level f_{op}. It also exemplifies how the total power contribution can be written as in (2.5), being the sum of the independent power contributions by the "k" number of interfaced DGUs. The "seam-less" interaction can be understood as the liberty of deviating from the nominal frequency value without compromising the power delivery forasmuch as the operational frequency is maintained under the allowed minimum and maximum values.

$$P_{total} = \sum_{n=1}^{k} P_{DGUn} \tag{2.5}$$
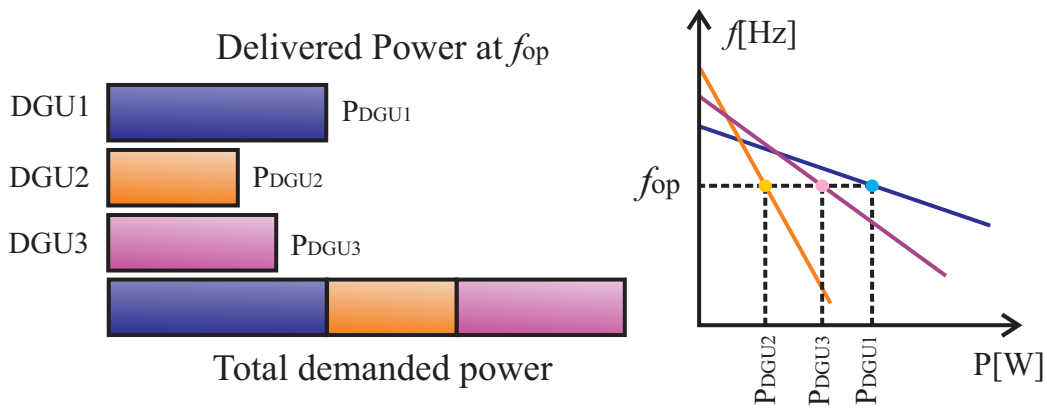
Fig. 2.10: Power contribution example

Overall, droop methods offer simpler power distribution among multiple interfaced distributed generation units, nonetheless, these are far from perfect, primary control deviations can be introduced due to the voltage and current controllers that are commonly used ahead of the droop methods, the voltage and frequency controllers are mostly based on conventional controllers such as PI and PID, offering an easy and fast implementation, however, it's correct tuning is a difficult task to achieve, therefore, most the PID implementations found in the literature tend to use the trial and error method to accomplish the desired control performance. The right tinning of the conventional controller's gains is not part of this works' scope.

2.5 Transitions Between Operation Modes

As described in the previews section, microgrids are systems that can operate either with or without a direct connection to the power grid. This characteristic of the microgrid allows the possibility of deciding the operational mode of the system. In the best-case scenario, connecting and disconnecting events can be scheduled, the former can be done with the intention of wanting active participation of microgrids in the power grid network through power exchange while the latter case can be motivated by minor power grid faults or planned maintenance events within the power grid. Nonetheless, transition events can also be unintentional, commonly caused by faults or power mismatches on the power network side. In either case, transition events are handled differently in the literature, and these are treated as separate problems among microgrid systems.

2.5.1 From Island to Connected operation

To achieve a seamless reconnecting with the main grid and sustain an uninterrupted and reliable power supply during the process, variables such as voltage, phase angle, and frequency need to be synchronized. That is, the mentioned electrical variables of both entities, the

power grid, and the microgrid, need to be within a specific delta range to properly achieve the reconnection of the microgrid and avoid causing transients. Figure 2.11 shows how these deltas can be displayed between the microgrid and the power grid.
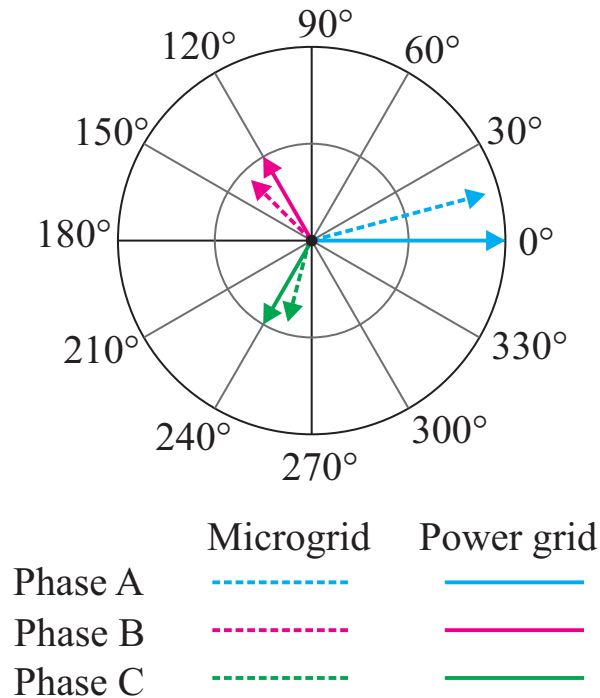
Fig. 2.11: Phase angle delta between the power grid and the microgrid

Nonetheless, due to the high penetration levels of power-electronic-based generation systems, the synchronization process can present some challenges. The fast dynamics, small inertia, and low to none overload capabilities of power converter systems require additional strategies to achieve a seamless reconnection [93]. Due to these characteristics reconnection transients can occur, generators over-current, voltage phase jumps, and frequency drifts represent a threat to the connected loads.

Virtual inertia-bases methods are proposed across the literature to counter any over-current effect on the generators, however, this strategy can not overcome the issues regarding the phase angle jump [93]. To better synchronize the phase angle, the authors in [94] propose a low-bandwidth communication-based method. the proposal synchronizes droop controllers to match the voltage, frequency, phase angle levels moments before the reconnection, the communication network helps to adjust the active and reactive power outputs of each DGU.

Reconnection events can be seen as a "simple´´ challenge in the transition between the island and grid-connected mode. This can be attributed to the fact that in cases where microgrids

need to be reconnected to the main grid all actions are intentional. In this sense, high-level controllers can coordinate the may participating assets to prepare a successful reconnection. This implies that a certain communication level needs to be established between high and low-level controllers to properly allow the flow of information from the high-level to the low-level components of the microgrid.

2.5.2   From Connected to Island operation

On the other hand, it is the unintentional and unplanned transition events that present the most challenging scenarios for seamless transitions. In fact, it is the case of transitions from a connected state to an autonomous operation of the microgrid that can cause greater damage, especially if these are not dealt with properly. Since these tensions can occur at any moment in time, several algorithms to detect these disconnection events have been proposed in the literature. These many algorithms can be found under the name of Islanding Detection Methods (IDMs). However, most of them rely on a communication network o can deteriorate the quality of the delivered energy across the microgrid. Further details in regards to this transition between operating modes are given in Chapter 3, where the state-of-the-art review of *island detection methods* is discussed.

The current proposal is given in the context of a transition between a grid-connected to an island operation of the microgrid. However, contrary to other proposals or island detection methods reviewed in the literature, this work proposes a decentralized island detection algorithm operating under the principles of individual droop characteristics deviations, meaning that only local parameters are used to detect any islanding events. By relying on local measurements to integrate the island detection capabilities within the primary control layer of the microgrid hierarchical control scheme. In this manner, the proposed algorithm can act locally, without the disadvantages that come with the implementation of harmful methods based on the introduction of electrical disturbances into the microgrid's power lines. Furthermore, this proposal is validated by constructing a digital and RT simulation test-bed. The following section of this chapter will discuss how RT simulation aids in the development of microgrid technologies, cutting the line between creation, validation, and implementation of an idea for accelerating the technology transfer process.

2.6   Real-Time as support for microgrid development

The raising challenges that come with the development of microgrids as a participating entity in today's electrical network have been undertaken by many researchers across the world in their respective fields such as management, control, planning, communication, and optimization, just to mention a few. However, the many proposals that surround such topics of interest

require the development of new testing and validation techniques to catch up with the increasing complexity of microgrid systems, especially in areas such as control and management. According to Vijay et al. [95], these new techniques must consider crucial testing characteristics such as scalability, flexibility, and ease of implementation, without compromising the accuracy of the results or the economy of the researchers.

Nowadays, the evolution of simulation and tests systems is directly proportional to the availability of more capable computing technologies. Simulators work on the available computational power and are known for being dependent on the accuracy and complexity of the simulated model. This evolution has led to more capable systems, such as the case of RT simulation that allows the simulation and testing of complex systems while ensuring the dynamic consistency of the tested model [96]. This new testing and validation technique has opened the door for other simulation strategies that can be better suited for specific scenarios. Figure 2.12 illustrates the different types of simulation that can be applied to the development of microgrid technologies [95].

In the past, the validation process of a given proposal was carried out in analog and digital simulation systems, also known as continuous and discrete simulations respectively [95]. With the evolution of computational tools, acquiring higher processing power, other simulation types could be added to the discrete simulation realm, for instance, Offline software, Real-Time software, and Real-Time software and hardware simulation strategies. Offline software simulation remains one of the most popular simulation strategies at the undergraduate level, its ease and low cost of implementation make it an attractive testing strategy for simpler tests that do not require an extremely accurate dynamic representation of the tested system. Particularly, this simulation type is characterized for an accelerated computation of results, that is, the results of a tested system can be given in a shorter time than the programmed simulation time. However, the fast computational time of offline software simulation can be slowed down by the complexity of the simulated model, in addition, due to the accelerated characteristics, the real dynamics of the tested system are not guaranteed, making this test and simulation type insufficient for a technology transfer process.
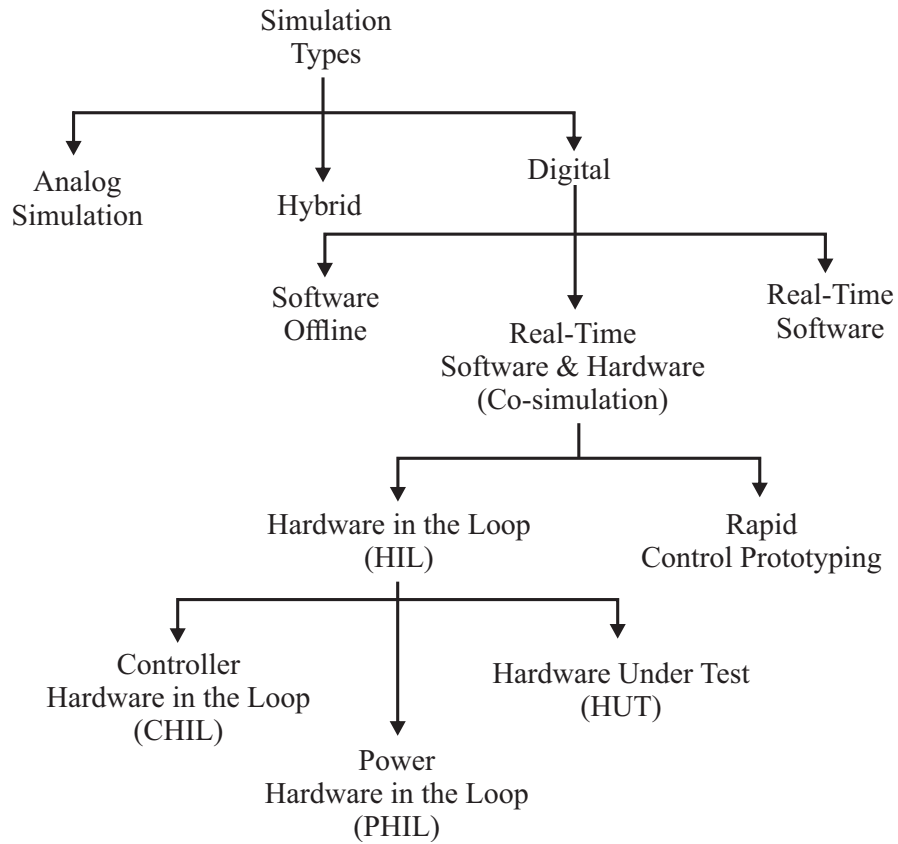
Fig. 2.12: Simulation types for microgrid development

Although the offline software approach can be adequate for certain manufacturing and iterative design processes, the many and different dynamics of the various assets within a power system such as the microgrid can challenge the effectiveness of computational simulation, especially since the complexity of the tested system is one of the main hindering factors for this digital simulation type. To overcome such paradigms of an offline software simulation, researchers have adopted other discrete simulation strategies such as RT simulation. RT simulation has been used to counter the added complexity of power systems, allowing a high degree of accuracy across simulation results [96].

In particular, RT simulation can be divided according to the employed tools in RT Software and in RT Software and Hardware as illustrated in figure 2.12. RT Software is characterized by allowing the construction of digital replicas of a real system, its application in the energy sector has been limited to areas concerning the information technologies behind the operation of microgrid systems. In recent years, this approach has been applied to the cyber security area of networked microgrids is presented in [97]. Alternatively, RT software and hardware deal with the operational technologies of complex electrical systems such as the microgrid. The operation technologies side of the microgrid is more complicated since it requires highly

accurate models concerning the complex dynamics of multiple generations and consumption agents within a single organization.

Microgrid and Smartgrid studies can be severely benefited when applying RT simulation technologies to their development process. The use of RT simulation is extensively reviewed in the literature [98, 99] for such fields of study. The RT technology attends the present issues of control and management techniques, distributed generation integration, grid state estimation, grid automation, protection, and high-level field-oriented applications for microgrids and Smartgrid systems [96]. The main advantages include not only reduction of risks of real implementation, but also aid to diminish the cost of extensive testing [100].

RT software and hardware category can be further divided to accelerate the design and validation of particular microgrid applications, for instance, *Rapid Control Prototyping* (RCP) offers a fast, intuitive, and iterative process in the right tuning of a designed controller. By running the proposed controller in RT and interfacing it with the real hardware, an online tuning procedure can be conducted by the researcher to guarantee the desired controller response. Alternatively, if the plant is too complex or difficult to attain in a laboratory environment, *Hardware in the Loop* (HIL) techniques can be integrated into the validation process.

HIL techniques are ideal for complex systems such as microgrids that deal with the nonlinear dynamics of an electrical network. HIL applications for an electrical system can be segregated into (i) *Controller Hardware in the Loop* (CHIL), (ii) *Power Hardware in the Loop* (PHIL), and (iii) *Hardware Under Test* (HUT). All of these categories divide the simulation problem into two systems connected via an interface that allows the translation of IO signals. One of the divisions is the RT simulator, which is commonly programmed with the plant or the environment in which the designed system is going to operate, the second system is the designed system, which is commonly programmed in an external device and interfaced to the plant via corresponding IO ports. The main differences between these strategies are the tested system (external) and the interface between both systems (internal and external). The former can be an embedded controller with minimum power requirements or a power device with actual power exchange, hence, the given names on CHIL and PHIL respectively. The latter difference is the interface, in the case of a PHIL approach, a power interface is required to translate high power signals of currents and voltages to digital and analog signals that can be interpreted by the RT simulator.

Overall, RT simulation is an attractive validation tool in the power control area due to the closest approximation of reality through the dynamic consistency of its simulation process. The dynamic consistency characteristic reefers to a deterministic time-step at which the simulation process needs to run. On the contrary to classical computational simulation, where

the simulation time-step can be set to fix or continue. RT assures that all the required operations be concluded before the next time-step is set, this is not true for classic simulation methods, where the required operations can delay their outcome to a specified or convenient time step to finish a certain task. In a sense, by completing every crucial operation before the next time-mark begins, the dynamic consistency of the simulated system is guaranteed [101]. Figure 2.13 show how these simulation types differentiate from each other when it comes to the time-step per operation, where the time-step is represented by the variable Ts_n, and the tasks by the variables Tn.
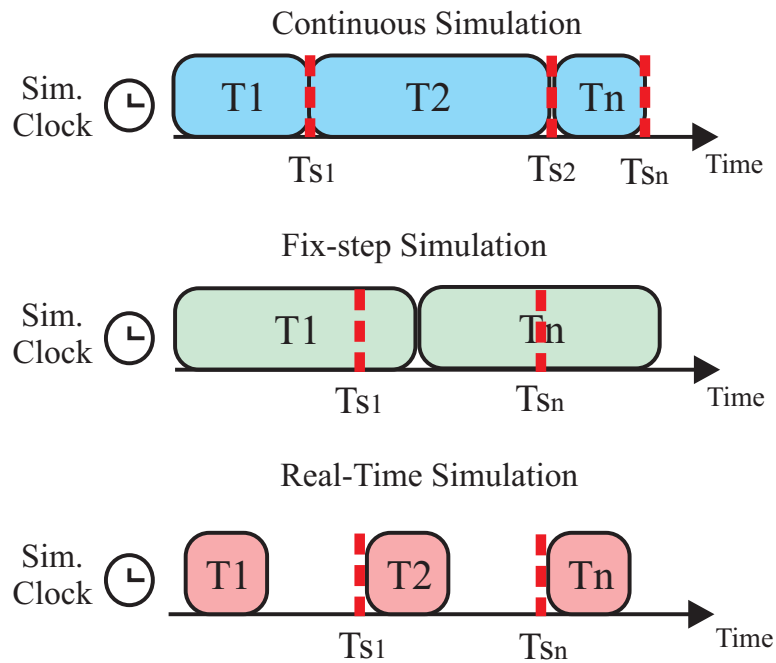
Fig. 2.13: Simulation time-step comparison

As mentioned, RT simulations are a fixed-step simulation type, meaning that for a given number of tasks, these must be performed at a certain time step, and its accuracy is found to be highly dependant on the length of time of each time step to obtain the desired results. To achieve RT simulation the obtained outputs of a given number of tasks must occur before the next time step mark, if a certain task takes a long time than the time step to produce the desired output, the simulation is considered erroneous, generally, this is denominated as an overrun fault. Figure 2.14 illustrates how an RT execution is carried out as the overrun fault at a step time C_n.
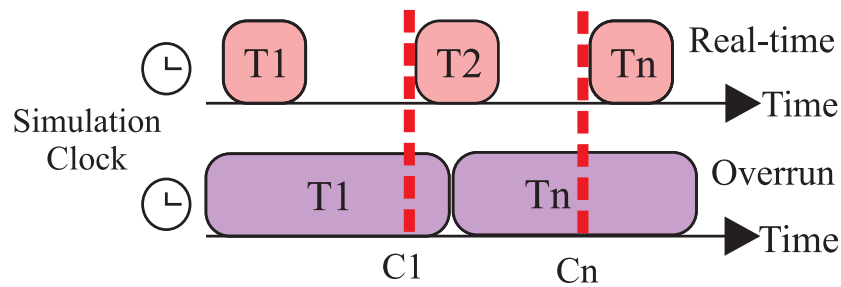
Fig. 2.14: Real-Time simulation overrun fault

2.6.1 Co-simulation

As a strategy to simulate complex and large power systems, co-simulation separates the problem into different modules and simulates each module in different RT simulators. In this manner, each simulator can solve independently a certain task, leading to a more realistic behavior between modules. This strategy is an advantage for power system-related proposals since the connection of real hardware is not necessary for its proper implementation, thus the risk of manipulating high-power devices is omitted.

One common application of the co-simulation strategy in Microgrid oriented applications is to have a control or management proposal executing in one RT simulator, while the plant or the test system is being executed in a second RT simulator. By having bidirectional communication between simulation platforms through analog and digital inputs and outputs ports, the information exchange is achieved in an efficient fashion. By following this array, obtaining a real-life behavior and dynamics of the programmed control or management proposal over a more realistic behavior of the executed test system.

As an example, authors in [102] propose a platform between two differently geolocated RT simulators to evaluate power systems. The communication and data exchange between simulators is performed using point-to-point User Datagram Protocol (UDP), while the user interaction is through an Internet connection to a public web server, simulators are also connected to the webs server to provide the user with information over the simulator work. Another approach is taken by authors in [103] to make use of HIL and co-simulation strategy to deliver a platform capable of delivering in detail the dynamics of a wind turbine as the behavior of the tested controllers.

In another work presented by Zhang et al. [104], co-simulation strategy is used to validate the electromagnetic transients of a 500 kV transformer within a hybrid power grid, the system is divided into three modules, where the simulation for the electromagnetic transients is allocated in an RT environment, the remaining modules take place in different platforms, one for finite element analysis calculation and other in a MATLAB-based platform.

2.6.2 Hardware-In-The-Loop

Alternatively to the co-simulation strategy, HIL, PHIL, and HUT deal with physical components in a bidirectional communication link with the RT simulation environment. The main difference between these strategies is that HIL and HUT deal in a different manner with the dynamics of the physical components. HIL interacts with embedded systems that represent the real product response to the simulated environment, while HUT interacts with the real artifact rather than its embedded version. On the contrary, PHIL incorporates a power exchange layer between the RT environment and the physical components, allowing the testing of high-power systems in a safe simulation space. In reality, all three strategies help in the early detection of faults in the operation of the tested system in a close to a real scenario. These strategies help by cutting the simulation cost of extensive testing and saving time in the validation process of a given product.

HIL simulation strategy turns into a safe practice for validating hardware and software [105]. In microgrid studies, HIL is a powerful tool to test and validate embedded controllers or proposed systems and foresee the correct operation before its actual implementation. HIL simulation replicates the dynamic of a system according to natural circumstances in an embedded platform, leading to a more complete analysis of the simulated system ahead of the real implementation. In this manner, system and controller faults can be identified in the early stages of a project.

HIL is the next stage in the process of validating the performance of a given proposal. The main difference between HIL and the co-simulation strategy is how the proposal is implemented and how its response gets analyzed, in the latter, the proposed system is simulated in a secondary simulator, while in the former, the proposed system is brought down to an embedded system that reads the simulator outputs and computes the triggering or feedback signals in an external process. The architectural difference is illustrated in Figure 2.15.
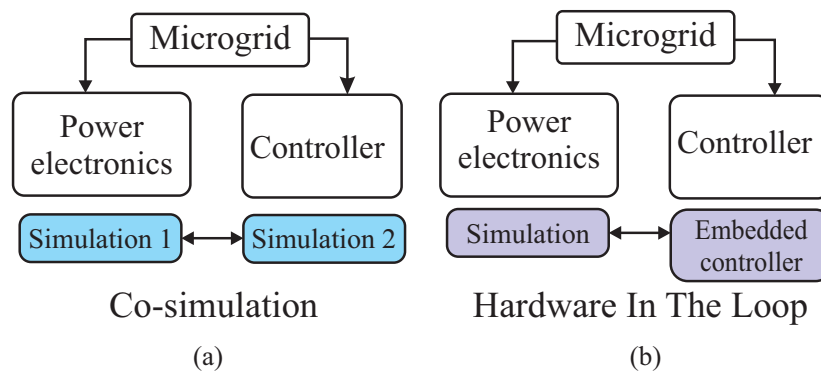
Fig. 2.15: RT simulation strategies: (a) Co-simulation; (b) Hardware in the loop

A combination of both simulation strategies is carried out in [103], authors establish an RT co-simulation platform with a HIL interface for a wind energy source. HIL of tested controllers is achieved by having in a Programmable Logic controller as an intermediate link between simulators, the co-simulation is carried out to model the wind turbine, while the controller is running in a HIL implementation. The is no doubt that RT has a huge area of opportunity in the planning and development of complex power systems such as the future electrical network and its smaller instances like microgrids. Other works have taken advantage of this technology to simulate and validate parts of these complex systems, relying on different RT strategies to achieve the final goal of validating their proposals, proving that RT is a reliable validation tool.

Chapter 3

State of the art review

3.1 LC filter

As the many DGU based on renewable assets depend on power electronic devices to generate electrical power, it is important to consider that the basis of such power converters is the implementation of high-frequency switching devices driven by PWM techniques. However, PWM techniques can cause the high-frequency switching devices to introduce high-frequency harmonics producing electrical noise in the delivered energy [106]. Furthermore, the electrical noise can disrupt the performance of power controllers and represent a hindering factor for electrical machines and other loads feeding of such generation. To tackle this problem, power converters are interfaced with electrical filters, these a divided according to the type used components which also drive the pricing and complexity of their design. Two main types can be found across the literature, those with passive components, with high reliability and low cost, and the ones based on active components, with improved performance but with higher costs, and these are commonly interfaced with external sensors that impose an additional investment cost [107].

Although active filters are a good solution to the noise problem, their complex design and higher implementation cost have led to the development of new strategies based on control methods to improve the performance of passive filters. An example is shown in [108] where the filter equations in a synchronous reference frame are used to develop a Sliding Mode current controller for an interfaced VSI, such equations are also used as the basis for an adaptive power-sharing controller in [109]. With these cases in mind, it can clearly be seen how the filter parameters can have an impact on low-level controllers, also, equations in a synchronous reference frame (3.1) and (3.2) show how these are critical variables in the power output of an interfaced VSI as demonstrated in [109, 108].

$$\begin{cases} L_f \ \dot{i}_d = v_d - v_{cd} + \omega_s \ L_f \ i_q \\ L_f \ \dot{i}_q = v_q - v_{cq} - \omega_s \ L_f \ i_d \end{cases} \tag{3.1}$$

$$\begin{cases} C_f \ \dot{v}_{cd} = i_d - i_{cd} + \omega_s \ C_f \ v_{cq} \\ C_f \ \dot{v}_{cq} = i_q - i_{cq} - \omega_s \ C_f \ v_{cd} \end{cases} \tag{3.2}$$

where the variables v_{cd} and v_{cq} represent the measured voltage at the capacitor of the LC filter, v_d and v_q represent the output voltage in their dq components, i_{cd} and i_{cd} are the currents passing through the capacitor C_f. i_d and i_q are the measured currents after the inductor L_f, ω_s being the frequency of the system in rad/sec, and lastly, $\dot{v}_d$, $\dot{v}_q$, $\dot{i}_d$, and $\dot{i}_q$ are the changing voltages and currents in a synchronous reference frame respectively.

From the latter examples and equations, it's clear to see the role of the LC filter in the control area and in regards to the quality of the delivered electrical energy. For that reason, Several design methodologies have been proposed across the literature, where most of them contemplate the integration of a VSI with a direct connection to the utility grid [110, 111, 112]. As an example, the work presented by Cheng et al. [61] introduces a fuzzy logic-based design methodology to determine the parameters of interfaced LC filters in a single-phase inverter system. Such a proposal establishes triangular membership functions with inputs such as the voltage error obtained from the measured voltage at the terminals and a reference voltage, the rate of change in the voltage error, and the voltage magnitude. Overall, the fuzzy logic design process for the LC filter obtains promising results in the attenuation of the harmonic content of the output voltage. Although this method is effective, the complexity of the Fuzzy Logic algorithm for a three-phase inverter would result in a setback for the design procedure. However, the advantage of not requiring the filter model makes this proposal an attractive solution.

Another design procedure for the LC filter in a single-phase VSI system is presented by Ahmad et al. [113], the work contemplates critical variables such as the cut-off frequency, modulation factor, and switching frequency to meet the *IEEE Std. 1547* for harmonic attenuation. Overall, the designed LC filter is able to maintain the harmonic distortion under 1.1%, full-filling the *IEEE Std. 1547* standard on harmonic attenuation.

By contemplating that LC filters are complex and their performance is dependent on external system variables, authors in [23] propose a design methodology is based on a metaheuristic optimization algorithm to better handle the multivariable problem. Particle swarm optimization is then used to find the optimal setting for the LC filter parameters, controller gains, and power-sharing coefficients in both operating modes of the microgrid, that is, the optimization algorithm is executed for each operating mode. Although the authors successfully find the optimal values for a specific microgrid model, the multivariable optimization problem is

rather complex since different systems are contemplated in a single objective function. In addition, the obtained parameters change are different for each operating mode of the microgrid, this would indicate that such variables would require modification in case of sudden disconnection, despite this being possible for the controller gains and power-sharing coefficients through the implementation of look-up tables, the physical components of a passive LC filter would be difficult to change, meaning that the optimized LC filter for a connected state may under-perform for an island operation since the controllers are not tuned to its specific dynamic.

Despite these crucial points, it is important to consider an optimization methodology for the LC filter parameters that can guarantee adequate performance in both operating modes and controller settings. Optimization algorithms are a good option to achieve such a goal since these can contemplate the vast number of variables and objectives in such convex and nonlinear problematic. For that matter, one of the proposals of this work deals with a heuristic optimization algorithm to find such LC values that can satisfy the *IEEE Std. 1547* standard on harmonic attenuation in both operating modes and minimize the introduction of transitories due to this *disconnection event*.

3.2 Genetic Algorithms

A large number of areas in the engineering field have benefited from the advantages of applying optimization algorithms. *Genetic algorithms* (GA) are one of the most widely used tools since it first appeared in 1970 [114]. GA is classified as an evolutionary optimization tool, this algorithm works under the dynamic principles of natural selection where only the fittest individuals in a population are chosen to continue in the iterative process of the algorithm as possible solutions [115].

GA works to find a minimum or maximum solution to an objective function by manipulating the initial population, each element of the population is evaluated with respect to the established objective function, acquiring a score with respect to it, at the end of the iteration only the inhabitants with the best scores are chosen as parents to create children, children are then created to contain characteristics of their parents. Figure 3.1 shows the functioning of these operations and the iterative evaluation process of GA optimization.

The basic structure of the GA is divided into operations such as selection, crossover, mutation, and evaluation [116]. The selection process separates the strong individuals from the weak ones as the former represents a potential solution due to their initial scores according to the established objective function, the selected individuals are then copied into children generations by the properties of crossover and mutation. The crossover operation takes the similarities of the best fit values from the parents in previous generations and creates a new

POPULATION & SELECTION
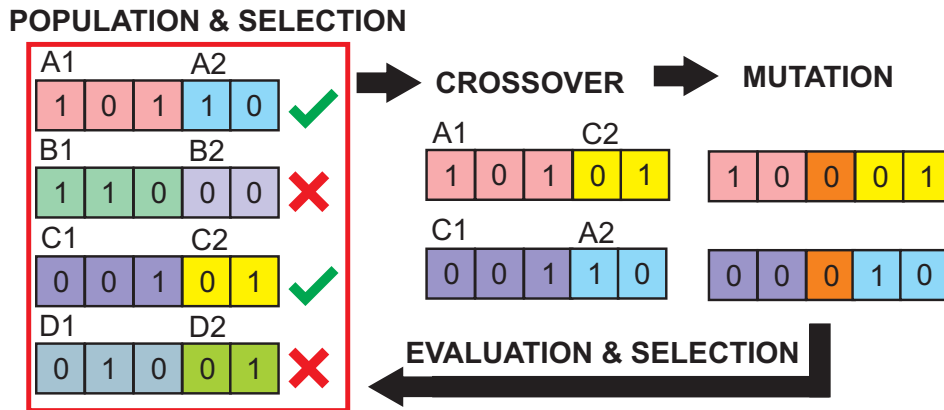
Fig. 3.1: Genetic algorithm flow of operation

population of children with common characteristics [114], at the same time, the mutation operation helps the optimization process to avoid falling in a local minimum or maximum value, this is achieved by changing one factor of a generated children according to certain probability [116].

3.3 Genetic Algorithms in Microgrid Applications

Optimization algorithms have been applied to a vast number of engineering fields. The action of optimizing a certain process, component, or area, is mostly constrained by complexity, a wide number of variables, the desired design, or behavior. Therefore, optimization algorithms contemplate such characteristics to optimize as key variables in a function that enables its resolution. Microgrids have adopted optimization algorithms in a wide range of areas, the scheduling of ESS, primary level controllers, management of resources, planning, just to mention a few. Genetic algorithms have been an important heuristic optimization method and used across many areas of opportunity in the development of microgrids. This optimization method is preferred thanks to its easy implementation and capability to adopt multivariable and multi-objective problematics that derive from nonconvex and nonlinear problems [117].

As an example, the work presented by Raghavan et al. [118] deals with the charging and discharging times for an ESS within a microgrid system. As reviewed in Chapter 2 microgrid management can introduce dynamic pricing strategies to motivate users to regulate their consumption during peak hours, this motivates the optimization problem to have an optimized charge/discharge scheduling strategy that aims to reduce the cost paid by users in a microgrid with subject to dynamic pricing. The optimization problem is carried out with genetic algorithms optimization, the variables of interest were the total demanded load, the generated power by the DGU, the price per kWh in an hourly format, and the charging and discharging

limits for the batteries in the ESS, these are used to formulate an objective function to evaluate in the optimization process. The results show how the genetic algorithms optimization process can help in the reduction of cost by a total of 11.31%.

Another application of genetic algorithm optimization can be found in the work presented by Askarzadeh [119]. In particular, this work deals with the generated power and how this is shared among the interfaced DGU within the microgrid. The optimization problem seeks to have an optimal power-sharing scheme to reduce strain in some of the DGUs during specific times of the day. The main variables considered in the optimization problem are the hourly cost of energy, the generated power by DGU, the efficiency of the DGU, and the type of generation (solar, wind, or CHP). Overall, the optimization by genetic algorithms successfully distributes the load among the DGU, resulting in a good alternative for microgrid power scheduling and power systems optimization.

Optimization can also be applied to in the planning stage of microgrids, this is proven in the work presented by Oulis Rousis et al. [120], where a genetic algorithm optimization procedure is conducted to solve the sizing problem of an AC/DC microgrid relative to the total installation cost of photovoltaic panels, wind turbines, and ESS. Another example of genetic algorithms applied to the design of distribution systems is presented by Ramirez-Rosado in [121], in such work the cost function is formed contemplating the investment cost of a future expansion in regards feeders and substations, then the objective function to minimize is formed by technical constraints such as power demand, number of nodes in the distribution network, number of mutual connection points, the results of such optimization problem show how genetic algorithms are a good alternative for planning distribution networks.

Lastly, the work in [107] resorts to a genetic algorithm optimization procedure find to damp the switching effect of the power electric devices in a current control scheme via the implementation of a control-based active damping method. The rectifier is interfaced with an LCL filter which parameters are obtained for a wide range of frequencies by means of genetic algorithms. This LCL filter genetic algorithm-based tuning leads to the development of an active damping method that does not require the addition of extra sensors as required by traditional active damping techniques.

3.4 Islanding Detection Algorithms

The integration of alternative generation sources at the power grid's distribution level has led to new challenges in the control, communication, and management areas of the electrical network [15]. Indeed, availing local resources comes with added complexity and requires coordination mechanisms to ensure their effective integration, leading to the organization of

local electrical agents into microgrids. [15]. Thanks to the introduction of microgrids, these paradigms can be enclosed in a single system definition.

As reviewed in Chapter 1, a microgrid is a cluster of (DGU) with power management and regulation capabilities that cover a local power demand [6, 15]. Microgrids add flexibility since their operation is not restricted to a permanent connection to the main power grid; they can act independently in what is known as *island operation*. However, switching between operating modes implies varying dynamics and dealing with a "weaker" network whenever the main power grid is disconnected.

However, the interchangeability between a grid-connected and an island operation of the microgrid is not a simple task to achieve. A microgrid interacts with the main grid through a single PCC. Disconnection events can be intentional, e.g., in the case of maintenance routines, or unintentional, caused by faults or disruptive events [50]. An unintentional disconnection would force an island operating state, potentially introducing harmful transients and degrading power quality.

Nonetheless, in any case, it is essential to detect the islanding event within the microgrid to trigger ancillary services and exert compensating actions [51]. Even having intentional disconnection events, a microgrid may follow a *distributed* control approach or not be fully communicated, requiring a detection mechanism typically referred to as *island detection algorithm*. Disregarding the case, the detection of a disconnection event should be acknowledged within 2 seconds of its occurrence to minimize any negative effects, this is a statement from the IEEE standard 1547.4-2011 [122].

Another important characteristic is the range of the operation efficacy that these *island detection methods* must have. This is known as the Non-detection Zone (NDZ), a parameter used to evaluate the efficiency of *island detection methods* in regards to possible false-triggering signals. Essentially, NDZ is an operational range in which an *island detection methods* can fail to detect the island condition or assume the occurrence of a disconnection event while the microgrid is still in grid-connected mode. Overall, *island detection methods* should perform as expected by the IEEE standard 1547.4-2011 with minimum effect on the quality of the delivered electrical energy and with a Small o zero NDZ to guarantee an optimal operation.

3.5   Main Island Detection Strategies

To avoid the hindering consequences that can occur from an unintentional disconnection, islanding detection algorithms. These operate with the objective of discovering any disconnection event in a fast and reliable manner, to promptly adjust any compensating actions due

to the sudden change in the mode of operation of the microgrid. Island detection algorithms can be classified in four categories as described in [52]:

1. *Remote* detection methods (RDM)

2. *Passive* detection methods (PDM)

3. *Active* detection methods (ADM)

4. *Hybrid* detection methods (HDM)

3.6 Remote Detection Methods

RDM can also be found under the description of communication-based methods across the literature [123, 124]. The definition of "Remote" is constructed due to the requirements of having a communication link between the utility grid and the microgrid to accurately detect the disconnection between the two networks. Mainly three types of RDMs stand out:, (i) Power Line Carrier Communication (PLCC); (ii) Signal of Disconnection (SoD); and (iii) Supervisory Control And Data Acquisition (SCADA).

3.6.1 Power Line Carrier Communication

As implied in the name, PLCC employs the established power lines to send a low-energy communication signal across the energy network. The masked signal is sent from the utility grid, meaning that microgrids are equipped with a device capable of identifying the presence of the masked signal at the PCC level, whenever the absence of the signal is identified the PCC is assumed to be open, then and a second communication signal can be sent to the operating assets of the microgrid to assume and island mode of operation [125].

One of the biggest advantages of PLCC is that its implantation is rather inexpensive when it comes to the availability of a communication network. PLCC uses established power lines to operate, meaning that installation costs can be shaved from the requirement of installing another communication line. Nonetheless, the transmitter and receiving devices in charge of sending and reading the masked signal can be expensive and uncommon in the market [124].

Also, PLCC can be susceptible to electrical interference, the carrier signal can be disrupted by other electrical components in the network, for example, transformers, motors, and non-linear loads. These components can have a negative effect on the NDZ characteristic of the PLCC, widening the area in which the *island detection methods* fails to detect the island conditions [126]. However, in a purely restive network PLCC methods have shown a close to

zero NDZ, meaning that most microgrids can rely on this *island detection methods*. On the other hand, the shortcomings of being a communication-based technique still apply, communication latency and pirate attacks being the most threatening, also the masked signal is sent from the utility grid, meaning that low flexibility is expected from this method.

To overcome the flexibility concerns, the authors [126] propose a modified scheme that adds flexibility to the PLCC strategy. This is achieved by having a distributed signaling device that can be installed in between substations and the microgrid. This approach also indicates that all the intended DGU within the microgrid should operate with their own signal detection device. This characteristic would only increase the cost of investment since more detection devices should be acquired to match the number of DGUs. Although, this approach decentralizes the *island detection methods* the investment cost would represent a huge setback in its further development.

3.6.2   Signal of Disconnection

In a similar approach, SoD methods base their operation on a direct communication link from the utility grid and each DGU within the microgrid. In this case, the utility grid sends a signal via a reserved communication channel, whenever the signal is broken up the island condition is assumed. Alternatively to PLCC methods, this method does not interfere with the quality of the delivered electrical energy, and the direct and independent connection from the DGU and the utility grid would allow greater coordination of the distributed assets.

With old communication technologies, it is clear how this *island detection methods* would represent a huge investment on physical communication lines and represent a challenge for old wireless methods with a narrow coverage area and slow transmission speeds. Today's wireless solutions have been evaluated as a way around the high implementation costs of physical communication lines and dependency on physical components. Ideally, these wireless signals can adopt a centralized and distributed communications architecture, where a given DGU can communicate with the utility grid and can report back in a one-to-one communications scheme. Several wireless communication protocols can be found in the literature applied to microgrid communications, i.e, Wi-Fi, ZigBee, Bluetooth, Cellular 3G, Cellular 4G, and Cellular 5G [127].

For that matter, the IEEE 802.15.4 standard on control access of wireless networks with a low data transmission rate is taken into consideration in the microgrid and Smartgrid context [68]. This standard opens a scenario where networking devices and features, such as routers, access points, firewalls, and Virtual Private Networks (VPN) can be adopted with WiFi protocols to carry out the data exchange.

Moreover, other studies have shown how the latency factor behind wireless communication plays a crucial role in the microgrid performance, especially affecting significantly the control actions of power electronic devices [128]. For that matter, communication speed has a higher priority when implementing a wireless communication-based microgrid. On the other hand, cellular networks have also been considered as an alternative solution to the Wi-Fi approach, particularly since the range limitations can be overlooked as long as the microgrid is located within the cellular coverage area, which may not always be the case when implementing microgrids outside the urban zones.

3.6.3 Supervisory Control And Data Acquisition

Lastly, SCADA techniques are typically based on supervisory control. These methods rely on closed communication infrastructure, monitoring some electrical variables at the PCC and the utility grid [52]. Although this *island detection methods* can be considered the most robust in the communication side among other RDM, their implementation can be the most challenging. SCADA operates under a network of sensing devices that can be allocated locally or only in the PCC. This *island detection methods* would require a higher involvement of the utility grid operator in the planning and deployment of microgrids, especially if a distributed architecture is preferred.

RDMs are commonly based on supervisory control techniques and are heavily dependent on reliable communication infrastructure, even power line communication techniques are implemented to avoid the higher cost of installing a proprietary communication network, one of the biggest disadvantages of RDMs is the possible communication delay and communication interference in power-line based methods. The disadvantages of *island detection methods* based on SCADA are the high implementation cost, and added complexity to the planning of microgrid, not to mention, the scalability features can be compromised.

3.7 Passive Detection Methods

Since microgrids have a unique point of connection with the main grid, it would be adequate to establish an islanding technique at the PCC level. This technique is dedicated to comparing any mismatches between the electrical variables within the microgrid and the reference values dictated by the main grid. That is, a direct comparison between the voltage phase angles, voltage amplitude, or frequency deviations can be done in a closed format.

To reduce the communication network dependency, PDMs are introduced at the PCC level [52], these methods operate by monitoring any drifts in electrical parameters such as the voltage, frequency, phase angle, and harmonic distortion, creating a tripping signal if any of the mentioned parameters goes beyond a certain threshold. Since PDMs are based on the PCC, the

need for a reliable communication network to effectively carry out the islanding signal is still present, meaning that all the disadvantages of a communication-dependent method still apply to PDMs.

The monitoring approach of PDMs opens a wide range of analysis strategies. In this case, the "local" electrical variables are constantly evaluated against an established threshold, rate of change of voltage (ROCOV), rate of change of frequency (ROCOF), over/under voltage, over/under frequency, active power mismatch (APM), and reactive power mismatch (RPM) are the most popular analysis techniques among PDM to find the operating mode of the microgrid [57].As expected, PDM techniques' performance relies on the type of acquired measurements and their location, sometimes needing additional systems to verify or broadcast the detection signal as discussed next.

3.7.1 ROCOF

Similarly, a ROCOF PDM is presented in [129]. The authors use the difference between the generated active power and the demanded power by the load, the rating of the generation units, and the fundamental frequency value to find the ROCOF over a defined sample window. Then, the ROCOF is compared to a threshold value every time the sample window is closed, adding to the overall detection time. The algorithm also introduces small frequency deviation through q-axis control of a grid side converter, since the injected frequency disturbance can cause a small periodic deviation in a "weaker" grid, the frequency deviations resulting from an islanding event can be used as trigger signals. In the end, the proposed ROCOF-based method is able to detect the island condition successfully in a time range from 100 ms to 200 ms.

However, the efficacy of this method can be undermined by the presence of externally introduced frequency drifts, causing false detection signals jeopardizing the operation of the microgrid. In addition, this method requires the presence of a communication infrastructure to acknowledge the actual power demand. this critical term then is required to compute the frequency deviation index. It is important to highlight that, in the pursue of a fully decentralized island detection method, the dependency on a communication infrastructure can not be an option.

A ROCOF PDM is presented in [129], the authors use the difference between the generated active power and the demanded power by the load, the rating of the generation units, and the fundamental frequency value to find the ROCOF over a defined sample window, the ROCOF is then compared to a designated threshold value for the frequency deviation every time the sample window is closed, adding to the overall detection time. In both island detection strategies, the behavior of the "local" electrical variables is studied. Tripping signals are produced

when certain variables get out of a permissible range of operation according to predefined thresholds [54].

One crucial factor of current proposals around the PDM strategy is that these require a certain level of communication between the island detection point and the rest of the microgrid since the signal must be shared throughout the different electrical agents within the distribution system. PDMs implies the need and disadvantages of communication infrastructure. Then, some of their main disadvantages are the possible communication delay and interference, especially in power-line-based methods [53].

3.7.2 ROCOV

Another popular strategy that falls in the category of PDM is known as ROCOV. As mentioned, ROCOV alternatives are based on comparing the rate of change of a defined voltage index to a designed threshold, whenever the threshold value for the proposed variable index is surpassed, the island conditions are assumed. For example, the work presented in [130] proposes a ROCOV based *island detection method*, the authors measure and compare the voltage and frequency variations at the PCC level to the measurement when a sudden rise in the voltage value occurs due to the rippled current caused by the disconnection event. However, it is important to note that the authors state that the proposed PDM is capable of detecting the island event, they fail to provide the reaction time of their proposal.

On the other hand, the work presented by Abd-Elkader *et al.* [131] proposes a ROCOV PDM based on a voltage index, this index is defined as the product of two variables, the former variable being the rate of change in the system voltage over one cycle of operation of the fundamental frequency, while the latter variable is defined as the average sum of the sampled voltage values in one cycle of the fundamental frequency. This index is later used to find voltage drifts in the main bus, subsequently, the active power mismatches caused by the voltage drifts are evaluated according to an established threshold. Mainly, large and small active power mismatches are analyzed to determine the operating state of the microgrid. Results from this method indicate that for large active power mismatches the algorithm is capable of detecting the island operation within 200 ms after the disconnection. However, in the case of small active power mismatches, a secondary strategy is required to increment the size of the power mismatch, this is achieved by implementing a load disconnection strategy that adds 84 ms to the detection time, which is the time required to disconnect the loads. In any case, the algorithm can detect the island operation within 300 ms, however, the dependency on controllable loads and the response time of these assets make this proposal far from ideal if the power mismatch is considered as small.

Another approach concerning the ROCOV strategy is presented in [132]. In this case, the author's proposal consists of two PDM operating in a parallel configuration, and an optional

ADM in a series configuration. The parallel PDMs consist of a ROCOV and a ROCORP, the latter measures the rate of change in the delivered reactive power at the PCC, while the former evaluates the rate of change in the voltage levels. Since the voltage and reactive power levels can be correlated by means of classic droop control strategies, this proposal takes advantage of this relationship and simultaneously compares both values to a designed threshold value, whenever both PDM agree on having an islanded signal the island signals is triggered. However, since this proposal also integrates the possibility of an ADM, it resorts to it whenever only one of the PDM detects the island condition. In this proposal, the hindering terms of the ADM can be skipped if the threshold values for the ROCOV and ROCORP are adequately designed. Overall, the *island detection algorithm* is tested in a three-phase inverter system feeding a three-phase RLC parallel load, the detection time is reported as 250 ms with a 30 % error rate.

3.8   Active Detection Methods

PDMs and ADMs can be described as local detection techniques according to [57] due to the continuous monitoring and analysis of "local" electrical variables with different approaches. In any case, variables such as voltage, frequency, and active and reactive power are studied to determine the operating conditions of the microgrid.

To further reduce the communication-network dependency. ADMs are introduced as a method that does not depend on established communication lines but operates under the introduction of minor electrical disturbances to the grid to analyze the response and determine the operational state [55]. The main drawback of this island detection strategy is the reduction of the power quality due to the introduction of electrical disturbances. On the other hand, its performance may be sub-optimal due to the countering effect of multiple DGU acting on the same island detection scheme [56].

Since ADMs operate by introducing an electrical disturbance, the analysis of the variable of interest is done after the disturbance is introduced. The work presented by Bakhshi-Jafarabadi & Sadeh [133] analyzes the active power output of a grid-connected photovoltaic system after a disturbance is introduced in the d-axis reference current of an inverter in a closed system, causing ripples in the voltage level of the microgrid if the island conditions are met.

A similar approach is taken by Murugesan & Murali [134], where the introduced disturbance is changed from the reference current's d-axis to the q-axis, leading to the analysis of the frequency response to indicate a grid-connected or island operation. Another approach is taken in[135], where a q-axis current disturbance is injected to achieve a decentralized *island*

detection algorithm, the authors state that the ADM is capable of detecting the island conditions within the 160 ms mark with minimum effect on the delivered power quality by the interfaced DGUs.

Another example of an ADM is proposed in [136], where a harmonic current disturbance-based method is proposed, in this case, harmonic distortion is periodically introduced by modifying the output impedance of the interfaced inverters. The authors state that the proposed ADM can be used in a multi-inverter system without major interference since the harmonic order of the disturbance can be changed for each DGU. However, it is seen that the introduction of non-linear loads can affect the performance of the proposed method. In addition, the proposed ADM is shown to introduce a THD percentage than the allowed by the *IEEE Std 519-2014* [137], Overall, the proposed ADM achieves a decentralized operation with setbacks such as the amount of THD and the long detection time of 3.3 seconds, 1.3 seconds more than the recommended by the IEEE standard 1547.4-2011 [122, 56].

ADMs fulfill the operational requirements for a decentralized system by not bounding their operation to a communication link, however, the introduction of disturbances that promote the degradation of the energy quality due to their operating nature can represent a future threat in the island microgrids with a volatile stiffness level. On the other hand, common PDMs still require the presence of a communication link to complete their islanding algorithm as in [129], where the proposed algorithm requires information about the load power demand, a critical data point that may not be available in a fully decentralized system. Therefore, other proposals have emerged where two of the three categories are merged into a hybrid island detection algorithm.

3.9   Hybrid Detection Methods

To minimize these shortcomings HDMs are proposed as a combination of island detection strategies. Figure 3.2 shows these strategies can be combined to form the fourth category of HDMs.
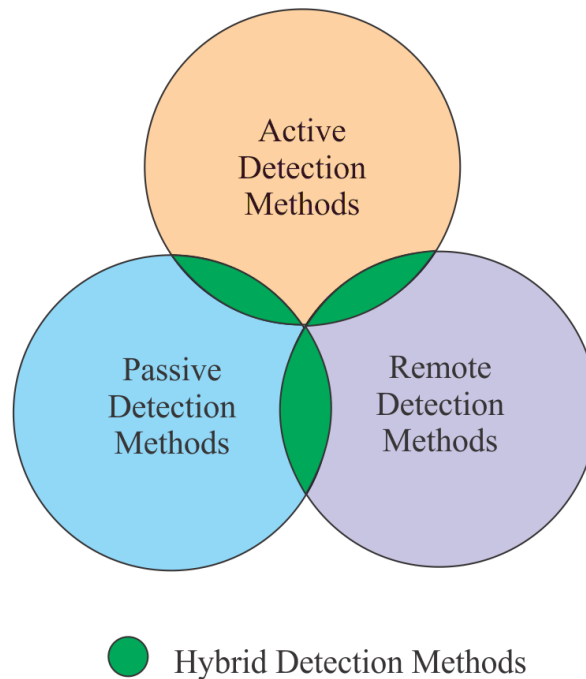
Fig. 3.2: Hybrid detection methods Venn diagram

Commonly, HDMs are classified as series or parallel. Series methods comprise two detection layers: a PDM or an ADM, and a high-level monitoring-based strategy. Only when the monitoring layer detects an islanding event, the PDM or ADM is activated to verify, limiting the ADM disturbances as they are only needed if the first condition is met, and minimizing false tripping. However, the detection time increases if a window-based technique is used at the second layer. A parallel configuration comprises both detection layers running concurrently, generating a tripping signal if both "agree" on a disconnection event. However, this configuration combines the weaknesses of the selected methods [56, 57]. Indeed, the detection systems are improved by combining different strategies, but some of the advantages can be lost as well. Figure 3.3 shows the flow diagram of how the operation of HDMs is carried out in a series configuration.
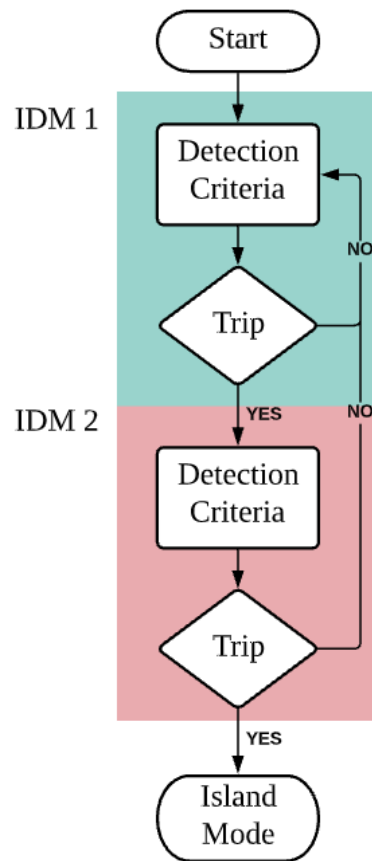
Fig. 3.3: Series configuration of HDM

Alternatively, a parallel architecture can also be implemented by having two different *island detection methods*s operating at the same time, and only tripping when both agree on the presence of an island condition. However, parallel configurations comprise both detection layers running concurrently and generating a tripping signal only if both agree on a disconnection event can compromise even further the reliability of the HDM. In addition, this configuration combines the weaknesses of the selected methods [56, 57]. Indeed, the detection systems are improved by combining different island detection strategies. However, some of the advantages can be lost as well, e.g., ADMs not requiring a communications layer might be combined with communication-based methods. Figure 3.4 shows the flow diagram of a parallel HDM.

For example, the work presented in [56] proposes combining a PDM and an ADM in a series configuration. The ADM was placed at the second layer to minimize its polluting actions and avoid false tripping. The PDM strategy monitors the ROCOV and the rate of change of the voltage harmonic content at the PCC. A voltage index is then calculated as the negative and positive sequences ratio of the delivered voltage. Subsequently, by comparing the obtained

voltage index to a previews voltage index value, a percentile delta can be computed, this percentile delta between the two values is exactly correspondent to the difference in one cycle of the fundamental frequency. The total harmonic distortion index is then calculated by obtaining the percentile difference of the harmonic content in one fundamental frequency cycle. Then percentile differences can be compared to a specific threshold, however, the authors do not provide further information on how the threshold values are obtained. Overall, the proposed method is capable of detecting the island event in 138 ms with minimum disadvantages such as the injection of polluting by the ADM.
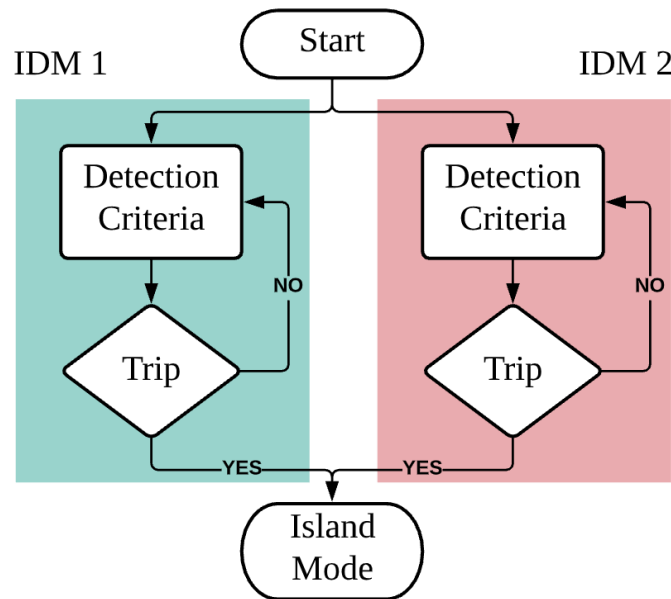
Fig. 3.4: The parallel configuration of HDM

Pouryekta *et al.* [52] present an RDM paired with a PDM in a series configuration. Their objective was to minimize the NDZ and provide fast detection with added reliability. The chosen RDM was based on the detection of injected signals through the power-line, while the PDM is based on a ROCOV method. The ROCOV the voltage index to obtained based on the rate of changes of the voltage phase angle during the defined time window, the analyzed HDM successfully identifies the disconnection event in 200 ms. Nonetheless, the method relies heavily upon a communication infrastructure due to the presence of an RDM, meaning that a fully decentralized system can not be achieved by relying on this detection method.

As an example, Ganivada et al.[138] propose an HDM formed by an ADM and an RDM based on provoked frequency disturbances by modifying the d-axis current reference. The proposed *island detection method* is tested for a photovoltaic system feeding a three-phase RLC load.

The proposed ADM adopts a communication infrastructure to imitate the injection of hindering electrical disturbances, this is achieved by having two frequency disturbance recorders at the interfaced power electronics device terminal and the nearby substation, whenever frequency slips are detected a communication signal is received at the DGU side, activating the ADM. Overall, this HDM is able to identify the islanding event in 170 ms.

Finally, Bakhshi-Jafarabadi & Popov [139] introduced an HDM based on the series combination of a PDM and an ADM. The PDM is based on a ROCOV technique that monitors the voltage at the PCC. If a defined threshold is surpassed, the ADM verifies by distorting the reference current d-axis. Then, the active power is analyzed for any variation that would indicate an island operation. Overall the method is effective in detecting the island condition within 300 ms in large power mismatch scenarios, however, in cases of small and active power mismatch, the analyzed method can underperform and extend or neglect the presence of island conditions.

Despite the advantages that come with hybrid detection methods, it is important to notice the future operational challenges of their implementation of these techniques in fully *distributed* microgrids, all hybrid methods include at least one island detection layer which operation if bound to critical data that can only be obtained through an established communication network. Therefore, its implementation in future systems will be unfeasible, requiring methods that operate only in a "local´´ fashion such as ADM. Nonetheless, the pollution nature of these strategies can also have a negative effect as previously discussed. In any case, there is a need for "locally´´ driven island detection methods that do not compromise the quality of the delivered energy.

Indeed, by combining various island detection strategies the disadvantages and hinder effects can be minimized. However, some of the advantages can be lost as well, especially the non-communication dependency of ADMs by binding their performance to communication-based methods. The independent nature of ADM makes it ideal in the decentralization goal of the DGUs, creating more reliable and intelligent generation agents by eliminating one more task that depends on an established communication network.

3.10   Test systems for island detection

Although many island detection algorithms have been introduced over the years, they were evaluated under different configurations and test-beds, hindering a direct comparison and the evaluation of new techniques. In order to effectively locate this work's proposal, the relevant literature was reviewed, from which three test-beds stand out:

1. Standard microgrid model. Usually, the IEEE 34-bus model is adopted.

2. Microgrid equivalent model. The structure shown in Figure 4.8 is used to emulate a simplified microgrid, using a three-phase parallel RLC load. Such a structure is recommended in the IEEE Std. 929 and IEEE Std. 1547 [140, 141] to test islanding detection algorithms.

3. Proprietary system. A specific model that fits some desired microgrid specifications.

It would result obvious that results coming from different test-beds can not be compared directly. Since the first category treats directly with an established microgrid model, it would appear to be logical that all tests should be conducted using the established systems. However, the lack of availability of the IEEE 34-bus model can be a huge limiter towards the homogenization of the islanding tests. Alternatively, the use of a proprietary system is even more limiting in availability for the purpose of validating current proposals under the same system.

For that matter, the literature has adopted the microgrid model equivalent represented by a three-phase RLC parallel load. As this last test-bed (three-phase RLC load) is being used to validate current proposals, it offers the easiest implementation and is readily replicable, therefore, it is the one considered in this work. Table 3.1 enlists other reported proposals divided into the mentioned categories.

It is important to notice that it was reported a detection time of 2.56 ms in Table 3.1; however, it was confirmed by simulated tests only [142]. Although that work also included an experimental section, it failed to demonstrate the same level of effectiveness and did not report any experimental detection time. Additionally, the proposed PDM was intended for intentional disconnection events.

Table 3.1: State of the art review of islanding detection systems.

Test system	Type of detection method	Island detection strategy	Detection time	Simulation validation	Experimental validation	Reference
IEEE 34 Bus model	PDM	Voltage unbalance and Current THD	129 ms	yes	no	[143]
	PDM	PMU monitoring	N/A	yes	no	[144]
3 phase RLC load	PDM	Active ROCOF	100 ˜ 200 ms	yes	no	[129]
	HDM	ROCOV, Voltage THD, and reactive power mismatch	138 ms	yes	yes	[56]
	ADM	Frequency drifts	140 ms	yes	yes	[145]
	PDM	Voltage and frequency drifts	2.56 ms	yes	no	[142]
Proprietary system	HDM	Voltage Threshold and MPPT disturbance	300 ms	yes	yes	[146]
	PDM	ROCOV	200 ˜ 300 ms	yes	no	[131]
	HDM	Power line signal and Voltage phase	200 ms	yes	yes	[52]
	HDM	ROCOV and d-axis current disturbance	300 ms	yes	no	[139]

Chapter 4

Proposed Solution & Methodology

4.1 LC filter optimization proposal

4.1.1 Bounded LC filter tuning procedure

Given the possible methods to obtain the LC filter values and the need for the system characteristics in the LC filter design, another approach is suggested where the system characteristics are not essential to obtain the values of the LC filter. Moreover, this new approach focuses on a desired design response of the VSI voltage output during and after a transition event. The system is tested through an extended number of LC filter parameters where the attenuation of the harmonics can be evaluated. The tests are exhorted to search for such a correlation of values that meet the *IEEE STD 519-1992* on harmonic limits for a THD average below 5% and maintain a voltage within the $\pm$ 5%. All the performed tests evaluate the attenuation performance by computing the THD during and after the transition event occurs through equation (4.1).

$$THD = \frac{\sqrt{\sum_{n=2}^{\infty} V_{n\_rms}^2}}{V_{fund\_rms}} \tag{4.1}$$

Where V_{nrms} is the measured $n = 8$ harmonic voltage component and $V_{fundrms}$ is the measured fundamental frequency RMS voltage. The bounded region is dictated by the constraints in (4.2) and (4.3) highlighting the filter parameters that meet the desired constraints to form a bounded region of values as shown in figure 4.1.

$$0\% \leq THD \leq 5\% \tag{4.2}$$

$$0.95 \times V_{RMS} \leq V_{out} \leq 1.05 \times V_{RMS}\% \tag{4.3}$$
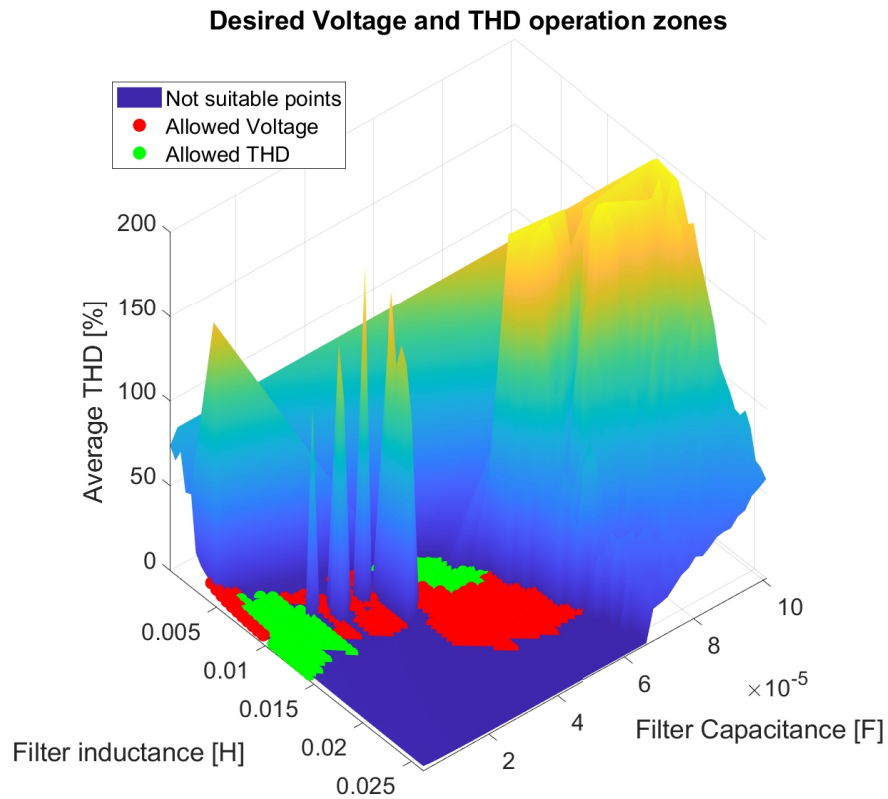
Fig. 4.1: Correlation of filter parameters and the THD output by the VSI after disconnection

figure 4.1 shows two sets of colored points, the points colored in green represent the combination of inductance and capacitance required by the LC output filer to meet the *IEEE Std 519-1992* on harmonic distortion, while the points highlighted in red represent the filter parameters that guarantee a voltage delivery level within the allowed $\pm$ 5%V. The *Z*-axis shows the THD average measurement at the PCC after the transition event occurs with the tested combination value for the LC filter. An optimization process using Genetic Algorithms is later implemented over the bounded region formed by the set of points that satisfy the system constraints on harmonic distortion and maximum voltage deviation of $\pm$ 5%, this optimization region is shown in figure 4.2. All simulations are carried out using *MATLAB Simulink* and the simulation parameters are listed in Table 4.1.
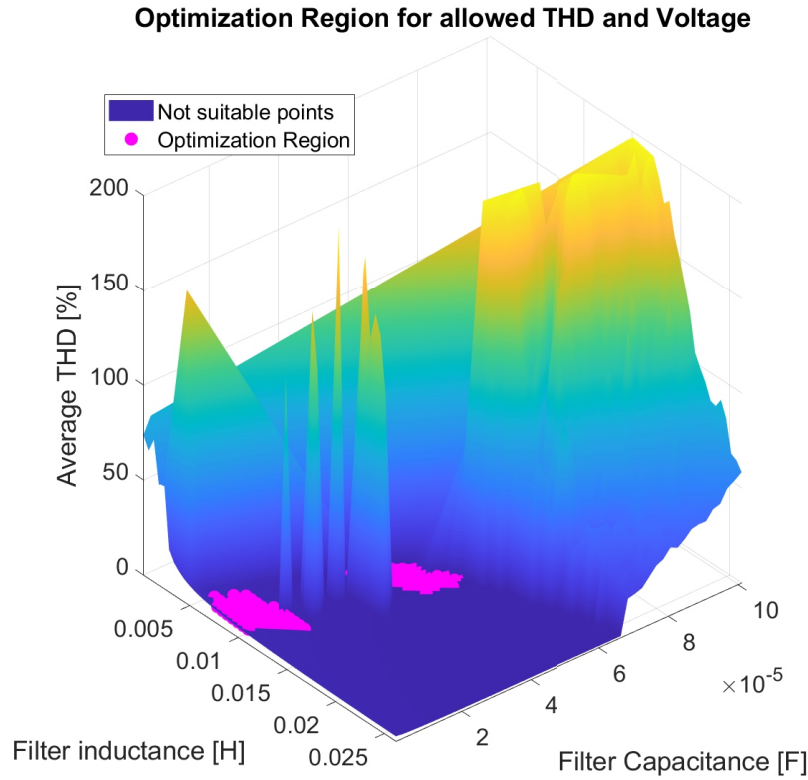
Fig. 4.2: Optimization Region for LC filter parameters after disconnection

Table 4.1: Simulation parameters

Parameter	Value
Sample time	$20\mu s$
Solver	ode4 runge kutta
Matlab Version	2020a
Clock rate	2.8 GHz

4.2 Microgrid Transition Case Study for LC filter analysis

4.2.1 LC filter optimization test-bed

To test the impact of the transition from a connected to autonomous operation in the LC output filter of a VSI fed microgrid, this work makes use of the *IEEE 13 node test feeder*. This particular system consists of 10 lines connecting 13 buses, with a radial distribution network

configuration, the system includes a generation unit, and different linear and nonlinear load configurations consisting of Δ and **Y** types in constant PQ, impedance, and current behavior; within the system, the loads have voltage and power unbalances and one transformer in a **Y** -**Y** configuration is included.

For practical purposes, the nominal RMS voltage is defined as balanced across the three-phase system for the different loads in the *IEEE 13 node test feeder* model, a breaker is added in the 650 node acting as the PCC between the utility grid and the microgrid, a VSI is added in the 650 node to feed the loads after the grid disconnection. The overall system specifications are brought down by a factor of 0.1 to feed the system with a single DGU with a $10KW$ rating without major voltage sags. According [147], an output voltage of $240V$ has been used for small photo-voltaic-based generation microgrids, hence, the nominal voltage is then scaled to $240V\,RMS$ with an operating frequency of $60Hz$. Figure 4.3 illustrates the system configuration used in this work.
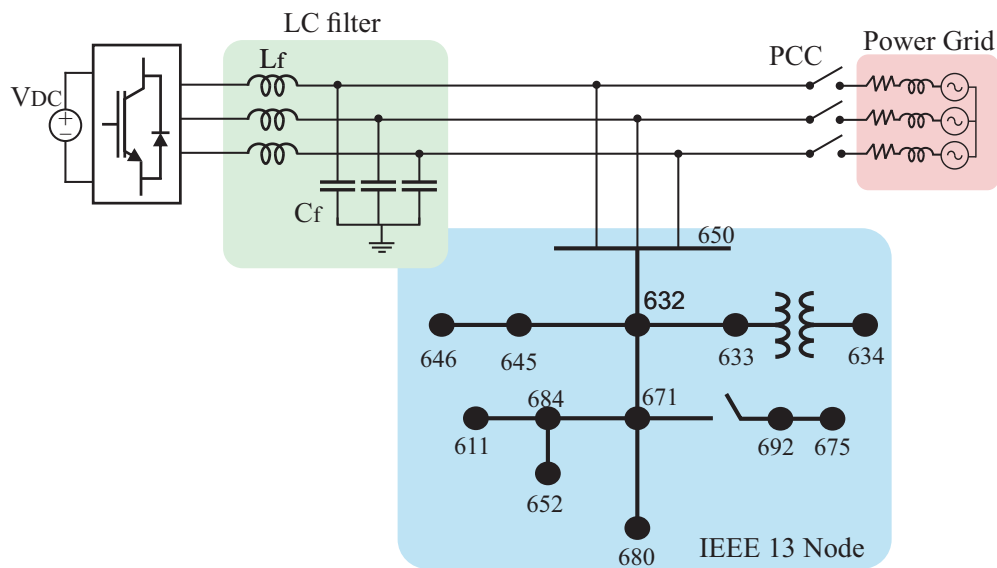
Fig. 4.3: Modified IEEE 13 node test feeder

The power grid is simulated by a constant three-phase generator in the **Y** grounded configuration, the simulated power grid feeds the system with a balanced three-phase line to line voltages in a swing generation type. The integration of VSI in a microgrid is a widely studied subject as reviewed in the literature, according to [80], three different control schemes for a VSI can be implemented in the microgrid system. Grid-supporting mode allows a VSI to operate in both modes of operation, acting as a grid-feeding unit in a connected state and switching to a grid-forming unit in autonomous operation of the microgrid.

The implemented VSI is set to operate under a grid-supporting control scheme. The grid-support control architecture includes three different control layers with different control objectives, all control layers in the grid-supporting architecture use local voltage, current, and power system measurements to compute the control signal output. However, the three control strategies are gain-dependent, where Proportional Integral (PI) controllers can be found in the external voltage and internal current control loops. Since the correct tuning of the gains is not the objective of this work, the different gains for the PI controllers are tuned by the trial and error method. The VSI is fed by a constant DC source, later, SVPWM is used and controlled to give the switching signals to the VSI in order to meet the desired voltage reference. The attenuation of the high order harmonics resulting from the switching signals is performed by the LC output filter implementation.

As a case study, the LC filter parameters are tested in the proposed microgrid system described in Section 4.2.1. Consisting of a modified version of the *IEEE 13 node test feeder* to test the disconnection effect over the VSI's LC filter performance. The microgrid's LC filter values were obtained through two different approaches. The first approach sorts to a design procedure proposed in [113], this design methodology is selected due to the fulfillment of the *IEEE Std 519-1992* on harmonic distortion, the obtained LC filter can be calculated according to the set of equations (4.4) and (4.5)

$$L = \frac{R_{Lm}}{\omega_1} \sqrt{\alpha^2 - \frac{\omega_1^4}{\omega_r^4}} \tag{4.4}$$

$$C = \frac{1}{R_{Lm}} \sqrt{\frac{\omega_1^1}{\alpha \omega_r^4 - \omega_1^4}} \tag{4.5}$$

The equations used to obtain the LC filer are dependent on system variables such as maximum load, fundamental frequency, cutoff frequency, and resort to a design coefficient that depends on the switching frequency and the maximum ripple current, RLm, $f1$, fr, and α respectively. Table 4.2 shows the system parameters used for the calculation of the LC filter.

Table 4.2: System parameters for LC filter calculation

Variable	Value
Vout	240 VRMS
fs	3 KHz
f1	60 Hz

4.2.2 Optimization Problem Formulation

Calculating a set of LC filter parameters able to output the desired THD at the instant of the transition is an unfeasible mathematical task. Therefore, an optimization methodology over a series of system tests is required to guarantee the filter performance in such conditions. The second approach optimizes according to a bounded region of LC filter values shown in figure 4.2 to obtain the LC filter values that satisfy the tuning constraints using GA optimization. For a connected and autonomous operation of the microgrid, the problem constraints are as follows.

$$0\% \leq THD_m \leq 5\% \tag{4.6}$$

$$0\% \leq THD_t \leq 12\% \tag{4.7}$$

$$Lf_{min} \leq L \leq Lf_{max} \tag{4.8}$$

$$Cf_{min} \leq C \leq Cf_{max} \tag{4.9}$$

Where Lf_{min} and Lf_{max} correspond to the minimum and maximum possible value for the filter inductor, and Cf_{min} and Cf_{max} the values that restrain the possible capacitor values. THD_m is the average measured THD in the voltage output signal after the transition, THD_t is the THD measured at the instant of the transition event, this constraint is set according to the standard *IEEE Std 519-2014* which states that a maximum of 12% THD is allowed over a maximum period of 3 seconds [86].

The objective function is defined as a weighted sum of the three design parameters for the filter. The geometrical area formed by the capacitor and the inductor values in the XY plane of figure 4.2 is considered as the main design criteria since the size of the components matter in final physical system implementation and are a crucial factor to minimize the system cost [148]. The formed geometrical area can be easily defined as (4.10).

$$Area = L \times C \tag{4.10}$$

The second design parameter is the THD produced during and after the transition event. To meet the standards *IEEE Std 519-2014* and *IEEE Std 519-1992* the system's THD is evaluated using equation (4.1) up to the 8th harmonic. Since the latter is already guaranteed by the bounded region of values shown in figure 4.2 its emphasis is reduced in the optimization problem, hence, the variable TDH_t has a greater weight in the final objective function.

The third design parameter is the bandwidth of the filter. As demonstrated in Section 2.3.1, the voltage ripple attenuation due to high switching frequencies of the VSI depends on the bandwidth of the implemented LC filer, thus, one of the optimization objectives is to minimize the bandwidth by the given LC filter without compromising the overall component size

of the filter and the disturbance response of the VSI. Each bounded filter parameter is evaluated in the frequency domain by following the second-order transfer function (4.11), and finding the bandwidth (BW) at the $-3\,dB$ points.

$$G(s) = \frac{1}{LCs^2 + 1} \tag{4.11}$$

The final objective function is then formulated as the weighted sum of the three design constraints and formulated in equation (4.12).

$$F_{objective} = min(k_1 Area + k_2(0.2 \times THD_m + 0.8 \times THD_t) + k_3 BW) \tag{4.12}$$

Where k_1, k_2, and k_3 represent the weights empirically assigned and fixed to each design constraint, the value of 0.7 is assigned to the coefficient k_1 which has a greater impact in the optimization process for an overall cost reduction [148], while 0.2 and 0.1 are chosen for the k_2 and k_3 variables. The GA optimization procedure is carried out with a population vector size of 25 with a uniform mutation vector equal to 0.01. The constraint and function tolerance are declared as 1×10^{-6}. The result of the bounded GA optimization procedures and the obtained LC values through conventional design methodology calculations are listed in Table 4.3.

Table 4.3: LC filter values in different approaches

Component	Calculated	GA Optimization
L	0.0108 H	0.0131 H
C	0.158 μF	50.506 μF

To validate the optimization results for the filter during a transition event in the modified *IEEE 13 node test feeder* described in Section 4.2.1, a comparison between the calculated values is done in a disconnection scenario. All tests and simulations are performed using *MATLAB Simulink* software in discrete time-space. The simulation is fixed to a $20\mu s$ step size with ode4 (Runge-Kutta) as the selected solver for the simulation, simulation time is set to 5 seconds.

The microgrid Voltage and frequency are measured at the PCC node, with a transition event programmed at 0.12 seconds within the simulation time, the RMS line to neutral voltages are set to $240V\,RMS$ for each phase with an equal 120° phase angle between each line. The transition is event is programmed to disconnect the three phases simultaneously, hence, entering in autonomous operation. The VSI is connected to a constant DC source of $600V$, the control creates the switching signals to the IGBT-based PC using SVPWM, the switching frequency is selected for a medium power standard to a $3Khz$ value according to the *IEEE Std 519-1992*.

4.3 Island Detection Proposal

Since the evolution of microgrids is expected to result in decentralized systems with minimal communication dependencies to increment the system reliability, some management mechanisms are required to migrate to a local format capable of operating along with the distributed nature of the many agents within the microgrid system. Some systems have already been migrated to cope with this distributed nature, such as the example of power controllers that were first introduced as a part of a control system based on a communication network. However, the evolution toward decentralized systems forced the adoption of decentralized power controllers based on droop control strategies. This evolution also motivates the transition of other control and management techniques such as secondary controllers and *island detection strategies*.

As reviewed in Chapter 3, the many proposals behind the *island detection* paradigm are far perfect. The communication dependencies frustrate the evolution of these management mechanisms towards becoming decentralized and distributed. On the other hand, the disadvantages of polluting the electrical network can have a severe effect on the delivered power quality and the long-term use of these methods, which can also represent a threat for the associated consumption agents within the microgrid system. Hence, this work proposes a novel *island detection method* that can cope with the distributed nature of DGU without relying on the contamination of the electrical network, the proposed solution is only based on available local measurements, basing its operation o the estimate and rate of change individual droop characteristics. This chapter dives deeper into the development of this proposal.

In addition, this Chapter also explains in more detail the test system used to validate the proposal of this work, multiple test scenarios are taken from the reviewed literature to test the performance of the proposed algorithm, these are later explained further in this Chapter. Also, the simulation test-beds are assembled, both, digital and RT simulation test-beds are explained in detail as the simulation parameters used in both simulation environments.

4.4 Islanding detection Algorithm based on Droop Characteristics

The proposed algorithm is based on the power-frequency drooping characteristics of the generating elements the microgrid takes its power from. Drooping is a natural phenomenon associated with turbines' loading at conventional power plants, and alternative sources commonly use the *virtual synchronous generator* approach, where the drooping characteristics are imposed by design depending on the DGU rating [80]. It mainly implies that the generating source will degrade its rotating speed as it becomes electrically loaded; exhibiting a

linear, inverse relationship between the taken active power and the output frequency.

The main grid is *stiff* as it is supported by multiple, massive generators, implying that its drooping will not be noticeable because the connected loads (and DGUs) are always relatively small. Then, it is expected that in grid-connected operation, the microgrid behaves like a stiff network for which power variations do not affect the main frequency. Nonetheless, in island operation, the microgrid relies on limited DGUs comprising a "weaker" grid with clear drooping characteristics. Then, the stiffness of a microgrid is variable as it transitions between connected and islanded states, showing different droop characteristics (slopes) as illustrated in Figure 4.4. This would indicate that a change in the estimated slope can be used as a local islanding detection event, eradicating the need for a communication infrastructure or the introduction of disturbances by ADMs.

For example to preview statement, in an autonomous operation, the obtained slope corresponding to the microgrid droop characteristics would be determined by the "no-load", "full-load" points, and the active or reactive power rating. However, in a connected configuration, the resultant slope value would be seen as zero due to the connection to the infinity bus of the power grid as illustrated in figure 4.4. Presumably, a faster response time to islanding events can be assumed if each DGU is able to detect this change on its own.

As a brief description, the proposed Local Island Detection (LISD) algorithm consists of the constant monitoring of local electrical variables with the purpose of finding their linear approximation that can be linked to individual droop characteristic m_p, corresponding to the active power vs frequency droop scheme. This linear approximation is implemented with a simple linear regression algorithm that computes the individual m_p value and determines the operational state of the microgrid based on its percentile jump to any electrical disturbance. The droop diagram of an island DGU indicates that for each frequency point f_{op} corresponds a unique power delivery P_g, due to the increased grid sensibility of an island system, several frequency data points can be acquired and paired with their corresponding power delivery points in the XY droop plane.
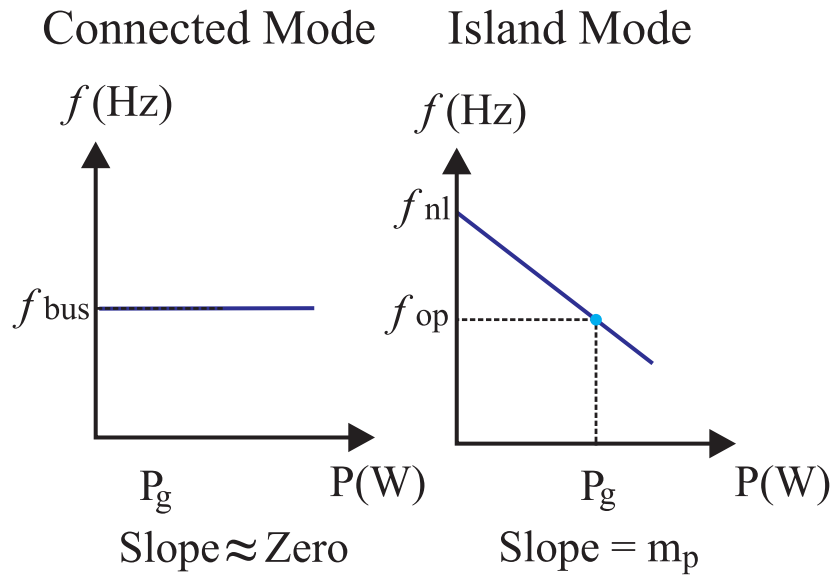
Fig. 4.4: Islanding detection through droop control characteristics

In more detail, the droop slope is noted by the variable m_p, this variable correlates the delivered active power P_g and the frequency of operation f_{op} in a linear fashion, meaning that every active power point in the x-axis, corresponds to a unique frequency point in the y-axis of the droop plane. Lastly, f_{nl} is known as the no-load point where the delivered active power is understood as zero, this point is defined as the maximum allowed frequency of the system. When the estimated slope is undefined, the frequency value is then driven by the main grid, this grid-driven frequency is noted by the variable f_{bus}. The resulting line crosses the vertical axis at f_{nl}, the no-load point, where the delivered active power is zero. This point is defined as the maximum allowed frequency of the system. If $m_p \approx 0$, the operating frequency is that of the main grid; then, $f_{op} = f_{bus} \, \forall P_g$.

The proposed LISD monitors local electrical variables to find the said linear approximation, i.e.,

$$f_{op} = m_p P_g + f_{nl}. \tag{4.13}$$

This linear approximation is implemented with a typical linear regression algorithm which determines the operational state of the microgrid based on m_p changes. In an island state, the system is prone to exhibit operating variations; out of this, the bijective relation between f_{op} and P_g can be analyzed.

The first stage of the proposed algorithm consists in constructing a defined stacked data set of the active power and frequency measurements by using delay units up to a desired delayed time value represented by the variable γ. Then, the stacked data sets are evaluated using the simple linear regression algorithm in a matrix configuration. The matrix that corresponds to

the collected data on the active power delivery points is represented by the matrix P, whereas the matrix containing the corresponding frequency points is represented by the matrix F. The matrix A contains the "no-load" and estimated slope points that better represent the linear droop equation of the DGU. Finally, the E matrix represents the error between the real and the approximated frequency values. These matrices represent the linear regression matrix equation in (4.14).

$$A = \begin{bmatrix} \hat{m}_p[k] & \hat{f}_{\text{nl}}[k] \end{bmatrix}^\top$$
$$\mathbf{F} = \begin{bmatrix} f(t) & f(t-1) & \cdots & f(t-\gamma) \end{bmatrix}^\top$$
$$\mathbf{P} = \begin{bmatrix} 1, P(t) & 1, P(t-1) & \cdots, \cdots & 1, P(t-\gamma) \end{bmatrix}^\top$$
$$E = \begin{bmatrix} (t) & e(t-1) & \cdots & e(t-\gamma) \end{bmatrix}^\top \tag{4.14}$$

In a sense, a shift-register is populated with input sampled data pairs $(f[k], P[k])$, where $k \in \mathbb{N}$ represents the kth sample of the signals, clocked at a given sample time T_s. Only $n \in \mathbb{N}$ samples are stored, then, one can build the vectors

$$\mathbf{F} = \begin{bmatrix} f[1] & f[2] & \cdots & f[n] \end{bmatrix}^\top$$
$$\mathbf{P} = \begin{bmatrix} P[1] & P[2] & \cdots & P[n] \end{bmatrix}^\top. \tag{4.15}$$

The performance of the proposed algorithm is constrained to the algorithm's *resolution* given by T_s, n, and τ. By increasing T_s the linear regression improves; however, the detection time significantly increases. On the other hand, the detecting time can be improved with low τ; nonetheless, it could also create false triggering signals. In the end, there is a trade-off between detection time and regression precision. The quadratic error threshold plays an important role in the amount of data that is further processed.

Where in matrix $\mathbf{P}$, the $P(n)$ value is the currently active power measurement while the subsequent data points are given up to the $P(n - \gamma)$ value. In the same fashion, the $\mathbf{F}$ matrix is formed following the staked limitation imposed by the variable γ. Consequently, the following step is to solve (4.16) for the matrix A which contains the desired droop characteristic value of the generator, m_p. Then, the solution for the simple linear regression is given in (4.17). Then the final form of the solution for the matrix A is then given in (4.18), depending only on the matrices formed by the collected frequency and active power data points.

$$F = PA + E \tag{4.16}$$

$$A = (\mathbf{F'}^\top \mathbf{F'})^{-1}(\mathbf{F'}^\top \mathbf{P}) \tag{4.17}$$

The expanded solution of (4.17) for line parameters is defined as:

$$\begin{bmatrix} \hat{m}_p[k] \\ \hat{f}_{nl}[k] \end{bmatrix} = (\mathbf{F'}^\top \mathbf{F'})^{-1}(\mathbf{F'}^\top \mathbf{P}) \tag{4.18}$$

where $\mathbf{F'} = \begin{bmatrix} \mathbf{F} \mid \mathbf{1} \end{bmatrix}$, i.e., a column with ones was appended to $\mathbf{F}$.

Once the solution for the matrix A is obtained, the estimated droop characteristics $\hat{m}_p[k]$ and $\hat{f}_{nl}[k]$ are used to compute an estimated running frequency point which is then compared to the real frequency of the system, this comparison results in an error that is evaluated in its quadratic form, if the quadratic error is greater than the desired tolerance represented by the variable e^*, then it enables the continuous operation of the droop characteristic estimation block. However, when the quadratic error is below the tolerance e^*, the estimated droop characteristic values are held and used for the following steps of the proposed algorithm. This enabling signal of the estimation block is crucial to avoid falling in a permanently connected state according to the LISD due to the weight a single data point would acquire, pulling the linear regression to a zero slope condition.

The line estimator includes a mechanism to discard incorrect or inessential estimates and avoid the zero slope condition. That is if no operating changes occur in the grid and $\mathbf{F}$ and $\mathbf{P}$ hold the same value n times, equation (4.18) will diverge and output non-numerical data. Programming languages are capable of detecting such issues (normally using a *not-a-number* value). Therefore, if divergence is detected, the estimated values are forced to

$$\hat{m}_p[k] := \hat{m}_p[k-1], \qquad \hat{f}_{nl}[k] := \hat{f}_{nl}[k-1]. \tag{4.19}$$

Initialization is also needed, i.e., $\hat{m}_p[1]$ and $\hat{f}_{nl}[1]$ must hold a value provided beforehand. Finally, a frequency estimate $\hat{f}[k]$ is computed using (4.13) with $\hat{m}_p[k]$ and $\hat{f}_{nl}[k]$, and the estimation error

$$e = \left(f[k] - \hat{f}[k] \right)^2 \tag{4.20}$$

is used to detect *relevant changes*, i.e., operating conditions incompatible with the estimated droop characteristic. The regression algorithm is only enabled if $e > e^*$, a threshold constant decided by the designer. The complete estimator is shown in Figure 4.5.
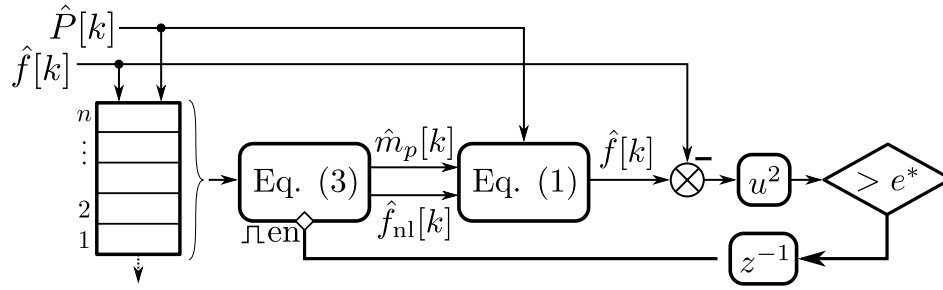
Fig. 4.5: Block diagram of the proposed linear regression algorithm.

In order to detect the islanding condition, the LISD computes the relative variation $\Delta \hat{m}_p$ between estimated slopes separated by τ samples (4.21).

$$\Delta \hat{m}_p = \left| \frac{\hat{m}_p[k] - \hat{m}_p[k - \tau]}{\hat{m}_p[k]} \right|. \tag{4.21}$$

Clearly, if $\Delta \hat{m}_p > \Delta \hat{m}_p^*$, a threshold constant set beforehand, the LISD triggers an islanding signal. It is possible for the system to vary m_p, mostly due to changes in DGUs operation. Then, $\Delta \hat{m}_p^*$ should consider an admissible interval representing island scenarios. The entire algorithm is represented in Figure 4.6.

The performance of the proposed algorithm is constrained to the algorithm's *resolution* given by T_s, n, and τ. By increasing T_s the linear regression improves; however, the detection time significantly increases. On the other hand, the detecting time can be improved with a low τ; nonetheless, it could also create false triggering signals. In the end, there is a trade-off between detection time and regression precision. Also, the quadratic error threshold plays an important role in the amount of data that is further processed. These considerations are discussed in the sequel.
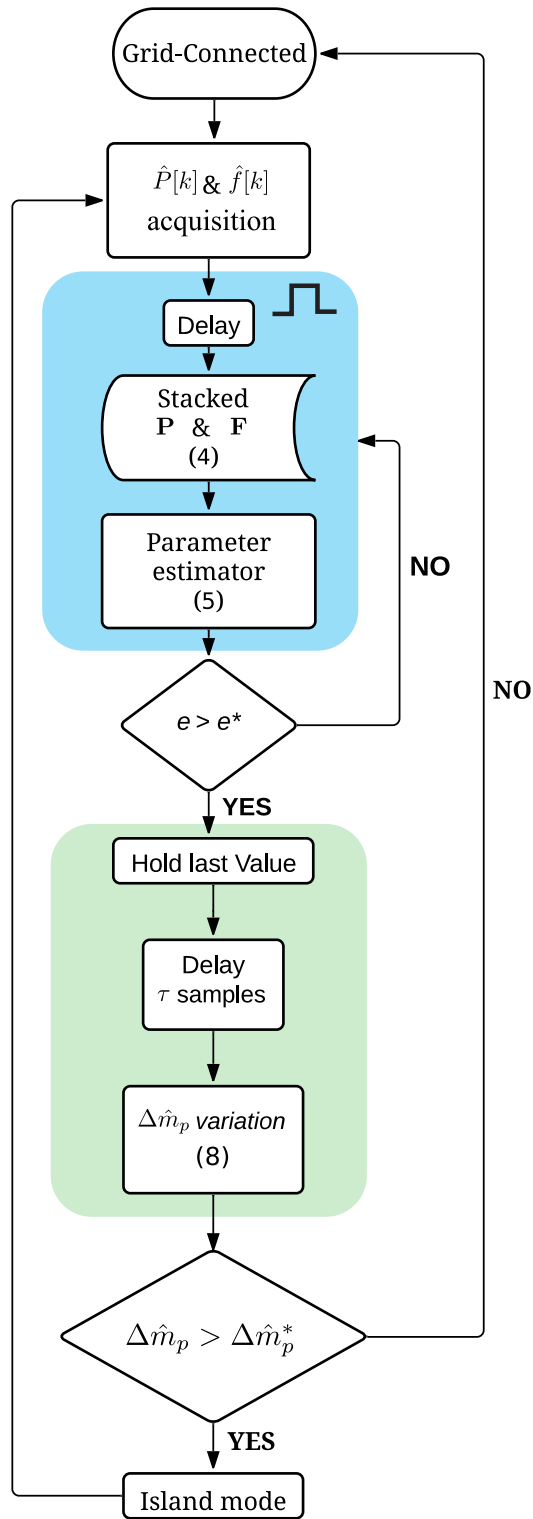
Fig. 4.6: Proposed local islanding detection algorithm flow diagram.

4.5 Constant Power approach for DGU control

Since the interfaced DGUs are expected to be operating under a grid-connected scheme prior to disconnection, a constant power approach is used to control all DGUs as done in [56]. This control strategy aims to deliver a constant amount of active and reactive power (P and Q, respectively). It comprises a cascaded control loop that computes the necessary inverter's outputs to uphold the measured power to given set-points, i.e., P^* and Q^* (see Figure 4.7). The instantaneous active and reactive powers are computed through

$$\hat{P} = \mathbf{V}_{dq}^{\top}\mathbf{I}_{dq}, \quad \hat{Q} = \mathbf{V}_{dq}^{\top}\begin{bmatrix} 0 & -1 \\ 1 & 0 \end{bmatrix}\mathbf{I}_{dq} \tag{4.22}$$

where $\mathbf{V}_{dq} = \mathbf{T}\mathbf{V}_{abc}$ and $\mathbf{I}_{dq} = \mathbf{T}\mathbf{I}_{abc}$, being $\mathbf{V}_{abc}$ and $\mathbf{I}_{abc}$ the three-phase voltages and currents sensed at the DGU's output, and $\mathbf{T}$ the Park transformation aligned to the α axis.

$$\mathbf{T} = \sqrt{\tfrac{2}{3}}\begin{bmatrix} \cos(\hat{\theta}) & \cos(\hat{\theta} - \tfrac{2\pi}{3}) & \cos(\hat{\theta} + \tfrac{2\pi}{3}) \\ -\sin(\hat{\theta}) & -\sin(\hat{\theta} - \tfrac{2\pi}{3}) & -\sin(\hat{\theta} + \tfrac{2\pi}{3}) \end{bmatrix}. \tag{4.23}$$

In addition, a three-phase *phase-locked loop* (PLL) is used to track the voltage's frequency f and phase θ at the DGU's output (a MAF-PLL was used in this work [149]). The estimated phase $\hat{\theta}$ is used as an input to (4.23), whereas the estimated frequency $\hat{f}$ and the previously computed $\hat{P}$ are fed to the proposed LISD.
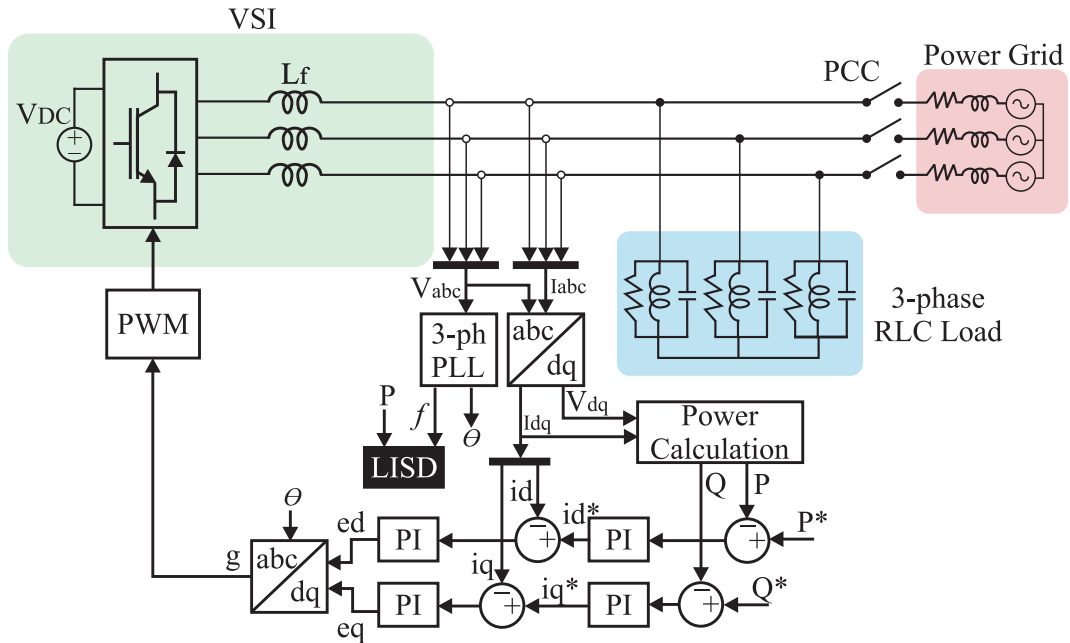

Fig. 4.7: Control block scheme for interfaced DGU and proposed LISD.

The control loop comprises a parallel PID arrangement that processes the d and q components individually, first using the *power error* to compute current set-points, i_d^* and i_q^*, and then the *current error* to output the required inverter's voltage, i.e., $\mathbf{V}_{dq}^* = \begin{bmatrix} v_d^* & v_q^* \end{bmatrix}^\top$. In this work, a 3-phase 2-level inverter was considered together with a *space-vector* PWM technique. To provide the three-phase input required by the switching technique, $\mathbf{V}_{abc}^* = T^{-1}\mathbf{V}_{dq}^*$ was computed as shown in Figure 4.7. Finally, the PID controllers were tuned by trial and error (a customary practice) with the help of the simulated test-bed. The reader is referred to [56] where the described controller is presented in depth.

4.6 The 3-phase RLC load testbed

Such a test system is illustrated in Figure 4.8, comprising one or many DGUs connected to the power grid, depending on the test scenario. The enabled DGUs feed a single three-phase parallel RLC load at Bus 1. Each enabled DGU comprises a three-phase two-level *voltage source inverter* (VSI) operating under constant-power conditions.
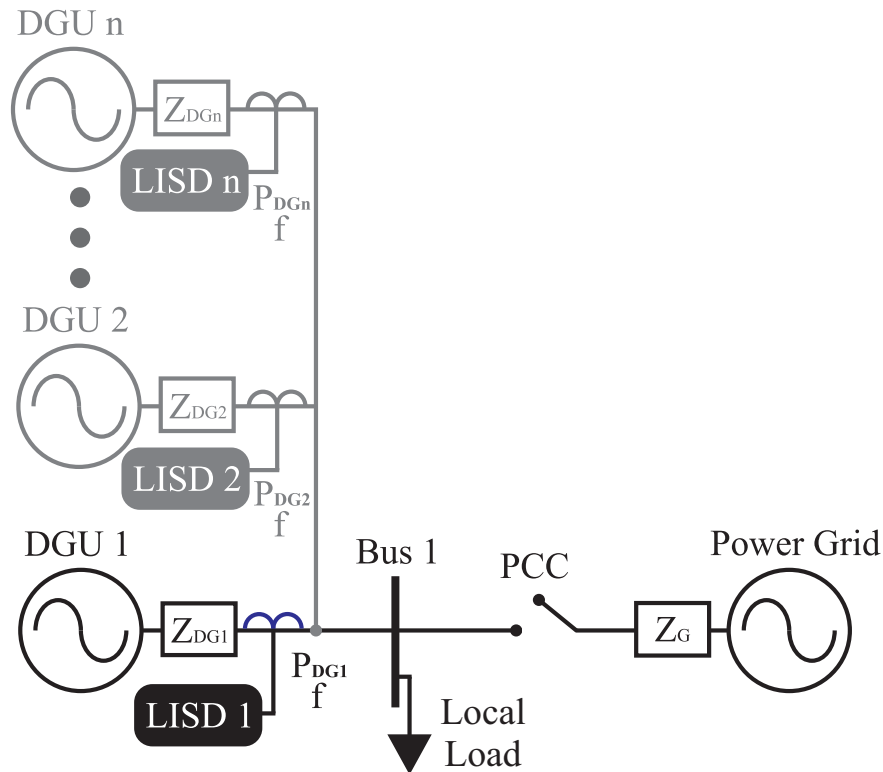

Fig. 4.8: Basic test system schematic, from a single DGU to n number of DGUs

The employed test systems are illustrated by figure 4.8, it consists of a single DGU connected to the power grid while feeding a single three-phase parallel RLC load represented

by Bus 1, the dynamic of the DGU are of a three-phase two-level inverter operating under constant power output conditions. The power control block scheme is shown in figure 4.7, where the three-phase voltages and currents are taken from the inverter output and processed to obtain the dq components through a park transformation block, a three-phase PLL block is used to squeeze the running frequency value necessary for the proposed islanding detection algorithm; for further information regarding the low-level power control, see the described control configuration in [56]. Lastly, the employed system has its unique point of connection to the grid, indicating the operational state of the microgrid. Furthermore, the LISD algorithm, which is the proposal of this work, is represented by the LISD black box in the illustration and fed with the running frequency and calculated active power.

As commented in Chapter 3, such a test system is not only used by other works in the literature but is also recommended for islanding detection tests by the IEEE Std. 929 and IEEE Std. 1547 [140, 141]. It comprises one or many DGUs connected to a single bus feeding a three-phase parallel RLC load. Each enabled DGU comprises a three-phase two-level *voltage source inverter* (VSI) operating under constant-power conditions [56].

Due to the easy implementation and high flexibility of the described test systems, some secondary tests become available to guarantee a safe performance. Other electrical agents can add disturbances coming from large load switching, nonlinear load integration, and voltage dips on the power grid side. Those disturbances are prone to cause the wrong triggering of the island detection technique, enabling the testing of false positives. Such secondary tests are described later in Section 4.7.

4.7 Validation protocol cases

The elaboration of a test protocol to homogenize the results of various proposals in equal conditions has been designed in this section. In this manner, the detection time, introduction of electric disturbances, and false island detection results can be compared equally under the same operating conditions. This test protocol can be applied in off-line and RT simulation conditions. The performance tests consist of the verification of the functionalities within scenarios that can trigger false islanding signals to corroborate the performance in simple disconnection events even in a multi inverter configuration to demonstrate that the algorithm under test is capable of withstanding common circumstances within today's microgrid implementations. The system used for validation of islanding algorithms consists of a single DGU feeding a three-phase RLC load in a grid-connected configuration, to later enter into an island state at $t = 1.4$ seconds of the simulation. This system is shown in figure 4.8.

All disconnection, load integration, and voltage dip events should be programmed to happen at the same instant for off-line simulations, in the case of an RT implantation, these events

should be treated as triggering events to correctly measure the detection time in disconnection cases. These cases are further described and noted in Table 4.4. The expected results of the validation test should fall under two possible outcomes, "triggered" and "not triggered", the former indicates that an island condition is detected by triggering the island detection signal, the latter outcome implies that the island condition has not been detected. For islanding events, the former outcome must occur while the latter should only be obtained in scenarios that test the reliability of the islanding algorithms through disruptive events.

Overall, these performance tests are required to verify the correct operation of the islanding detection algorithm, especially in scenarios that could cause false or real triggering signals. For instance, dynamic changes within a connected microgrid must not trigger an islanding event. Similarly, a disconnection must trigger it within 2 s according to the IEEE standard 1547.4-2011 [122]. Finally, to cope with current and expected microgrid operating conditions, multiple DGUs (multi-inverter configuration) must be tested together.

The reported testbeds based on an interfaced three-phase RLC load (see Table 3.1) validate their proposals differently. For example, the work reported in [129] presents load switching tests, including resistive, inductive, and capacitive load switching scenarios. Similarly, the work presented in [145] tests different quality factors on the interfaced RLC load. In contrast with these proposals, the work reported in [142] conducts a validation test addressing the dynamics of two interfaced DGUs, feeding a single three-phase RLC load; however, it did not analyze switching load conditions. Lastly, the work presented in [56] considered the dynamics of load switching scenarios, grid faults, and the interaction of multiple DGUs. Despite the differences, all reported test-beds comprise one or multiple DGUs feeding a single three-phase RLC load in a grid-connected configuration as shown in Figure 4.7.

In an attempt to aggregate the reported test conditions, the proposed test protocol consists of 5 different cases [56]:

- Case 1: Simple disconnection event with a single DGU.

- Case 2: Large load integration in grid-connected mode.

- Case 3: Non-linear load integration in grid-connected mode.

- Case 4: Voltage dip on the supply system.

- Case 5: Simple disconnection event in a multi-inverter system.

The details about each case study are analyzed next so that the detection time and false island detection results can be compared under fair conditions. As the test-bed and its parameters

are those used in [56], the obtained results would be directly comparable to that work. More-over, the results in [56] were proven superior to another typical detection approach proposed in [150], making the comparison twofold. As the used test-bed is the one recommended by the IEEE Std. 929 and IEEE Std. 1547 [140, 141], the present results could be compared in the future with new proposals.

The details about each case study are analyzed next so that the detection time and false island detection results can be compared under fair conditions. It is worth mentioning that all cases are verified in simulated and experimental tests later in this work.

4.7.1   Case 1: Simple disconnection event with a single DGU

The disconnection occurs at a specific time during the test. By opening the PCC, the single interfaced DGU assumes the task of feeding the connected RLC load. For this disconnec-tion scenario, it is expected that the tested LISD triggers an islanding signal within the 2 s according to the IEEE standard 1547.4-2011 [122]

4.7.2   Cases 2 and 3: Load integration in grid-connected mode

The incorporation of new loads, especially large and nonlinear loads, can cause small fre-quency ripples when connected to the microgrid, even in a grid-connected configuration. Those ripples may trigger a false islanding signal.

In more detail, case 2 integrates a large load equal to half of the original power demand, while case 3 integrates a three-phase rectifier feeding a load equal to half of the supplying power demand (nonlinear load integration). Both tests integrate their corresponding load at a specific instant. It is the objective of this case to evaluate if the proposed algorithm can avoid producing false tripping signals due to the caused frequency ripples.

It is important to highlight that in island detection strategies that require some comparison against a specific threshold, false tripping is possible during load variations. In the context of the proposed LISD, the frequency ripple created due to the load integration leads to variations in the estimated droop characteristic of the generator. Then, false tripping could occur if $\Delta \hat{m}_p^*$ is set incorrectly. Such threshold can be obtained by executing this test and obtaining the maximum variation of $\Delta \hat{m}_p$.

4.7.3   Case 4: Voltage dip on the supply system

Case 4 treats with the effect of any grid faults that do not cause an islanding event, a common fault is that of low-magnitude, sudden voltage dips, affecting the delivered voltage with little

to no effect on the delivered frequency. For that matter, any islanding algorithm should be capable of avoiding false tripping during voltage dips.

4.7.4   Case 5: Simple disconnection event in a multi inverter system

The presence of multiple DGUs can significantly change the dynamics of a microgrid. During islanding events, all DGUs must trip to sustain a reliable operation during and after the transition event. Due to communication dependencies, any islanding event signal can be delayed or even lost in large microgrids. As the LISD proposal is decentralized, this case tests if many interacting DGUs are capable of tripping, considering that communication does not exist among them. A four-DGU system is tested to evaluate the performance of the proposed LISD in a multi-inverter arrangement. Each inverter is equipped with its own LISD.

Table 4.4: Validation cases description

Case	Description	Expected Result
Simple disconnection	Programmed disconnection between the DGU and the power grid at instant t.	Trigger
Large load integration	A large three-phase load equal to half of the nominal load is connected at instant t.	Not trigger
Non-linear load integration	A non-linear load equal to half of the nominal load is connected at instant t. This load is integrated trough a three-phase rectifier that introduces the non-linear term.	Not trigger
Voltage dip	A voltage dip fault by the grid supply system is introduced atinstant t. The voltage dip is equal to 0.13 p.u.	Not trigger
Disconnection in a multi inverter system	Programmed disconnection between the multiple DGU system and the power grid at instant t. The multi inverter system consists in 4 DGU in a constant power supply operation, feeding a 32 KW three-phase load.	Trigger

4.8 Simulink digital simulation test-bed

To validate the proposed solution on a distributed islanding detection algorithm through the monitoring of individual droop characteristics the test system described in the previews section of this Chapter is assembled in *MATLAB Simulink* 2020a. All the described simulation cases are carried out using the *Specialized Power Systems toolbox* of *MATLAB Simulink*, using the simulation parameters listed in Table 4.5. The voltage's amplitude, frequency, and

the variations of $\Delta\hat{m}_p$ were acquired and plotted. In the simulation, $\Delta\hat{m}_p$ is not latched when the island condition is detected, allowing the visualization of $\Delta\hat{m}_p$ changes after the disconnection event and during island operation.

All simulated tests were programmed to disconnect from the main grid or modify the existing loads at $t = 1.4$ s after the system reached a steady state. It is important to mention that, the impedance values corresponding to each of the DGU are taken from [151] as the authors suggest such values to conduct validation tests in a multi-inverter configuration. All the simulation parameters are also used to validate the proposal in the RT simulation environment that is later described in this Chapter.

Table 4.5: Simulink and system simulation parameters.

Parameter	Value	Parameter	Value
Step size	50 μs	Disconnection time	1.4 s
Solver	ode1(Euler)	Rated power	8 kW
Step size LISD	1 ms	Load resistance	26.45 Ω
Simulation time	3 s	Load inductance	23.109 mH
e^*	0.01	Load capacitance	0.438 mF
$\Delta\hat{m}_p^*$	0.35	Grid Resitance	0.01 Ω
n	10	Grid inductance	0.3 mH
τ	10	ZDGU1	$0.012 + j0.0052\ \Omega$
V_{abc}	460 V_{RMS}	ZDGU2	$0.015 + j0.0053\ \Omega$
f	50 Hz	ZDGU3	$0.019 + j0.0055\ \Omega$
V_{DC}	800 V	ZDGU4	$0.019 + j0.0055\ \Omega$
L_f	3.8 mH	–	–

The first stage of the simulated test system in *MATLAB Simulink* is shown in figure 4.9. This figure illustrates the system for a single DGU islanding test. The block containing the power electrics system, the DGU's output filter, and the power control is connected to the three-phase RLC parallel load and the three-phase breaker block which acts as the programmed PCC, separating the microgrid from the main grid. In this general view of the test system, the proposed LISD block is positioned next to the block containing the VSI system, the active power and frequency outputs of the latter block are then fed into the LISD block.
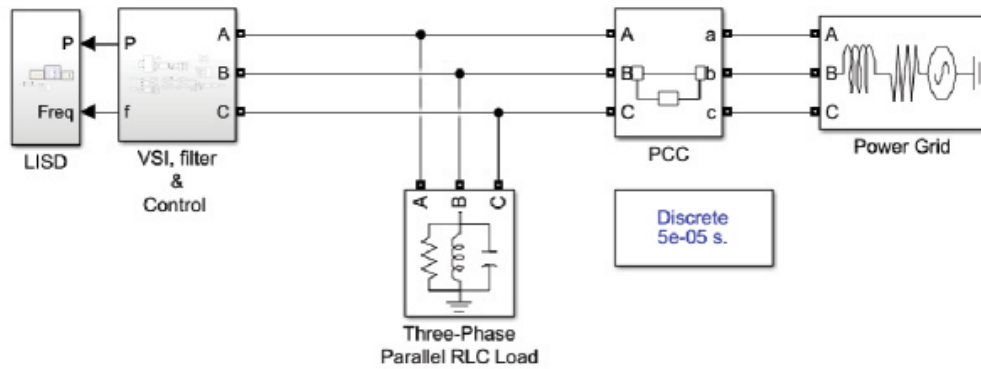
Fig. 4.9: Overview of test-system in Matlab Simulink

In more detail, the block containing the VSI system with its respective power control and output filter is shown in figure 4.10. The VSI system is assembled by using the "Universal Bridge" block configured with IGBT /diodes as the interfaced power electronic device. At the output of the inductance filter, the voltage and current measurements are acquired via the "Three-Phase V-I Measurement" block, these measurements are done from phase-to-ground and fed into three different blocks for further analysis. The "three-phase PLL", "three-phase instantaneous Power measurement", and "abc to dq0" blocks are used to obtain the frequency of the system, instantaneous active and reactive power, and the dq components of the measured current. Lastly, the power control described in Section 4.5 of this Chapter is assembled to output the gate signals for the interfaced power electronic devices.
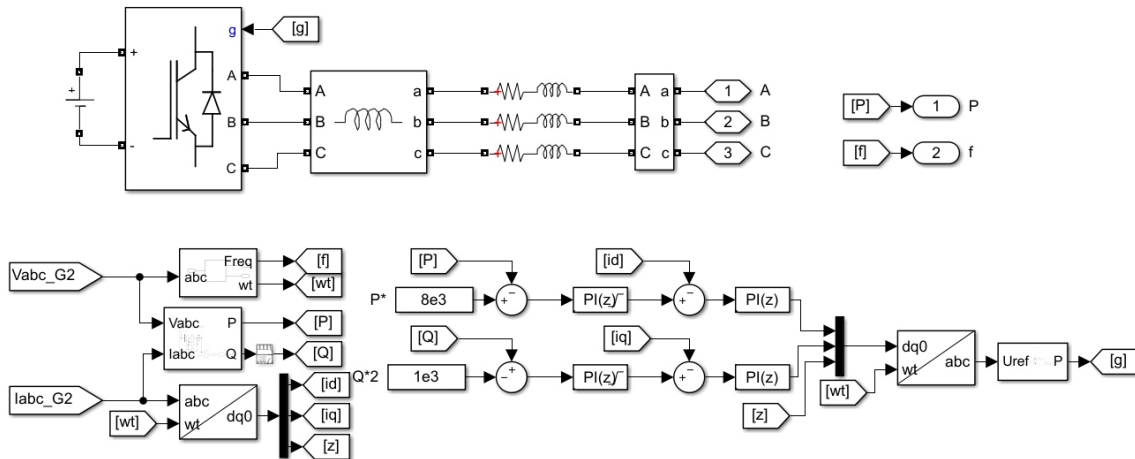

Fig. 4.10: VSI, filter, and power control block in *MATLAB Simulink*

Figure 4.11 shows an overview of the proposed LISD block. The active power and frequency inputs are interfaced with "Rate transition" blocks to change the fixed step size of the general simulation to the desired step size for the proposed algorithm. In doing this, the algorithm can output be comprehended as an "independent" system despite running in the same simulation file. Then the transformed active power and frequency are fed into the LISD proposal.
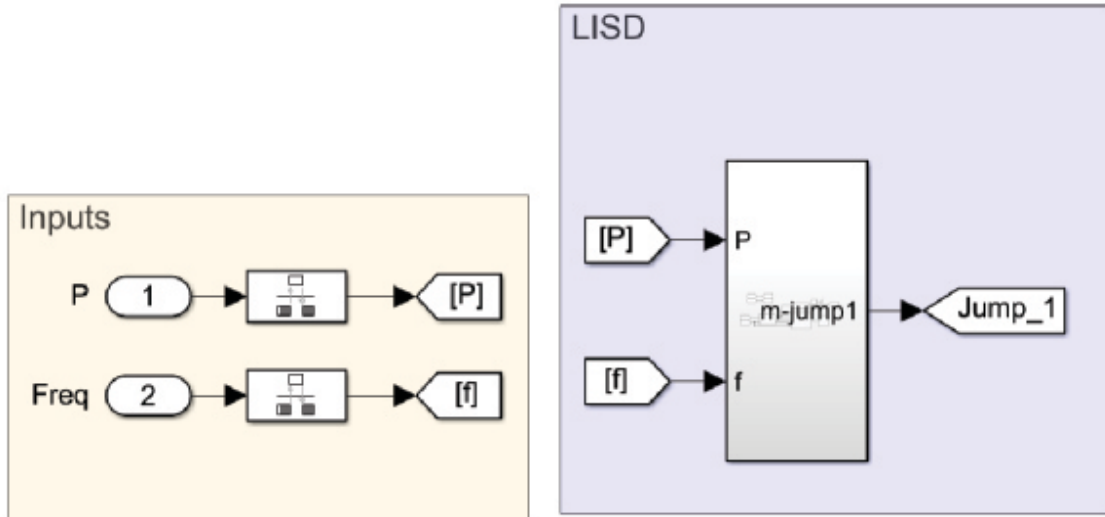
Fig. 4.11: Overview of LISD block in *MATLAB Simulink*

In more detail, figure 4.12 shows the threshold $\Delta\hat{m}_p^*$ constant value to identify the disconnection event. In this figure the line regression block and the block that calculates the $\Delta\hat{m}_p$ value are shown in a series configuration.

Fig. 4.12: The first block of LISD in *MATLAB Simulink*

The line regression block is shown in more detail in figure 4.13, the block is divided into the analysis system, which is in charge of the stack and analysis of input data, and the enabling system, which outputs an enabling signal by comparing the estimated frequency to the real frequency of the system as shown in equation 4.20.
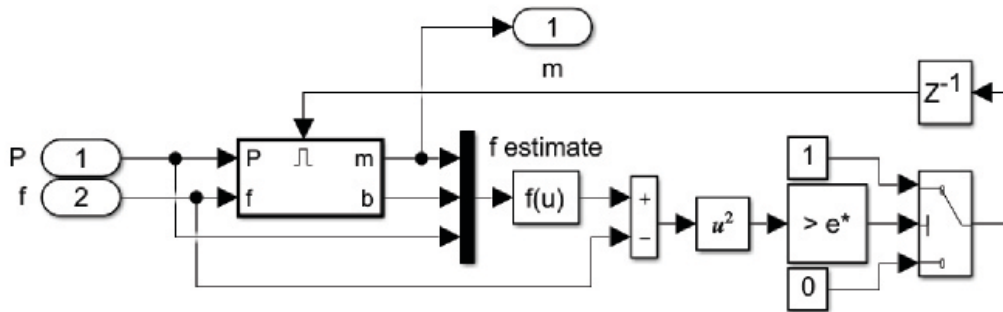

Fig. 4.13: Enabled system block of LISD in *MATLAB Simulink*

Finally, figure 4.14 shows the core stage of the proposed LISD algorithm. The stack subsystem acquires n number of samples of the active power and frequency inputs, feeding the formed vectors of data to the "*MATLAB* function" block which is in charge of carrying out the simple linear regression to obtain the droop characteristic estimate m_p. The results of the *MATLAB Simulink* simulation are shown in the following Chapter, these are compared to the results obtained by the experimental approach.
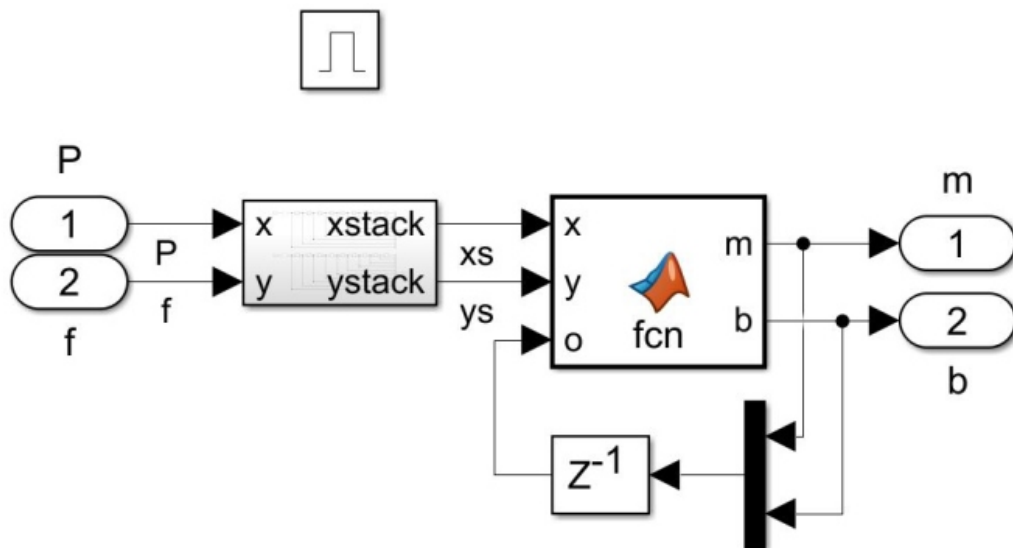

Fig. 4.14: Stacked data and line regression function in *MATLAB Simulink*

4.9   Real-Time simulation test-bed

In order to validate the dynamic consistency proposed LISD, the proposed test system in Chapter 4 is assembled a Real-Time environment. The experimental component in this work consists of a HIL RT simulation test-bed. To validate the proposed LISD, a separate RT cable platform is employed only from the test system, this is to guarantee its correct individual operation and avoid crossing dynamics if simulated in the same RT platform as the test system. This would imply that the test system is simulated in a separate RT platform, in this sense, the decoupling of the two system dynamics is assured, resulting in a certain dynamic behavior of both systems.

The two RT-capable systems are interconnected via their analog I/Os. The first RT simulator is an OP5700 from OPAL technologies [152], this simulator runs and controls the system described in Figure 4.8 but not the LISD blocks. The second RT simulator is a Boom-Box by Imperix [153], ideal for rapid control prototyping and validation of diverse power electronic applications, in this work this platform is employed to run the proposed LISD algorithms separately in an embedded format. This simulator is in charge of running the proposed LISD algorithms separately. The relevant signals are acquired with an oscilloscope.

The RT simulation system by OPAL technologies is programmed to have a user-controlled switching signal to indicate the disconnection of the PCC or the instant at which the different loads are integrated into the microgrid. This switching signal also triggers the oscilloscope where the microgrid's three-phase voltage and islanding signal are collected. The primary control of the DGU is fed in a loop-back configuration through the multiple analog I/O ports of the OP5700. The active power and frequency signals are also taken from the analog output ports and connected to an Imperix proprietary simulator interface which is the communication bridge between both RT simulation systems. Finally, the OP5700 is programmed to run at a 50μ s step time.

On the other end of the experimental validation, the Imperix Boom-Box receives the active power and frequency signals required for the operation of the proposed LISD. The algorithm runs at a step time of $1m$ s and outputs the islanding signal if such conditions are detected. The islanding signal is carried out through a single analog output port and fed to the oscilloscope for its visualization and reaction time compared to the precise triggering event instant. Figure 4.15 shows the experimental configuration and connections between RT time simulation platforms.
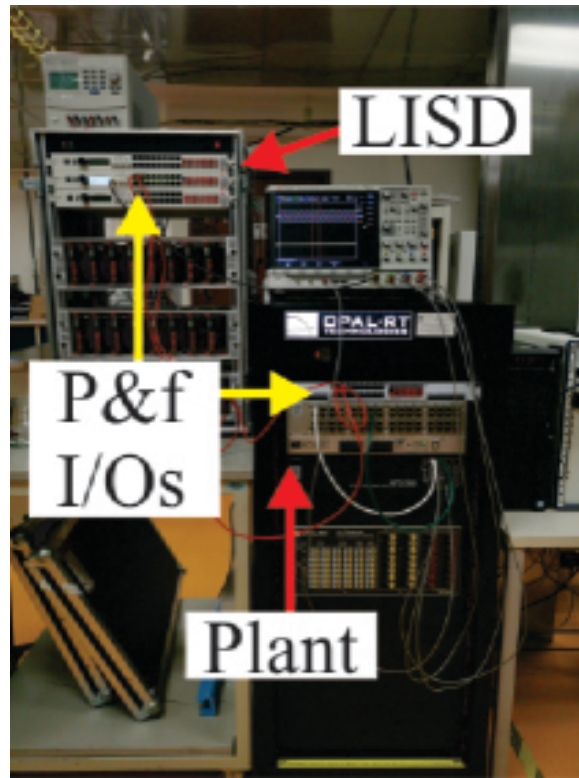
Fig. 4.15: Real-Time Experimental Test-bed

4.9.1 OPAL code

In this work, the OPAL-RT platform is designated to run the test system thanks to the proprietary software of the company. RT-LAB, being the proprietary software, is capable of running *MATLAB Simulink* models after minor modifications in the structure of the original model. Figure 4.16 shows the root layer of the proposed LISD modified to operate along with the RT-LAB environment. In this layer the *MATLAB Simulink* code is divided into two blocks, the "SM_Master" and "SM_Console" block. The former encloses the computational work of the test system, meaning that all the controllers, variable measurements, mathematical operations, and I/Os are placed inside this particular system. Meanwhile, the latter block receives them and sends back data related to monitoring or manual control actions, in sense, the "SM_Console" allows user control over certain variables in the "SM_Master" block. By allowing this, the disconnection event can be programmed to be user-controlled, this user-controlled action is also sent via a digital output channel to serve as the triggering signal of the oscilloscope.
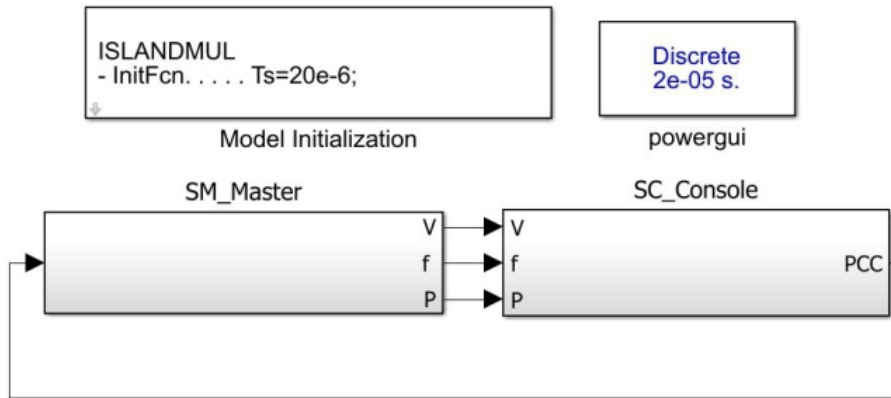
Fig. 4.16: The root of the main code in the OPAL-RT platform

One of the important components inside the "SM_Master" is the tested system. This system is showcased in figure 4.17 for a single DGU connected to the main grid through the PCC, also its multi-inverter configuration is shown in figure 4.18. This latter configuration shows how each DGU voltage and current measurements are taken at the output of their corresponding impedance. In addition, the PCC block is triggered by an external signal, this signal is generated by the user through the "SM_Console" block.
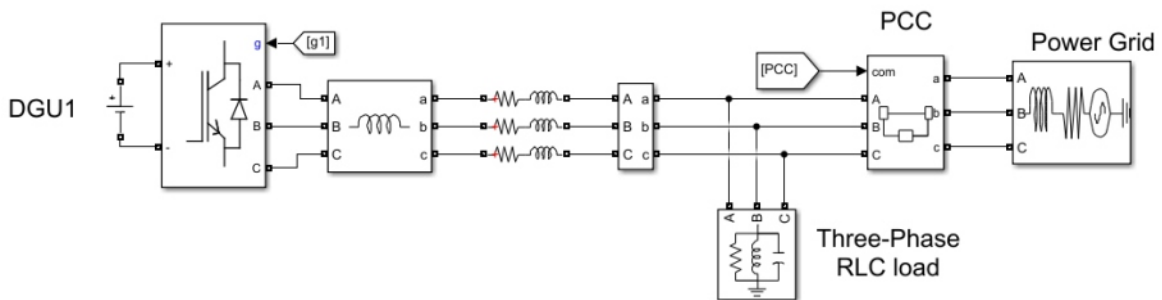

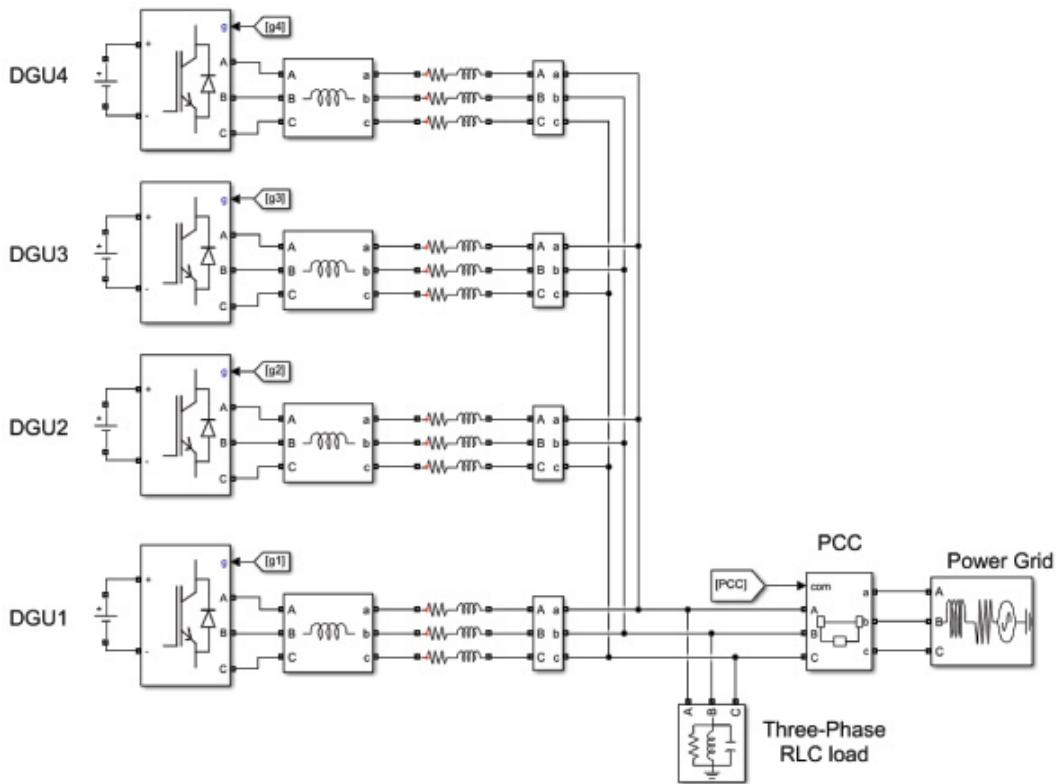Fig. 4.17: Test-system in Opal-RT for a single DGU

Fig. 4.18: Test-system in Opal-RT for multiple DGUs

Essentially the same *MATLAB Simulink* code described in section 4.8 of this chapter is implemented in the OPAL-RT platform. The only additions are in the definition of the analog and digital I/O ports to connect both simulation platforms. Figure 4.19 shows how these blocks are arranged. Clearly, the active power and frequency readings of each DGU are sent to the secondary RT simulation platform via analog output channels, these readings are scaled-down and limited through again and saturation blocks to stay within the $\pm 10\ V$ range allowed by the OPAL-RT simulator. In a similar configuration, the PCC signal is sent via the Digital output channel, this signal is used to trigger the oscilloscope for accurate reading of the action of the proposed LISD.
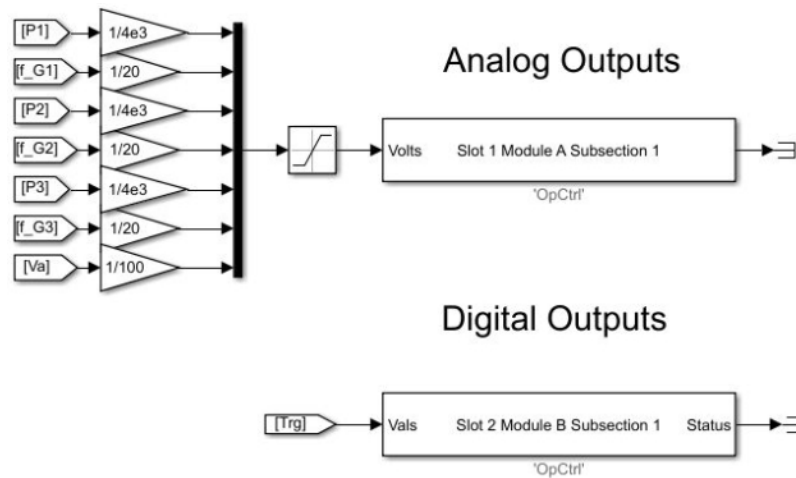
Fig. 4.19: Analog and Digital ports in OPAL-RT for multiple DGUs

4.9.2   Imperix code

Subsequently, to the first RT simulation platform, the proposed LISD is assembled in the Imperix equipment. Since the Boombox by Imperix can be programmed using *MATLAB Simulink*, the previously described LISD block in section 4.8 can be directly migrated to this simulation environment. A key element in the Imperix simulation environment is the use of the analog-digital converter blocks, which outputs are later upscaled to be reestablished and fed into the LISD block. As mentioned the LID block remains unchanged as described in section 4.8. At the output side of the LISD blocks, the island signals are interfaced with a digital to analog converter block and assigned to a specific analog output channel of the BoomBox simulator. These analog outputs are then fed into the oscilloscope for further analysis in regards to the obtained results.
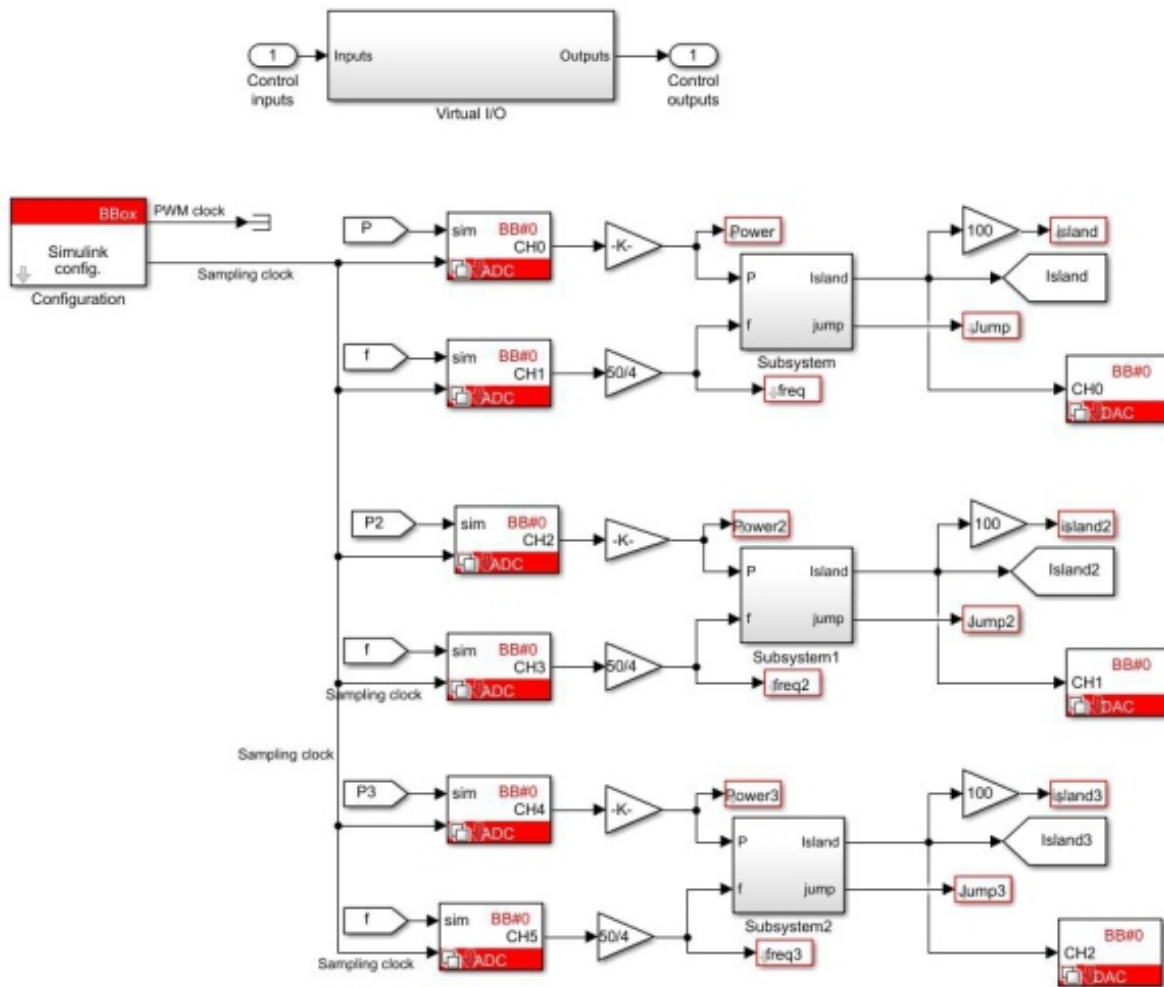
Fig. 4.20: Multiple LIDS in Imperix simulation platform

Chapter 5

Results & Discussion

5.1 Results of LC filter optimization though Genetic Algorithms

The optimization process evolved over the bounded area of values shown in figure 4.2 is shown in figure 5.1. Finding the local minimum value within the problem constraints in 31 generations of the optimization algorithm. Overall, the total employed time in the GA optimization procedure is $4.28s$, the optimization sample time is obtained as $0.002835ms$. The CPU usage is defined as CPU%=$\frac{Employed\ time}{Optimization\ sample\ time} \times 100$, resulting in 1.21%. The evolution plot of each filter component is obtained, showing the optimized values for each individual.

Fig. 5.1: GA Optimization fitness evolution

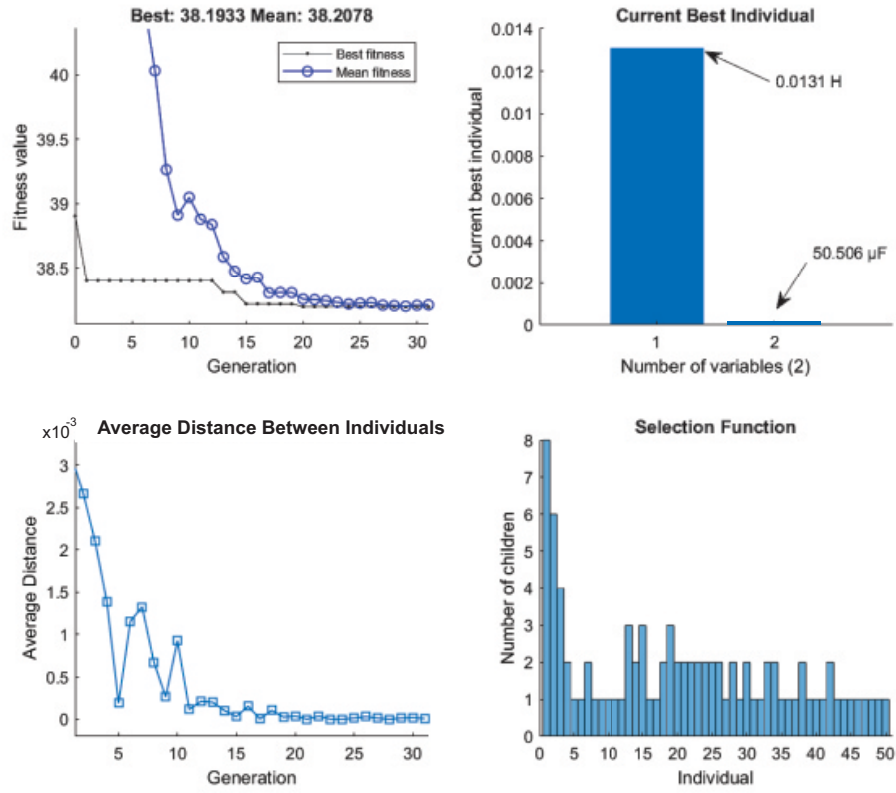The first optimization criteria design is shown in figure 5.2, where the geometric area formed by the obtained filter parameters by the GA optimization process is highlighted. The illustrated area represents the filter parameters that best attenuate the injected THD and deliver a small bandwidth without compromising the size of the filter components.

Area =6.6163e-7[L*C]
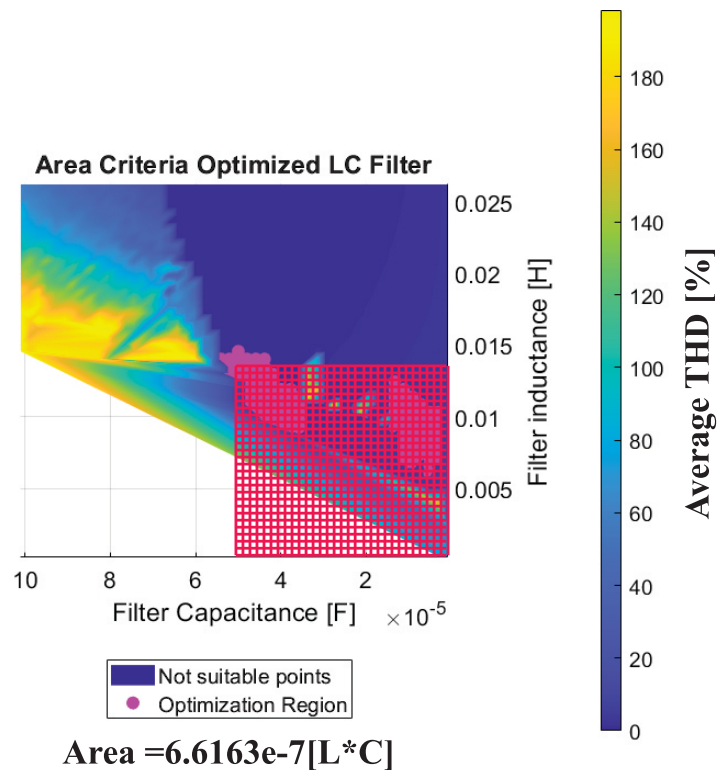
Fig. 5.2: Area criteria formed by Optimized LC filter

figure 5.3 shows the two different frequency characteristics, each representing the calculated and the optimized filters in the frequency domain. The calculated LC filter shows a bandwidth equal to $3.77x10^4 rad/s$, whereas, the LC parameters obtained through the genetic algorithm optimization process display a smaller bandwidth equal to $1.9x10^3 rad/s$. The optimization results in the minimization of the bandwidth, leading to a greater THD mitigation in the voltage output of the VSI as shown in Figures 5.5 and 5.6.
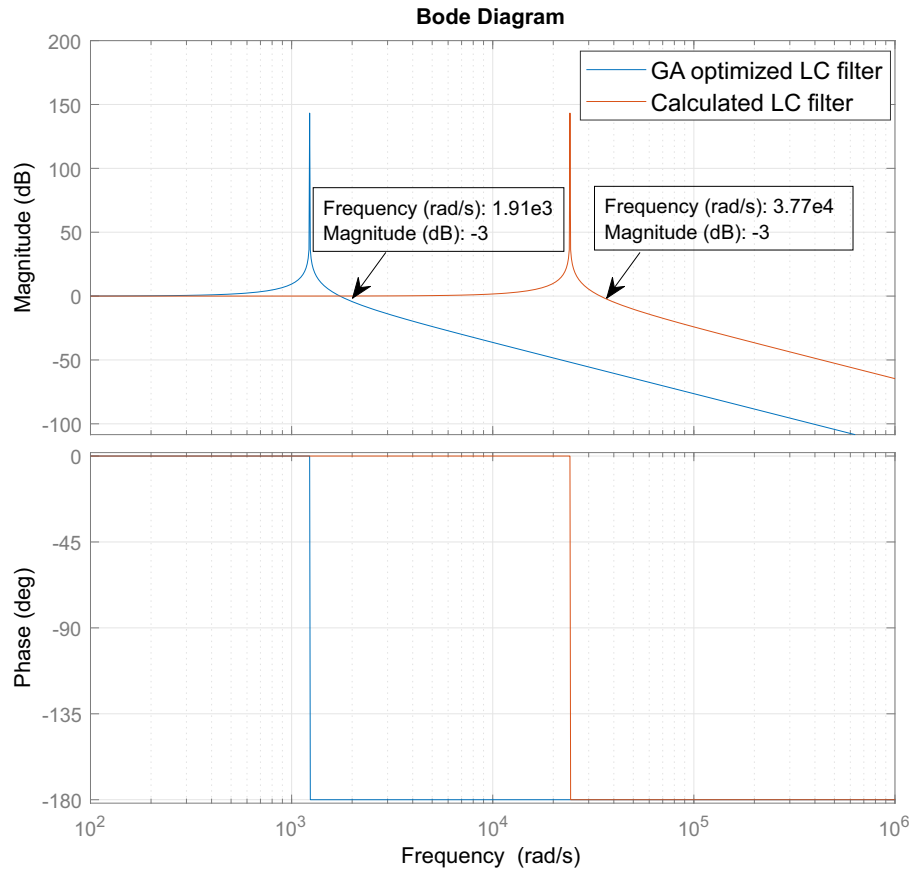
Fig. 5.3: Bode plot for LC filter parameters

As discussed a transition event can lead to high harmonic injection. Figure 5.4 illustrates the measured voltage output THD per phase of the VSI before, during, and after the transition occurs at 0.12 seconds during the simulation time. Results in figure 5.4a show the filter performance of the calculated LC filter using conventional methods, showing that the filter meets the *IEEE Std 519-2014* of a limit of 12% THD over a maximum of 3 seconds in the voltage output of the VSI. However, the conventional method fails in the fulfillment of the standards *IEEE Std 519-1992* by maintaining a THD above 5% after the transition. The case of the optimized LC filter values, illustrated in figure 5.4b, show a greater THD injection of $+1.14\%$ during the transition in the C phase of the VSI, differently, phases A and B display a better transition behavior in the maximum THD injection per phase with -4.1% and -2.03% respectively to their associated values with the calculated LC filter.
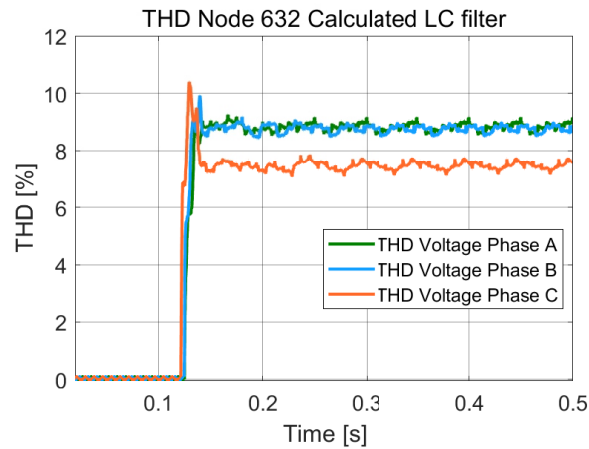
(a) Calculated LC filter by conventional method
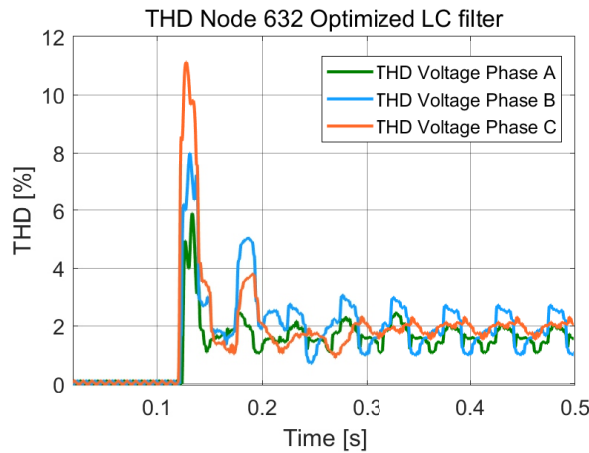
(b) GA Optimized LC filter values in a bounded region

Fig. 5.4: Measured THD in Voltage output signal per phase during simulation

Figure 5.5 shows how the calculated LC filter fails in attenuating the high switching harmonics after the transition. The voltage ripple is increased and present due to the loss of connection to the grid. The calculated filter through the switching frequency leads to an increment in the injected THD measured up to the 8th harmonic going from a $THD = 0.003\%$ to an average of $THD = 8.3\%$ between the three phases of the VSI.
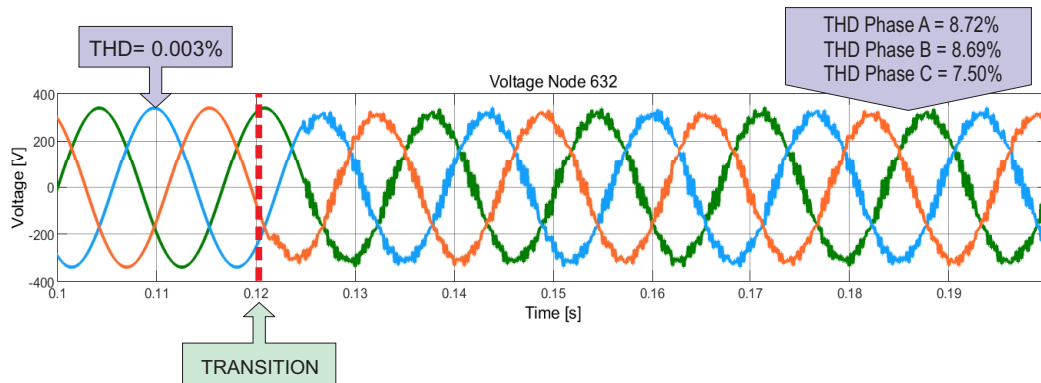
Fig. 5.5: Calculated LC filter performance after the transition

On the other hand, figure 5.6 illustrates the performance of the LC filter obtained through the bounded optimization process during a transition event, the GA optimized LC filter meets the *IEEE Std 519-1992* and *IEEE Std 519-2014* standards on the maximum allowed harmonic distortion, attenuating the high switching harmonics even after the disconnection. The average THD generated up to the 8th harmonic due to the loss of connection to the grid results in a 1.6003% increment, going from a $THD = 0.003\%$ to an average per phase of $THD = 1.6033\%$.
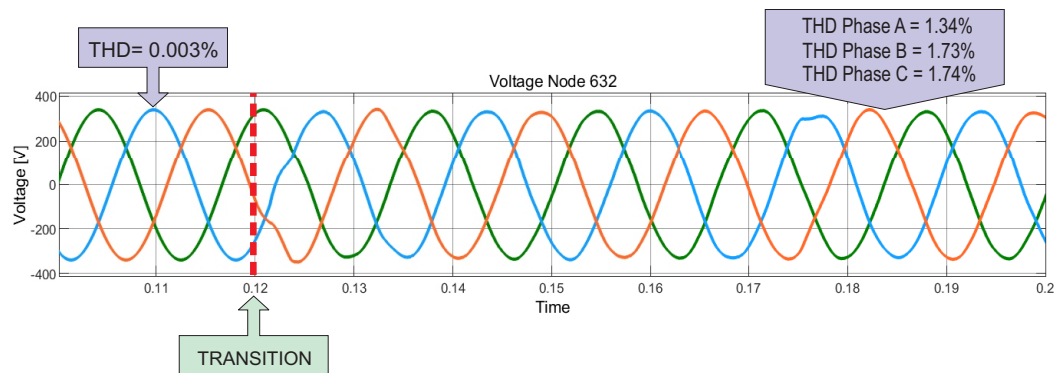
Fig. 5.6: Bounded GA Optimized LC filter performance after the transition

In Both cases, the maximum 12% THD set by the *IEEE Std 519-2014* is not exceeded. In the case of the calculated LC filter, the voltage distortion is greater when compared to the generated by the optimized LC filter, particularly the transition event leads evade the 5% THD limit. The optimized LC filter leads to a better VSI performance in transition events from a connected to autonomous operation. The transition can be improved by the right tuning of the grid-supporting controllers of the VSI. Overall, the GA-optimized LC filter has a better performance in the attenuation of harmonics in the voltage after the transition event occurs, leading to better power delivery.

5.2 Results in a Digital Simulation environment of LISD

All the described simulation cases are carried out using the *Specialized Power Systems tool-box* of *MATLAB Simulink*, using the parameters listed in Table 4.5. Notice that, as depicted in Figure 4.7, the load considered is a parallel RLC load having its resonance frequency $1/\sqrt{LC}$ matching that of the local utility operating frequency. This is assumed to be the worst-case scenario for successful detection of unintentional islanding [56]. The voltage's amplitude, frequency, and the variations of $\Delta\hat{m}_p$ were acquired and plotted. In the simulation, $\Delta\hat{m}_p$ is not latched when the island condition is detected, allowing the visualization of $\Delta\hat{m}_p$ changes after the disconnection event and during island operation. All simulated tests were programmed to disconnect from the main grid or modify the existing loads at $t = 1.4$ s after the system reached a steady state.

The $\Delta\hat{m}_p^*$ threshold was set to a constant value (35% as will be later explained) for all simulation results. As described in Section 4, it can be obtained by executing the test related to case 2. A more in-depth description is given in the results below. It is essential to notice that the proposed LISD is not constrained to operate in some load range and that the installed load value is not necessary for the LISD operation. As this algorithm evaluates the grid's stiffness, $\Delta\hat{m}_p$ would remain a valid metric in different load ranges as long as the island and grid-connected operation regimes exhibit different power-frequency slopes.

5.2.1 Case 1: Simple disconnection

The first simulation scenario consisted of a simple disconnection event. The microgrid was disconnected at 1.4 s from the main power grid, leaving all power-feeding requirements to the DGU. The performance of the LISD is shown in Figure 5.7. The disconnection event clearly affected the system's frequency and the proposed island detection algorithm was triggered at 1.414 s, i.e., with a delay of 14 ms. It can be seen that further frequency variations would have again triggered the detection algorithm. However, one can latch the first tripping signal and exert the compensation mechanisms from that point on.
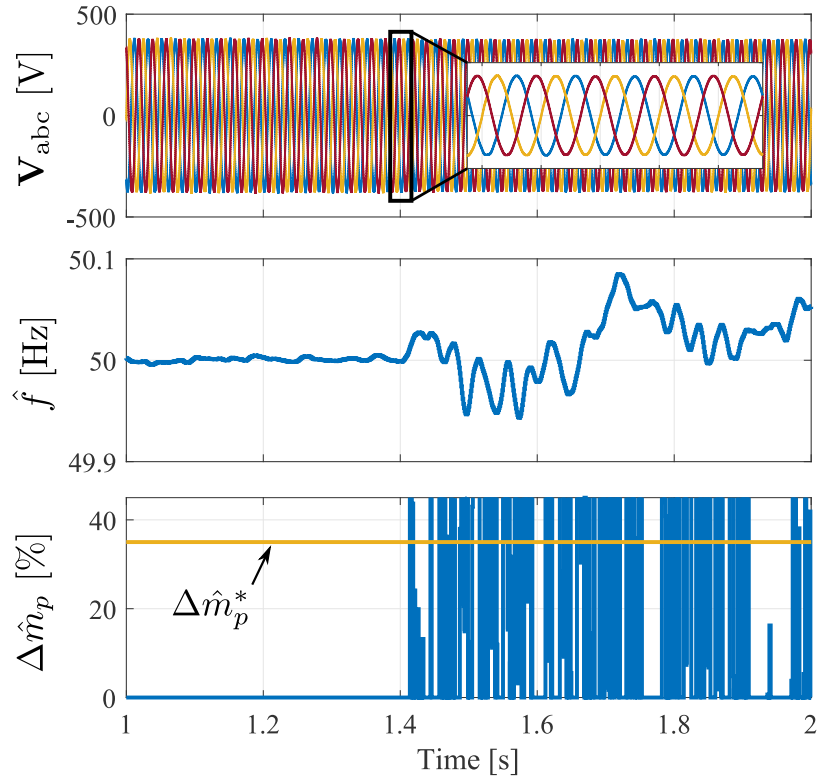
Fig. 5.7: Case 1: Island detection test to evaluate detection delay.

5.2.2 Cases 2 & 3: Load integration tripping detection

The system's load was first increased by 50% according to the parameters in Table 4.5. As shown in Figure 5.8, the $\Delta \hat{m}_p$ variations caused by the large load integration raised to 30%. Then, to avoid false tripping signals caused by load variations, the threshold value $\Delta \hat{m}_p^*$ must be above 30%. Hence, $\Delta \hat{m}_p^*$ was set to 35% as illustrated in the presented results.
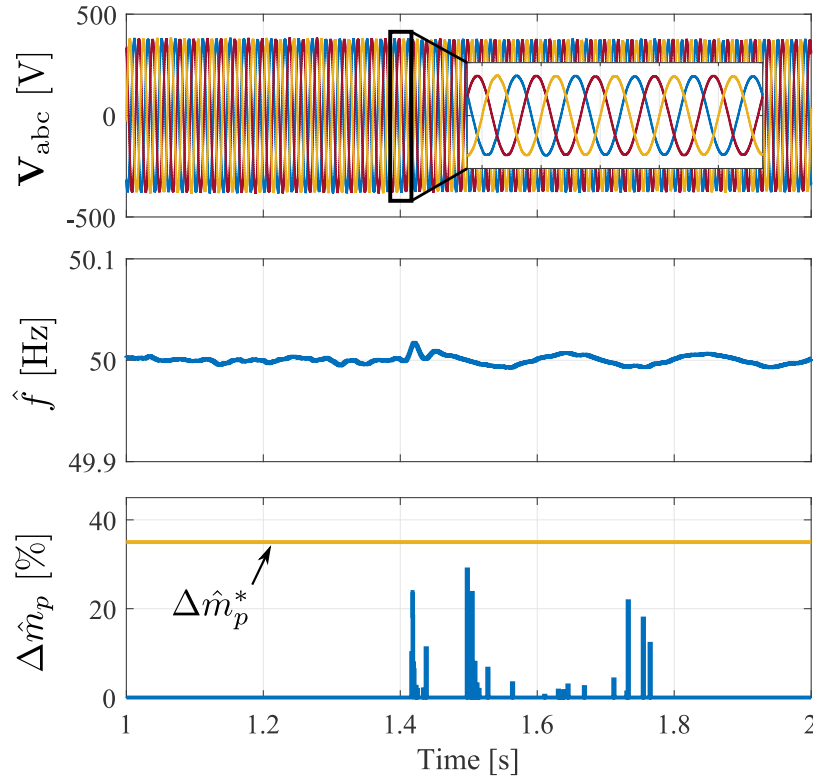
Fig. 5.8: Case 2: Large switching load test to discard false tripping.

As discussed above, it is recommended to first analyze the grid to find its usual m_p and weigh load variations to find admissible $\Delta\hat{m}_p$ values. Instead, and as done in this work, the threshold can be set after running simulations considering critical variations. It is essential to consider that $\Delta\hat{m}_p^*$ would vary depending on n, τ, T_s, and the grid parameters; as a result, it would be difficult to derive it analytically. In this case, the simulated approach was preferred.

Similarly, case 3 considered the integration of a nonlinear load, and its results are shown in Figure 5.9. The nonlinearity of the rectifier exhibited a negligible effect on the performance of the proposed algorithm. In this case, the estimated droop characteristic does not show a significant jump in the estimated slope change $\Delta\hat{m}_p$ that could trigger any false islanding signals. Thus, neither of the tested scenarios that deal with the integration of a large load or nonlinear load triggered a false positive signal during these tests.
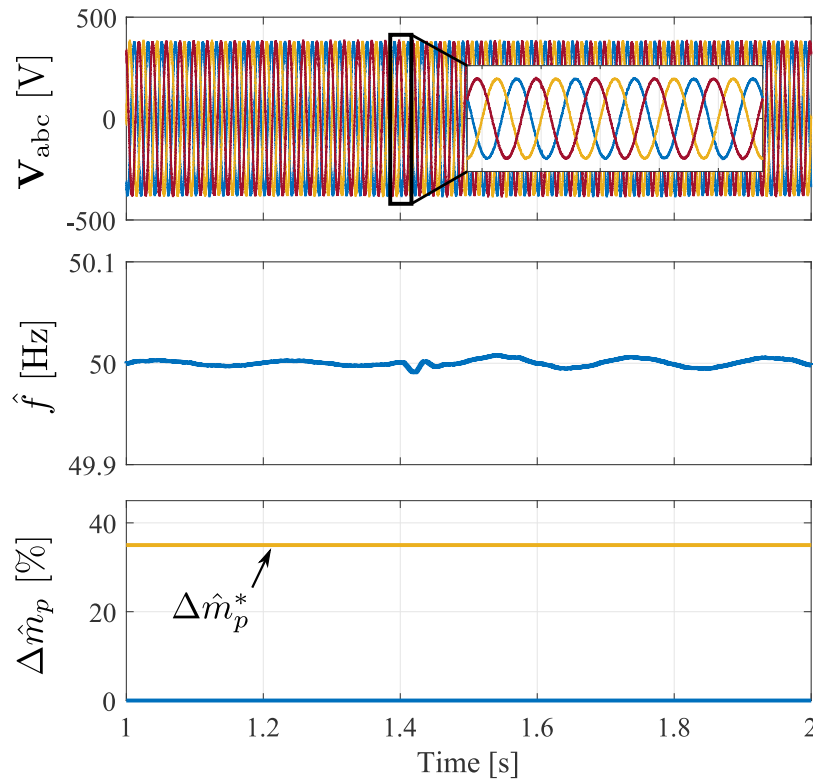
Fig. 5.9: Case 3: Nonlinear load integration test to discard false tripping.

5.2.3 Cases 4: Voltage dip tripping detection

This case treats with the effect of any grid faults that do not cause an islanding event, a common fault is that of a sudden voltage dips of a low magnitude, affecting the delivered voltage with little to no effect on the delivered frequency. For that matter, any islanding algorithm should be capable of avoiding any false tripping signal under this type of grid fault conditions. Since the proposed algorithm deals with the variations in the frequency and power delivery, it does not trigger a false islanding signal.

Figure 5.10 shows the performance of the LISD after a voltage dip of 0.13 p.u. occurred (as tested in [56]). As shown, the estimated frequency did not change drastically; therefore, there is no change in the estimated droop characteristics of the DGU. As the proposed algorithm deals with frequency and power variations and not directly with the voltage levels, the LISD did not trigger a false islanding signal, exhibiting reliability in the case of low magnitude grid faults. Recall that $\hat{m}_p[k]$ only changes if the variation is "relevant." Then, even in the presence of frequency variations, $\Delta\hat{m}_p$ would not necessarily change if e^* is not surpassed as discussed around (4.20).
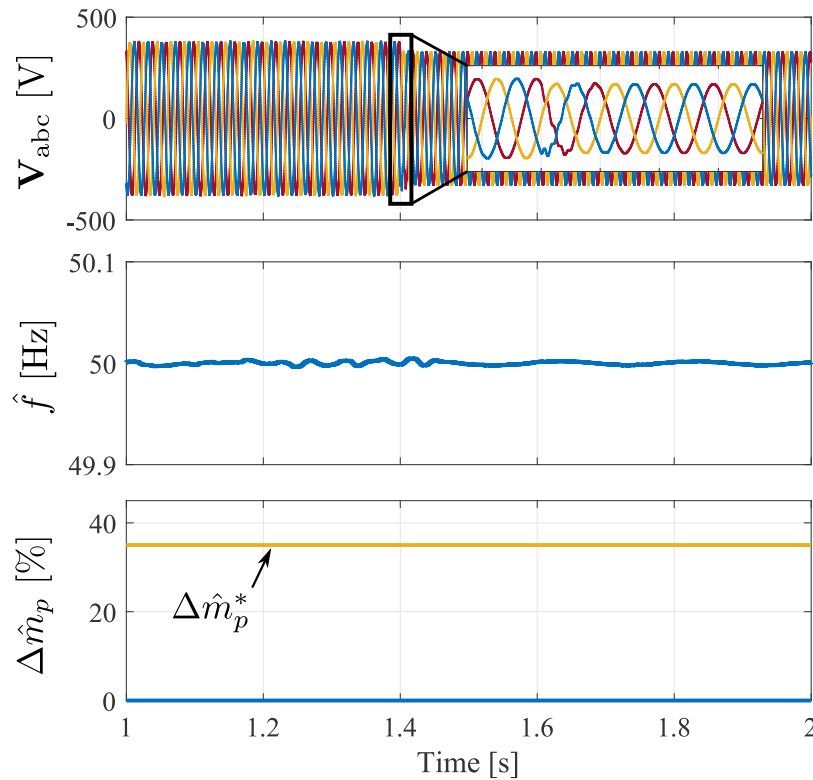
Fig. 5.10: Case 4: Voltage dip test to discard false tripping.

5.2.4   Cases 5: Island detection in multiple inverter system

Microgrid systems are conventionally governed by multiple-generation agents that contribute to the total power demand of the microgrid. The presence of multiple generation units can significantly change the dynamics of a microgrid in different conditions, one concern is set into islanding events where all DGU need to acknowledge the change in the operational mode of the microgrid in time to sustain a reliable operation during and after the transition event.

Due to communication dependencies, any islanding event signal can be delayed or even lost in large microgrids with an extant communication network, to eradicate the communication dependency and test the performance of the proposed islanding algorithm, a multiple inverter system is simulated, each inverter is equipped with their own LISD algorithm; by starting in a grid-connected configuration and transitioning into an island state at 1.4 seconds of the running simulation. The total demeaned power is set to 32 KW and remains unchanged during the simulation.

Figure 5.11 shows the result of the islanding test in the multiple inverter configuration. The proposed LISD algorithm was equipped locally at each inverter system (four in total), and each was capable of detecting the islanding event by calculating an individual m_p using

the variables locally available at the DGUs outputs. The islanding signal was triggered at 1.412 ms, exhibiting a 12 ms delay after disconnection. The performance of the LIDS was slightly faster in a multiple invert system due to the added variations by other inverter systems in the microgrid. It is important to mention that, the impedance values corresponding to each of the DGU are taken from [151] as the authors suggest such values to conduct validation tests in a multi-inverter configuration.

Fig. 5.11: Case 5: Multiple DGUs tests to check non-interference among DGUs tripping.

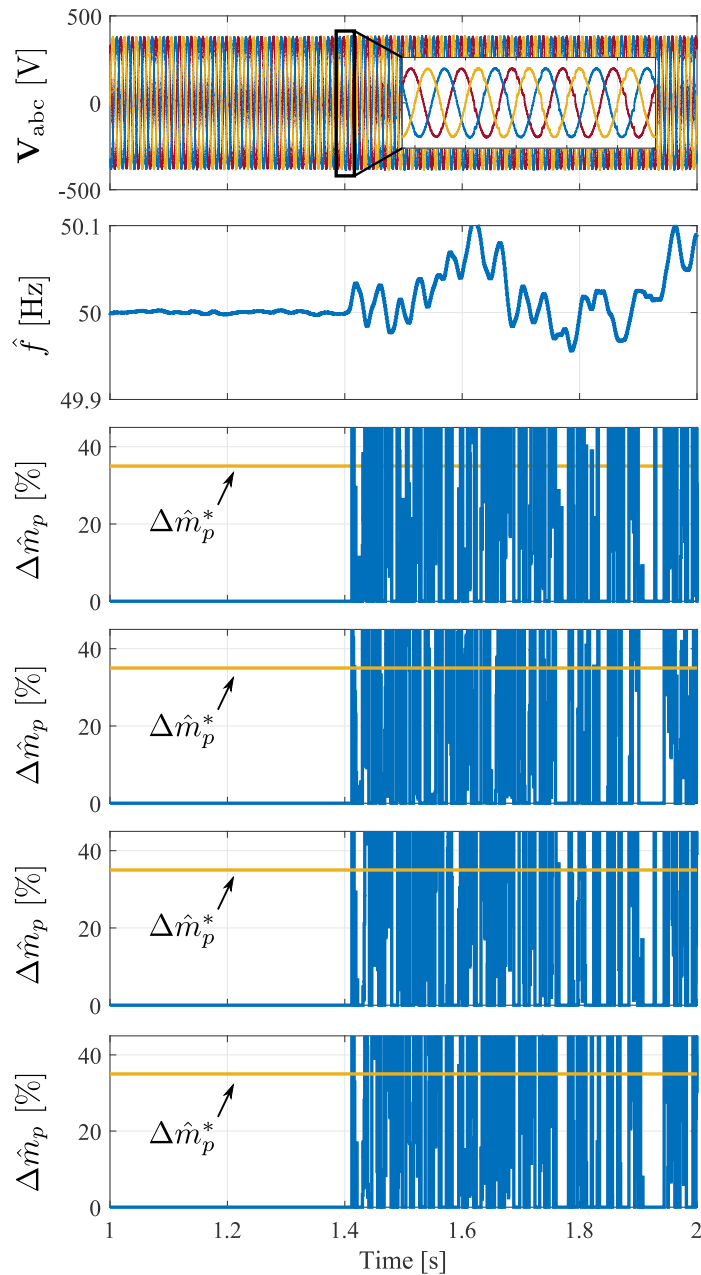Indeed the correct performance of any islanding detection algorithms is crucial in a multiple DGU system due to the different dynamics of each contributing agent, it is also important that no counteraction between DGU be provoked due to the islanding detection algorithms, as in the case of active detection methods that can introduce electrical disturbances that can have an effect on other electrical agents connected to the microgrid. Thus, the proposed algorithm achieves the local recognition of a disconnection, without relying on communication lines nor introducing other electrical disturbances into the microgrid's main bus. The LISD is a noninvasive implementation that can be attached to the DGU.

As shown from the different simulation scenarios, from case 1 through case 5, the proposed LISD algorithm is capable of acknowledging the microgrid disconnection from the electrical grid at a primary level in simulation, meaning that no communication link is required between the DGU and the MGC nor between neighboring DGU as in other active and passive methods. Also, the operation of this proposal does not introduce any electrical disturbances to the microgrid's main bus, resulting in a noninvasive implementation. Nonetheless, the threshold value defined by the large load switching event needs to be properly defined to avoid any false tripping signals in such conditions. In the following section, an experimental test-bed is assembled to validate the performance of the proposed LISD algorithm.

5.3 Results in a Real-Time simulation environment of LISD

5.3.1 Case 1: Simple disconnection

Case 1 was carried out as the first experimental validation test, consisting of a triggered disconnection. The Boom-Box RT system output the islanding signal exactly 25 ms after the disconnection event as shown in Figure 5.12. Since the triggering signal occurs at $t = 0$, a manual offset was used to align the rising islanding signal to the horizontal center of the oscilloscope, then obtaining the delay time as the horizontal offset.
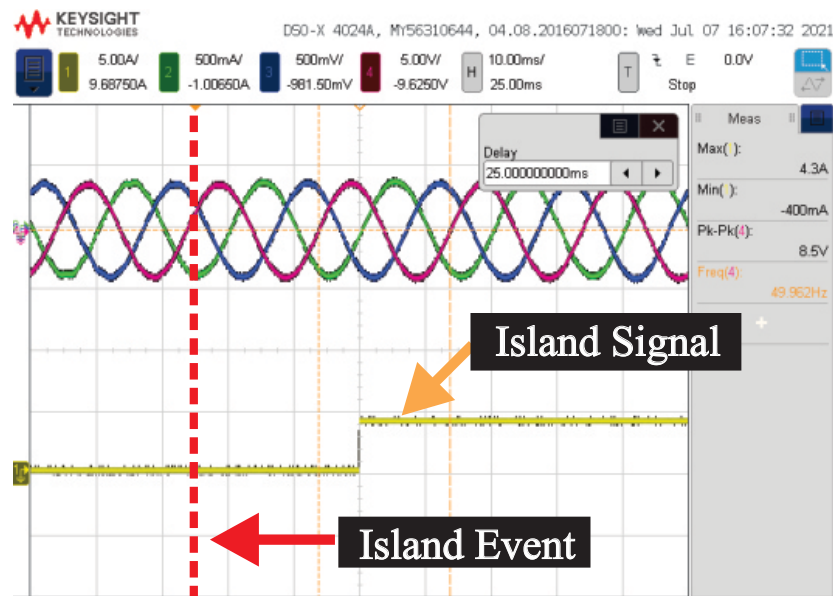
Fig. 5.12: Single load islanding experimental results

5.3.2   Case 2 & 3: Load integration tests

Subsequently, the load integration tests were performed in the same manner, again acquiring the islanding signal coming from the Boom-Box RT simulator. In both cases, the integration of an external load did not trigger a false islanding signal as shown in Figures 5.13 and 5.14 (three-phase parallel load and nonlinear load integration, respectively). This indicates that the proposed LISD algorithm can withstand large load switching events without tripping.
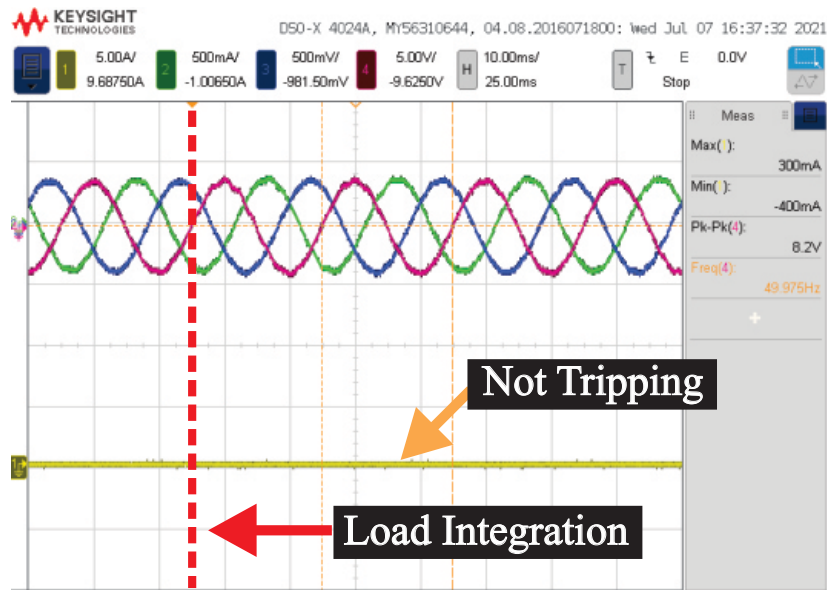
Fig. 5.13: Large load integration tripping experimental results
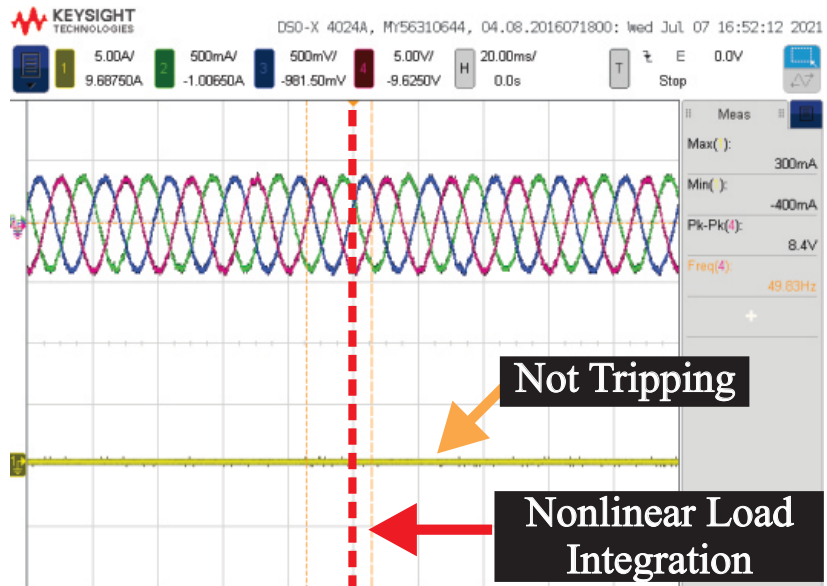
Fig. 5.14: Nonlinear load integration tripping experimental results

5.3.3   Case 5: Multiple System Island detection

Lastly, a multi-inverter system is assembled as the plant, consisting of four voltage synchronous inverters operating on a constant power control scheme while feeding a 332 kW load (the rated power was multiplied by the number of DGUs). In this case, only the active power and the frequency values available to the three-generation unit are fed into the

BoomBox, therefore, only the islanding signal for these particular generation units are generated. Each inverter is tasked to deliver a constant power output of 8 kW, and their output impedances are set to be different to represent different locations of DGUs (see Table 4.5). In this case, only the active power and frequency values of three DGUs were fed into the BoomBox due to the availability of I/O ports; therefore, only the islanding signal of these particular DGUs is graphically shown.

The four islanding signals were triggered after 27 ms (DGU1), 32 ms (DGU2), 40 ms (DGU3), and 40 ms (DGU4). The acquired signals from the first three DGUs are shown in Figure 5.15. It is noteworthy that the delay time seems to be associated with the distance from the PCC to the DGU, and that the simulated unit (DGU4) yielded the same delay as DGU3, both sharing the same output impedance. Each of the islanding signals was generated by monitoring only the local power and frequency measurements of each inverter. These results indicate that each DGU is capable of identifying the disconnection event even in a multiple inverter configuration without external communications.
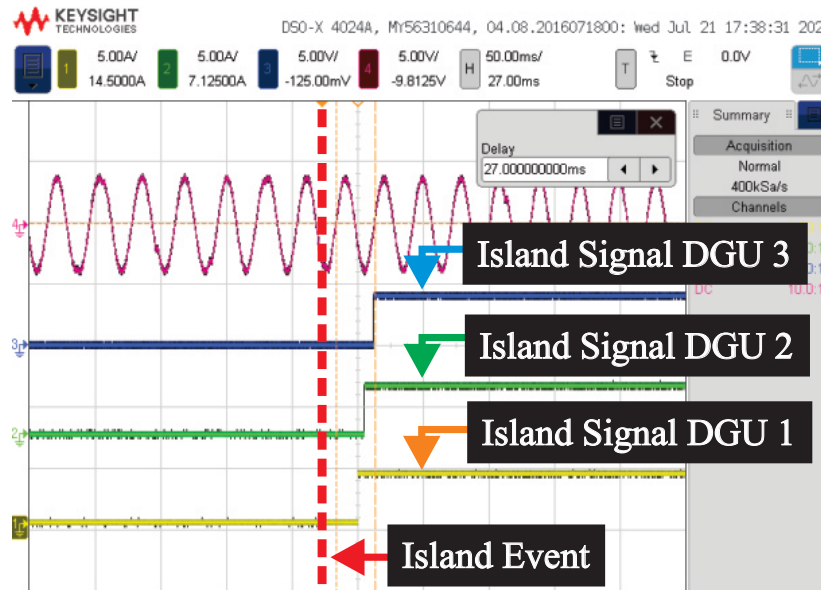
Fig. 5.15: Multiple inverter island experimental results

Table 5.1 shows a summary of the reported results compared to the work presented in [56], addressing a hybrid islanding detection algorithm based on voltage unbalances and total harmonic distortion. This comparison is relevant because the authors have compared their proposal to other hybrid detection methods and tested their islanding algorithm under the same simulation scenarios presented in section 4.7. Therefore, the LISD was validated as an improved detection mechanism over previously presented methods.

Table 5.1: Performance comparison of Islanding detection algorithms

ISD	Simulation Environment	Case 1	Case 2	Case 3	Case 4	Case 5
LISD	Off-line	14 ms	Not tripping	Not tripping	Not tripping	12 ms
	Real-Time	25 ms	Not tripping	Not tripping	Not tripping	27 ms 30 ms 40 ms
HISD VU/THD [56]	Off-line	98 ms	Not tripping	Not tripping	Not tripping	110 ms
	Real-Time	138 ms	Not tripping	Not tripping	Not tripping	132 ms

Chapter 6

Conclusion & Future Work

6.1 Conclusion

The present issues that come with sudden *disconnection events* have led to the development of new strategies to counter the hindering effects that such a scenario can introduce. This work is the extent of two proposals around the topic of microgrids transitioning from a connected state to an island operation. The former proposal deals with the computation of the LC filter parameters using a genetic algorithm optimization over a bounded region of values that meet the desired VSI response during *disconnection events*. The latter proposal introduces a novel island event detection algorithm based on low-level electrical measurements to avoid the dependency on communication lines, eliminating hindering factors such as packet losses and communications delays.

In regarding the optimization of the LC filter parameters, the proposal presented as a novel alternative to conventional switching frequency design-based methodologies. Unlike other methodologies, this proposal works on system measurements and does not need the system parameters to compute the LC filter values, therefore, it can be used in any particular system. The optimization procedure was designed to meet the *IEEE Std 519-1992* and *IEEE Std 519-2014* standards on harmonic distortion being below 5% and with a maximum of 12% during a period of 3 seconds respectively. The proposed optimization process utilized a total of CPU% of 1.21%.

A comparison to a calculated LC filter using the switching frequency the main design parameter is done and tested in a modified version of the *IEEE 13 node test feeder*. The performance of the GA optimized filter results in greater attenuation of the injected THD after the transition event and an improved transition behavior in the microgrid delivered voltage when compared to a conventional design method. The filter component size, bandwidth of the low-pass filter, and the injected THD are part of the optimization objective function and

minimized leading to a greater attenuation of high order harmonics, and improving output voltage signal of the VSI during and after the transition between a connected to autonomous operation of the microgrid.

With respect to the novel island event detection algorithm, motivated by the rapid development of microgrid systems and their trending evolution toward a decentralized operation to take advantage of the distributed nature behind the DGUs, which has led to the migration of crucial mechanisms of its core operation toward operating in a local fashion. The proposed LISD algorithm is based on the estimate of droop characteristics via the local reading of active power and frequency available to low-level controllers. This LISD takes advantage of the changing dynamics of the microgrid during transition events that introduce frequency and power fluctuations that eventually change the estimated droop plane for a given DGU.

This rate of change in the frequency of the estimated droop characteristics is the core of the proposed LISD algorithm, which can be implemented locally and operate in parallel with the primary controllers without interfering in the perforce of other DGU, this achieves a decentralized island detection system without the introduction of the electrical disturbances commonly found in active detection methods.

The LISD proposal is firstly validated in an offline digital simulation environment using *MATLAB Simulink* as the main interface. The results of the digital simulation verify the working principle of relying on the rate of change in the estimated droop characteristics to detect sudden *disconnection events*. Then the dynamic consistency validation of the proposed algorithm is achieved through a series of tests in an RT HIL simulation environment. This test emulates real-life scenarios with dynamic consistency to guarantee the performance of the proposed algorithm prior to the technology transfer stage. Overall, the detection of any disconnection event through the LISD is achieved in a faster and cleaner process.

In more detail, the proposed LISD was tested in various scenarios and directly compared to another proposal in the literature, results indicate the proposed LISD is capable o detecting an islanding event within 25 ms, meaning that the proposed LISD exhibits a performance 5.5 times faster than other works presented in the literature. In addition, the proposed LISD does not interfere with the quality of the delivered electrical energy, leading to a safer implementation in a multi-inverter system that adopts this island detection strategy. In such scenarios, the LISD is capable of detecting the island conditions in a maximum time of 40 ms depending on the impedance output value of the DGUs. This result indicates that the proposed LISD is 3.3 times faster than other island detection strategies under the same test-system condition.

6.2 Future Work

Around these proposals, some tests and experiments have been left out for future work. Such work consists mainly of the expansion of certain experiments and the scalability of the tested systems which can derive from new proposals or the improvement of certain mechanisms. For example, the optimization of the filter could be implemented in an online process, external to the tested microgrid system. It could be interesting to consider other optimization algorithms as the limits of the bounded region. In addition, the results of this first proposal could be integrated along with the proposal that deals with the island detection events. The dynamics of the optimized filter could have an effect on the detection time of such detection algorithm, therefore further analysis is required to derive in a holistic proposal that contemplates both methods.

On the other hand, the proposed LISD can be improved, an optimization algorithm can be coupled to find the optimal values in regards to the thresholds and sampling values for each system. In doing so, the LISD can be tested as a generic distributed island detection method, as currently the tuning of such variables is dependent on the system characteristics such as line impedance, voltage magnitude, and generated power. This leads to the scalability of the testbed for larger microgrid implementations. Additionally, the proposed LISD can be improved by having a mechanism that detects whenever the microgrid is back to a connected state, this addition can be achieved under the same droop principles. In doing so, complete decentralized disconnection and reconnection algorithms can be achieved.

Appendix A

Park Transform

A.1 From a natural reference frame to a rotating reference frame

The natural reference frame of an AC signal is composed of three components, these components are known for being separated by 120 degrees from each other. By assuming a symmetrical and balanced three-phase system of magnitude V and a phase angle ϕ, then the AC system can also be modeled in a rotating coordinate frame to enable the linearization of the AC components. Figure A.1 shows the relationship between the natural and the rotatory reference frame defined by its *d-axis* and *q-axis*, with a phase angle equivalent to ϕt with respect to the *A axis*.
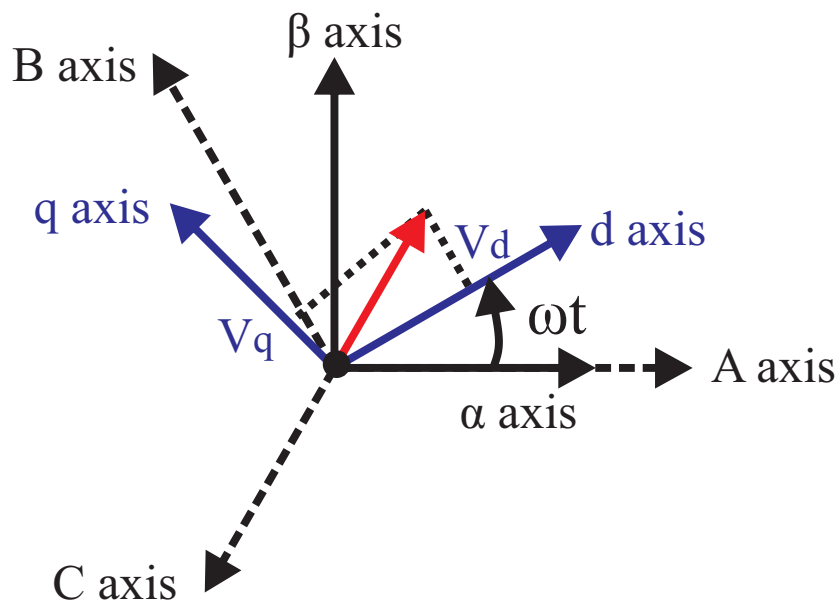
Fig. A.1: Rotatory reference frame scheme

The three-phase signals can be defined in a matrix configuration such as:

$$V_{abc} = \begin{bmatrix} V_a \\ V_b \\ V_c \end{bmatrix} \tag{A.1}$$

In more detail, these signals can be represented as a function of their magnitude and phase angle as:

$$
\begin{aligned}
V_a &= V \, cos(\omega t + \phi) + V_0 \\
V_b &= V \, cos(\omega t - \frac{2\,\pi}{3} + \phi) + V_0 \\
V_c &= V \, cos(\omega t + \frac{2\,\pi}{3} + \phi) + V_0
\end{aligned}
\tag{A.2}
$$

Essentially, these can be represented in its detailed matrix configuration such as:

$$V_{abc} = \begin{bmatrix} V \, cos(\omega t + \phi) + V_0 \\ V \, cos(\omega t - \frac{2\,\pi}{3} + \phi) + V_0 \\ V \, cos(\omega t + \frac{2\,\pi}{3} + \phi) + V_0 \end{bmatrix} \tag{A.3}$$

The reference transformation can assume its mathematical form as:

$$\begin{bmatrix} V_d \\ V_q \\ V_0 \end{bmatrix} = \mathbf{T} \begin{bmatrix} V_a \\ V_b \\ V_c \end{bmatrix} \tag{A.4}$$

where $\mathbf{T}$ is known as the transformation matrix, this term is then defined as:

$$\mathbf{T} = K \begin{bmatrix} cos(\omega t) & cos(\omega t - \frac{2\,\pi}{3}) & cos(\omega t + \frac{2\,\pi}{3}) \\ -sin(\omega t) & -sin(\omega t - \frac{2\,\pi}{3}) & -sin(\omega t + \frac{2\,\pi}{3}) \\ \frac{1}{2} & \frac{1}{2} & \frac{1}{2} \end{bmatrix} \tag{A.5}$$

where K is known as a scale factor, this K factor can be geometrically derived from the following diagram (see figure A.2).
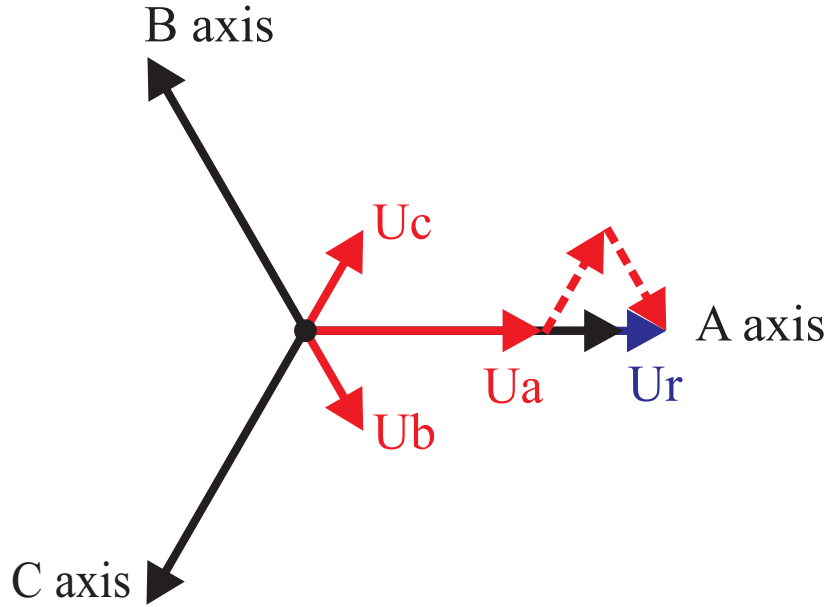
Fig. A.2: Geometric representation of the K scale factor.

where Ua, Ub, Uc represent the magnitudes of each phase in a three-phase system when the unity amplitude is reached by the A-phase of the system. The resultant vector Ur is then found according to the following relationship expressed in equation (A.6):

$$Ur = 1.5\, Ua \tag{A.6}$$

To maintain an equal amplitude during the transformation process the K factor is derived as:

$$K = \frac{2}{3} \tag{A.7}$$

By combining the equations (A.5), (A.7), and (A.3) into equation (A.4), the following expression can be obtained.

$$\begin{bmatrix} V_d \\ V_q \\ V_0 \end{bmatrix} = \frac{2}{3} \begin{bmatrix} cos(\omega t) & cos(\omega t - \frac{2\pi}{3}) & cos(\omega t + \frac{2\pi}{3}) \\ -sin(\omega t) & -sin(\omega t - \frac{2\pi}{3}) & -sin(\omega t + \frac{2\pi}{3}) \\ \frac{1}{2} & \frac{1}{2} & \frac{1}{2} \end{bmatrix} \begin{bmatrix} V\, cos(\omega t + \phi) + V_0 \\ V\, cos(\omega t - \frac{2\pi}{3} + \phi) + V_0 \\ V\, cos(\omega t + \frac{2\pi}{3} + \phi) + V_0 \end{bmatrix} \tag{A.8}$$

However, this expression can be simplified according to the rotating speed ω as:

$$V_{dq0} = \begin{bmatrix} V \ cos(\phi) \\ V \ sin(\phi) \\ V_0 \end{bmatrix} \qquad (A.9)$$

A.2 Inverse transformation

This work also considers the inverse transformation, that is changing from a rotatory reference frame to a natural reference frame, this can be achieved as expressed in the following expression.

$$\begin{bmatrix} V_a \\ V_b \\ V_c \end{bmatrix} = \mathbf{T}^{-1} \begin{bmatrix} V_d \\ V_q \\ V_0 \end{bmatrix} \qquad (A.10)$$

where the inverse transformation matrix $\mathbf{T}^{-1}$ is defined as:

$$\mathbf{T}^{-1} = \frac{2}{3} \begin{bmatrix} cos(\omega t) & -sin(\omega t) & 1 \\ cos(\omega t - \frac{2\pi}{3}) & -sin(\omega t - \frac{2\pi}{3}) & 1 \\ cos(\omega t + \frac{2\pi}{3}) & -sin(\omega t + \frac{2\pi}{3}) & 1 \end{bmatrix} \qquad (A.11)$$

Appendix B

Abbreviations and acronyms

DAN   Data Acquisition Network
RES   Renewable Energy Source
ESS   Energy Storage System
DGU   Distributed Generation Unit
PCC   Point of Common Coupling
EMS   Energy Management System
RDM   Remote Detection Methods
PDM   Passive Detection Methods
ADM   Active Detection Methods
HDM   Hybrid Detection Methods
RT   Real-Time
MGCC   Microgrid Central Controller
SoC   State of Charge
DSM   Demand Side Management
DR   Demand Response
AIbM   Artificial Intelligence Based Methods
UPS   Uninterruptible Power Supply
VSGC   Virtual Synchronous Generator Control
HIL   Hardware in the Loop
HUT   Hardware Under Test
PHIL   Power Hardware in the Loop
UDP   User Datagram Protocol
NDZ   Non Detectable Zone
PLCC   Power Line Carrier Communication

SoD	Signal of Disconnection
SCADA	Supervisory Control And Data Acquisition
VPN	Virtual Private Network
ROCOV	Rate of Change of Voltage
ROVOF	Rate of Change of Frequency
APM	Active Power Mismatch
RPM	Reactive Power Mismatch
PLL	Phase Locked Loop
VSI	Voltage Source Inverter
LISD	Local Island Detection

Bibliography

[1] S. A.R.F. and S. Haleem, "A survey: Smart cities for sustainable future," *International Journal of Innovative Science and Research Technology*, 11 2018.

[2] A. Lavalle, M. A. Teruel, A. Maté, and J. Trujillo, "Improving Sustainability of Smart Cities through Visualization Techniques for Big Data from IoT Devices," *Sustainability*, vol. 12, p. 5595, July 2020.

[3] "THE 17 GOALS | Sustainable Development."

[4] S. R. Rizvi, S. Zehra, and S. Olariu, "Aspire: An agent-oriented smart parking recommendation system for smart cities," *IEEE Intelligent Transportation Systems Magazine*, vol. 11, no. 4, pp. 48–61, 2019.

[5] M. Farmanbar, K. Parham, O. Arild, and C. Rong, "A Widespread Review of Smart Grids Towards Smart Cities," *Energies*, vol. 12, p. 4484, Nov. 2019.

[6] B. Kroposki, R. Lasseter, T. Ise, S. Morozumi, S. Papathanassiou, and N. Hatziargyriou, "Making microgrids work," *IEEE Power and Energy Magazine*, vol. 6, pp. 40–53, May 2008.

[7] O. US EPA, "Inventory of U.S. Greenhouse Gas Emissions and Sinks," Feb. 2018. Library Catalog: www.epa.gov.

[8] US EIA, "Short-term energy outlook," May 2021. Library Catalog: www.eia.gov.

[9] United Nations, "Energy statistics pocketbook," tech. rep., Department of Economic and Social Affairs, Statistics Division, United Nations, 2018.

[10] J. Lee and F. Zhao, "Global wind report 2021," tech. rep., Global Wind Energy Council, Mar. 2021.

[11] IRENA, "Renewable capacity statistics 2021," *International Renewable Energy Agency (IRENA), Abu Dhabi*, 2021.

[12] I. E. Agency, "Mexico energy outloopk 202." `https://www.iea.org/countries/mexico`, 2021. Accessed: 2021-10-30.

[13] "Rural electrification and mini grids in Mexico -."

[14] CENACE, "Programa de ampliación y de modernización de la red nacional de transmisión y redes generales de distribución del mercado eléctrico mayorista," tech. rep., CENACE, 2019.

[15] D. E. Olivares, A. Mehrizi-Sani, A. H. Etemadi, C. A. Canizares, R. Iravani, M. Kazerani, A. H. Hajimiragha, O. Gomis-Bellmunt, M. Saeedifard, R. Palma-Behnke, G. A. Jimenez-Estevez, and N. D. Hatziargyriou, "Trends in Microgrid Control," *IEEE Transactions on Smart Grid*, vol. 5, pp. 1905–1919, July 2014.

[16] EnergySage, "Utah solar incentives," 2021.

[17] L. Ibarra, J. R. Lopez, P. Ponce, and A. Molina, "Empowering Energy Saving Management and Microgrid Topology to Diminish Climate Challenge," in *Handbook of Climate Change Mitigation and Adaptation* (M. Lackner, B. Sajjadi, and W.-Y. Chen, eds.), pp. 1–31, New York, NY: Springer New York, 2020.

[18] R. Majumder, A. Ghosh, G. Ledwich, and F. Zare, "Power Management and Power Flow Control With Back-to-Back Converters in a Utility Connected Microgrid," *IEEE Transactions on Power Systems*, vol. 25, pp. 821–834, May 2010.

[19] M. Qu, C. Marnay, and N. Zhou, "Microgrid Policy Review of Selected Major Countries, Regions, and Organizations," Tech. Rep. LBNL–5782E, 1210907, U.S. Department of Energy Office of Scientific and Technical Information, Nov. 2011.

[20] C. A. Cortes, S. F. Contreras, and M. Shahidehpour, "Microgrid Topology Planning for Enhancing the Reliability of Active Distribution Networks," *IEEE Transactions on Smart Grid*, pp. 1–1, 2017.

[21] M. F. Zia, E. Elbouchikhi, and M. Benbouzid, "Microgrids energy management systems: A critical review on methods, solutions, and prospects," *Applied Energy*, vol. 222, pp. 1033–1055, July 2018.

[22] A. R. Busquet, G. Kardaras, J. C. R. Soler, and L. Dittmann, "Towards efficient energy management: Defining hems, ami and smart grid objectives," in *ICON 2011*, 2011.

[23] M. A. Hassan and M. A. Abido, "Optimal Design of Microgrids in Autonomous and Grid-Connected Modes Using Particle Swarm Optimization," *IEEE Transactions on Power Electronics*, vol. 26, pp. 755–769, Mar. 2011.

[24] A. F. Hoke, A. Nelson, S. Chakraborty, F. Bell, and M. McCarty, "An Islanding Detection Test Platform for Multi-Inverter Islands Using Power HIL," *IEEE Transactions on Industrial Electronics*, vol. 65, pp. 7944–7953, Oct. 2018.

[25] G. C. Kryonidis, E. O. Kontis, A. I. Chrysochos, K. O. Oureilidis, C. S. Demoulias, and G. K. Papagiannis, "Power flow of islanded ac microgrids: Revisited," *IEEE Transactions on Smart Grid*, vol. 9, no. 4, pp. 3903–3905, 2018.

[26] E. Barklund, N. Pogaku, M. Prodanovic, C. Hernandez-Aramburo, and T. C. Green, "Energy management in autonomous microgrid using stability-constrained droop control of inverters," *IEEE Transactions on Power Electronics*, vol. 23, no. 5, pp. 2346–2352, 2008.

[27] L. Steg, R. Shwom, and T. Dietz, "What Drives Energy Consumers?: Engaging People in a Sustainable Energy Transition," *IEEE Power and Energy Magazine*, vol. 16, pp. 20–28, Jan. 2018.

[28] A. Hussain, I.-S. Choi, Y. H. Im, and H.-M. Kim, "Optimal operation of greenhouses in microgrids perspective," *IEEE Transactions on Smart Grid*, pp. 1–1, 2018.

[29] B. V. Solanki, K. Bhattacharya, and C. A. Canizares, "A Sustainable Energy Management System for Isolated Microgrids," *IEEE Transactions on Sustainable Energy*, vol. 8, pp. 1507–1517, Oct. 2017.

[30] C. Jones, P. Gilbert, and L. Stamford, "Assessing the climate change mitigation potential of stationary energy storage for electricity grid services," *Environmental Science & Technology*, vol. 54, pp. 67–75, Jan. 2020.

[31] B. Zhao, X. Zhang, J. Chen, C. Wang, and L. Guo, "Operation optimization of standalone microgrids considering lifetime characteristics of battery energy storage system," *IEEE Transactions on Sustainable Energy*, vol. 4, no. 4, pp. 934–943, 2013.

[32] F. Yang, X. Feng, and Z. Li, "Advanced microgrid energy management system for future sustainable and resilient power grid," *IEEE Transactions on Industry Applications*, vol. 55, no. 6, pp. 7251–7260, 2019.

[33] D. Mackenzie, "Ieee smart village: Sustainable development is a global mission," *IEEE Systems, Man, and Cybernetics Magazine*, vol. 5, no. 3, pp. 39–41, 2019.

[34] Y. Zhang, N. Gatsis, and G. B. Giannakis, "Robust energy management for microgrids with high-penetration renewables," *IEEE Transactions on Sustainable Energy*, vol. 4, no. 4, pp. 944–953, 2013.

[35] M. A. Ebrahim, F. Wadie, and M. A. Abd-Allah, "An Algorithm for Detection of Fault, Islanding, and Power Swings in DG-Equipped Radial Distribution Networks," *IEEE Systems Journal*, vol. 14, pp. 3893–3903, Sept. 2020.

[36] S.-I. Jang and K.-H. Kim, "An Islanding Detection Method for Distributed Generations Using Voltage Unbalance and Total Harmonic Distortion of Current," *IEEE Transactions on Power Delivery*, vol. 19, pp. 745–752, Apr. 2004.

[37] R. Bakhshi-Jafarabadi, J. Sadeh, and M. Popov, "Maximum Power Point Tracking Injection Method for Islanding Detection of Grid-Connected Photovoltaic Systems in Microgrid," *IEEE Transactions on Power Delivery*, vol. 36, pp. 168–179, Feb. 2021.

[38] M. Arriaga, C. A. Cañizares, and M. Kazerani, "Northern lights: Access to electricity in canada's northern and remote communities," *IEEE Power and Energy Magazine*, vol. 12, no. 4, pp. 50–59, 2014.

[39] G. P. Holdmann, R. W. Wies, and J. B. Vandermeer, "Renewable Energy Integration in Alaska's Remote Islanded Microgrids: Economic Drivers, Technical Strategies, Technological Niche Development, and Policy Implications," *Proceedings of the IEEE*, vol. 107, pp. 1820–1837, Sept. 2019.

[40] U.S Energy Information Administration, "Alaska, state profile and energy estimates." https://www.eia.gov/state/?sid=AK#tabs-4, 2021. Accessed: 2021-04-08.

[41] H. Wilms, D. Mildt, M. Cupelli, A. Monti, P. Kjellen, T. Fischer, D. Panic, M. Hirst, E. Scionti, S. Schwarz, P. Kessler, and L. Hernandez, "Microgrid field trials in sweden: Expanding the electric infrastructure in the village of simris," *IEEE Electrification Magazine*, vol. 6, no. 4, pp. 48–62, 2018.

[42] M. Ganji, "Airport microgrids: Transportation energy as a service [viewpoint]," *IEEE Electrification Magazine*, vol. 8, no. 4, pp. 121–124, 2020.

[43] M. Hong, X. Yu, N.-P. Yu, and K. A. Loparo, "An Energy Scheduling Algorithm Supporting Power Quality Management in Commercial Building Microgrids," *IEEE Transactions on Smart Grid*, vol. 7, pp. 1044–1056, Mar. 2014.

[44] I. Beil, I. Hiskens, and S. Backhaus, "Frequency regulation from commercial building hvac demand response," *Proceedings of the IEEE*, vol. 104, no. 4, pp. 745–757, 2016.

[45] B. Washom, J. Dilliot, D. Weil, J. Kleissl, N. Balac, W. Torre, and C. Richter, "Ivory Tower of Power: Microgrid Implementation at the University of California, San Diego," *IEEE Power and Energy Magazine*, vol. 11, pp. 28–32, July 2013.

[46] G. G. Talapur, H. M. Suryawanshi, L. Xu, and A. B. Shitole, "A Reliable Microgrid With Seamless Transition Between Grid Connected and Islanded Mode for Residential Community With Enhanced Power Quality," *IEEE Transactions on Industry Applications*, vol. 54, pp. 5246–5255, Sept. 2018.

[47] D. S. Ochs, B. Mirafzal, and P. Sotoodeh, "A Method of Seamless Transitions Between Grid-Tied and Stand-Alone Modes of Operation for Utility-Interactive Three-Phase Inverters," *IEEE Transactions on Industry Applications*, vol. 50, pp. 1934–1941, May 2014.

[48] D. Das, G. Gurrala, and U. J. Shenoy, "Transition between grid-connected mode and islanded mode in VSI-fed microgrids," *Sādhanā*, vol. 42, pp. 1239–1250, Aug. 2017.

[49] Fang Gao and M. Iravani, "A Control Strategy for a Distributed Generation Unit in Grid-Connected and Autonomous Modes of Operation," *IEEE Transactions on Power Delivery*, vol. 23, pp. 850–859, Apr. 2008.

[50] R. Majumder, "Some Aspects of Stability in Microgrids," *IEEE Transactions on Power Systems*, vol. 28, pp. 3243–3252, Aug. 2013.

[51] M. M. Islam, M. Nagrial, J. Rizk, and A. Hellany, "General aspects, islanding detection, and energy management in microgrids: A review," *Sustainability*, vol. 13, no. 16, 2021.

[52] A. Pouryekta, V. K. Ramachandaramurthy, N. Mithulananthan, and A. Arulampalam, "Islanding Detection and Enhancement of Microgrid Performance," *IEEE Systems Journal*, vol. 12, pp. 3131–3141, Dec. 2018.

[53] M. Wasowski, T. Sikorski, G. Wisniewski, P. Kostyla, J. Szymanda, M. Habrych, L. Gornicki, J. Sokol, and M. Jurczyk, "The Impact of Supply Voltage Waveform Distortion on Non-Intentional Emission in the Frequency Range 2–150 kHz: An Experimental Study with Power-Line Communication and Selected End-User Equipment," *Energies*, vol. 14, no. 3, 2021.

[54] A. A. Arefin, K. N. B. M. Hasan, M. L. Othman, M. F. Romlie, N. Saad, N. B. M. Nor, and M. F. Abdullah, "A Novel Island Detection Threshold Setting Using Phasor Measurement Unit Voltage Angle in a Distribution Network," *Energies*, vol. 14, no. 16, 2021.

[55] S. Murugesan, V. Murali, and S. A. Daniel, "Hybrid analyzing technique for active islanding detection based on d-axis current injection," *IEEE Systems Journal*, vol. 12, no. 4, pp. 3608–3617, 2018.

[56] G. Wang, F. Gao, J. Liu, Q. Li, and Y. Zhao, "Design consideration and performance analysis of a hybrid islanding detection method combining voltage unbalance/total harmonic distortion and bilateral reactive power variation," *CPSS Transactions on Power Electronics and Applications*, vol. 5, pp. 86–100, Mar. 2020.

[57] K. Subramanian and A. K. Loganathan, "Islanding detection using a micro-synchrophasor for distribution systems with distributed generation," *Energies*, vol. 13, no. 19, 2020.

[58] S. A. Hosseini, H. A. Abyaneh, S. H. H. Sadeghi, F. Razavi, and A. Nasiri, "An overview of microgrid protection methods and the factors involved," *Renewable and Sustainable Energy Reviews*, vol. 64, pp. 174–186, Oct. 2016.

[59] X. Wang, J. M. Guerrero, F. Blaabjerg, and Z. Chen, "A Review of Power Electronics Based Microgrids," *Journal of Power Electronics*, vol. 12, pp. 181–192, Jan. 2012.

[60] M. Pastor and J. Dudrik, "Design of Output LCL Filter for 15-level Cascade Inverter," *Electronics and Electrical Engineering*, vol. 19, Oct. 2013.

[61] C.-H. Cheng, "Design of output filter for inverters using fuzzy logic," *Expert Systems with Applications*, vol. 38, pp. 8639–8647, July 2011.

[62] P. P. Vergara, J. C. López, J. M. Rey, L. C. P. da Silva, and M. J. Rider, "Energy Management in Microgrids," in *Microgrids Design and Implementation* (A. C. Zambroni de Souza and M. Castilla, eds.), pp. 195–216, Cham: Springer International Publishing, 2019.

[63] J. M. Guerrero, J. C. Vasquez, J. Matas, L. G. de Vicuna, and M. Castilla, "Hierarchical control of droop-controlled ac and dc microgrids a general approach toward standardization," *IEEE Transactions on Industrial Electronics*, vol. 58, pp. 158–172, Jan. 2011.

[64] F. Luo, G. Ranzi, S. Wang, and Z. Y. Dong, "Hierarchical Energy Management System for Home Microgrids," *IEEE Transactions on Smart Grid*, vol. 10, pp. 5536–5546, Sept. 2019.

[65] I. Serban, S. Céspedes, C. Marinescu, C. A. Azurdia-Meza, J. S. Gómez, and D. S. Hueichapan, "Communication requirements in microgrids: A practical survey," *IEEE Access*, vol. 8, pp. 47694–47712, 2020.

[66] "IEEE 2030-2011 - IEEE Guide for Smart Grid Interoperability of Energy Technology and Information Technology Operation with the Electric Power System (EPS), End-Use Applications, and Loads."

[67] A. K. Sahoo, K. Mahmud, M. Crittenden, J. Ravishankar, S. Padmanaban, and F. Blaabjerg, "Communication-less primary and secondary control in inverter-interfaced ac microgrid: An overview," *IEEE Journal of Emerging and Selected Topics in Power Electronics*, pp. 1–1, 2020.

[68] V. C. Gungor, B. Lu, and G. P. Hancke, "Opportunities and challenges of wireless sensor networks in smart grid," *IEEE Transactions on Industrial Electronics*, vol. 57, no. 10, pp. 3557–3564, 2010.

[69] H. Farhangi, "The path of the smart grid," *IEEE Power and Energy Magazine*, vol. 8, no. 1, pp. 18–28, 2010.

[70] W. Xu, G. Zhang, C. Li, W. Wang, G. Wang, and J. Kliber, "A power line signaling based technique for anti-islanding protection of distributed generators—part i: Scheme and analysis," *IEEE Transactions on Power Delivery*, vol. 22, no. 3, pp. 1758–1766, 2007.

[71] P. Palensky and D. Dietrich, "Demand side management: Demand response, intelligent energy systems, and smart loads," *IEEE Transactions on Industrial Informatics*, vol. 7, no. 3, pp. 381–388, 2011.

[72] H. Yang, W. Shen, Q. Yu, J. Liu, Y. Jiang, E. Ackom, and Z. Y. Dong, "Coordinated demand response of rail transit load and energy storage system considering driving comfort," *CSEE Journal of Power and Energy Systems*, vol. 6, no. 4, pp. 749–759, 2020.

[73] J. Xie, Y. Zheng, X. Pan, Y. Zheng, L. Zhang, and Y. Zhan, "A short-term optimal scheduling model for wind-solar-hydro hybrid generation system with cascade hydropower considering regulation reserve and spinning reserve requirements," *IEEE Access*, vol. 9, pp. 10765–10777, 2021.

[74] M. Alipour, B. Mohammadi-Ivatloo, and K. Zare, "Stochastic scheduling of renewable and chp-based microgrids," *IEEE Transactions on Industrial Informatics*, vol. 11, no. 5, pp. 1049–1058, 2015.

[75] E. Thalassinakis and E. Dialynas, "A monte-carlo simulation method for setting the underfrequency load shedding relays and selecting the spinning reserve policy in autonomous power systems," *IEEE Transactions on Power Systems*, vol. 19, no. 4, pp. 2044–2052, 2004.

[76] A. Parisio, C. Wiezorek, T. Kyntäjä, J. Elo, K. Strunz, and K. H. Johansson, "Cooperative mpc-based energy management for networked microgrids," *IEEE Transactions on Smart Grid*, vol. 8, no. 6, pp. 3066–3074, 2017.

[77] T. Alnejaili, S. Drid, D. Mehdi, L. Chrifi-Alaoui, R. Belarbi, and A. Hamdouni, "Dynamic control and advanced load management of a stand-alone hybrid renewable power system for remote housing," *Energy Conversion and Management*, vol. 105, pp. 377–392, 2015.

[78] C. Elkin and S. Witherspoon, "Machine learning can boost the value of wind energy," Feb. 2019.

[79] F. Katiraei, R. Iravani, N. Hatziargyriou, and A. Dimeas, "Microgrids management," *IEEE Power and Energy Magazine*, vol. 6, no. 3, pp. 54–65, 2008.

[80] J. Rocabert, A. Luna, F. Blaabjerg, and P. Rodriguez, "Control of Power Converters in AC Microgrids," *IEEE Transactions on Power Electronics*, vol. 27, pp. 4734–4749, Nov. 2012.

[81] J. Kim, J. Choi, and H. Hong, "Output LC filter design of voltage source inverter considering the performance of controller," in *PowerCon 2000. 2000 International Conference on Power System Technology. Proceedings (Cat. No.00EX409)*, vol. 3, (Perth, WA, Australia), pp. 1659–1664, IEEE, 2000.

[82] T. Wang, Zhihong Ye, Gautam Sinha, and Xiaoming Yuan, "Output filter design for a grid-interconnected three-phase inverter," in *IEEE 34th Annual Conference on Power Electronics Specialist, 2003. PESC '03.*, vol. 2, (Acapulco, Mexico), pp. 779–784, IEEE, 2003.

[83] S. Sen, K. Yenduri, and P. Sensarma, "Step-by-step design and control of LCL filter based three phase grid-connected inverter," in *2014 IEEE International Conference on Industrial Technology (ICIT)*, (Busan, South Korea), pp. 503–508, IEEE, Feb. 2014.

[84] Byoungwoo Ryu, Jaesik Kim, Jaeho Choi, and Changho Choi, "Design and analysis of output filter for 3-phase UPS inverter," in *Proceedings of the Power Conversion Conference-Osaka 2002 (Cat. No.02TH8579)*, vol. 3, (Osaka, Japan), pp. 941–946, IEEE, 2002.

[85] D. J. Cheng, "Compliances, Updates, Solutions and Case Studies." Informative Lecture.

[86] IEEE Standards Association, "Ieee std 519-2014. recommended practice and requirements for harmonic control in electric power systems," 2014.

[87] R. Turner, S. Walton, and R. Duke, "Stability and Bandwidth Implications of Digitally Controlled Grid-Connected Parallel Inverters," *IEEE Transactions on Industrial Electronics*, vol. 57, pp. 3685–3694, Nov. 2010.

[88] E. Unamuno and J. A. Barrena, "Hybrid ac/dc microgrids Part I: Review and classification of topologies," *Renewable and Sustainable Energy Reviews*, vol. 52, pp. 1251–1259, Dec. 2015.

[89] P. P. Cruz, *Maquinas Electricas Tecnicas modernas de control*. Alfaomega, 2016.

[90] G. K. Kasal and B. Singh, "Voltage and Frequency Controllers for an Asynchronous Generator-Based Isolated Wind Energy Conversion System," *IEEE Transactions on Energy Conversion*, vol. 26, pp. 402–416, June 2011.

[91] Q. Zhong and G. Weiss, "Synchronverters: Inverters that mimic synchronous generators," *IEEE Transactions on Industrial Electronics*, vol. 58, no. 4, pp. 1259–1267, 2011.

[92] J. Liu, Y. Miura, and T. Ise, "Comparison of dynamic characteristics between virtual synchronous generator and droop control in inverter-based distributed generators," *IEEE Transactions on Power Electronics*, vol. 31, no. 5, pp. 3600–3611, 2016.

[93] F. Tang, J. M. Guerrero, J. C. Vasquez, D. Wu, and L. Meng, "Distributed active synchronization strategy for microgrid seamless reconnection to the grid under unbalance and harmonic distortion," *IEEE Transactions on Smart Grid*, vol. 6, no. 6, pp. 2757–2769, 2015.

[94] C.-T. Lee, R.-P. Jiang, and P.-T. Cheng, "A grid synchronization method for droop-controlled distributed energy resource converters," *IEEE Transactions on Industry Applications*, vol. 49, no. 2, pp. 954–962, 2013.

[95] A. S. Vijay, S. Doolla, and M. C. Chandorkar, "Real-time testing approaches for microgrids," *IEEE Journal of Emerging and Selected Topics in Power Electronics*, vol. 5, no. 3, pp. 1356–1376, 2017.

[96] L. Ibarra, A. Rosales, P. Ponce, A. Molina, and R. Ayyanar, "Overview of Real-Time Simulation as a Supporting Effort to Smart-Grid Attainment," *Energies*, vol. 10, p. 817, June 2017.

[97] A. Saad, S. Faddel, T. Youssef, and O. A. Mohammed, "On the Implementation of IoT-Based Digital Twin for Networked Microgrids Resiliency Against Cyber Attacks," *IEEE Transactions on Smart Grid*, vol. 11, pp. 5138–5150, Nov. 2020.

[98] M. A. Hannan, Z. A. Ghani, A. Mohamed, and M. N. Uddin, "Real-Time Testing of a Fuzzy-Logic-Controller-Based Grid-Connected Photovoltaic Inverter System," *IEEE Transactions on Industry Applications*, vol. 51, pp. 4775–4784, 11 2015.

[99] T. Strasser, M. Stifter, F. Andren, and P. Palensky, "Co-Simulation Training Platform for Smart Grids," *IEEE Transactions on Power Systems*, vol. 29, pp. 1989–1997, 07 2014.

[100] J. R. López Gutiérrez, P. Ponce, and A. Molina, "Real-time power electronics laboratory to strengthen distance learning engineering education on smart grids and microgrids," *Future Internet*, vol. 13, no. 9, 2021.

[101] J. Bélanger and P. Venne, "The What, Where and Why of Real-Time Simulation," *Planet RT*, p. 13, 01 2010.

[102] M. Stevic, S. Vogel, M. Grigull, A. Monti, A. Estebsari, E. Pons, Tao Huang, and E. Bompard, "Virtual integration of laboratories over long distance for real-time co-simulation of power systems," in *IECON 2016 - 42nd Annual Conference of the IEEE Industrial Electronics Society*, (Florence, Italy), pp. 6717–6721, IEEE, 10 2016.

[103] F. Jia, X. Cai, Y. Lou, and Z. Li, "Interfacing technique and hardware-in-loop simulation of real-time co-simulation platform for wind energy conversion system," *IET Generation, Transmission & Distribution*, vol. 11, pp. 3030–3038, 08 2017.

[104] B. Zhang, W. Deng, L. Ruan, T. Wang, J. Quan, Q. Cao, Y. Teng, W. Wang, Y. Yuan, and L. Li, "Field–circuit cosimulation of 500-kv transformers in ac/dc hybrid power grid," *IEEE Transactions on Applied Superconductivity*, vol. 26, no. 4, pp. 1–5, 2016.

[105] A. Soriano, P. Ponce, and A. Molina, "A Novel Design of Virtual Laboratory," in *2019 20th International Conference on Research and Education in Mechatronics (REM)*, (Wels, Austria), pp. 1–6, IEEE, 05 2019.

[106] V. Dzhankhotov and J. Pyrhönen, "Passive ¡formula formulatype="inline"¿¡tex notation="tex"¿lc¡/tex¿¡/formula¿ filter design considerations for motor applications," *IEEE Transactions on Industrial Electronics*, vol. 60, no. 10, pp. 4253–4259, 2013.

[107] M. Liserre, A. Dell'Aquila, and F. Blaabjerg, "Genetic Algorithm-Based Design of the Active Damping for an LCL-Filter Three-Phase Active Rectifier," *IEEE Transactions on Power Electronics*, vol. 19, pp. 76–86, Jan. 2004.

[108] Z. Li, C. Zang, P. Zeng, H. Yu, S. Li, and J. Bian, "Control of a Grid-Forming Inverter Based on Sliding-Mode and Mixed $H\_2/H\_\ddot{A}\pm nfty$ Control," *IEEE Transactions on Industrial Electronics*, vol. 64, pp. 3862–3872, May 2017.

[109] Z. Li, C. Zang, P. Zeng, H. Yu, H. Li, and S. Li, "Analysis of Multi-Agent-Based Adaptive Droop-Controlled AC Microgrids with PSCAD: Modeling and Simulation," *Journal of Power Electronics*, vol. 15, pp. 455–468, Mar. 2015.

[110] M. A. Elsaharty, "Passive L and LCL filter design method for grid-connected inverters," in *2014 IEEE Innovative Smart Grid Technologies - Asia (ISGT ASIA)*, (Kuala Lumpur, Malaysia), pp. 13–18, IEEE, May 2014.

[111] H.-S. Kim and S.-K. Sul, "A Novel Filter Design for Output LC Filters of PWM Inverters," *Journal of Power Electronics*, vol. 11, pp. 74–81, Jan. 2011.

[112] K. Ahmed, S. Finney, and B. Williams, "Passive Filter Design for Three-Phase Inverter Interfacing in Distributed Generation," in *2007 Compatibility in Power Electronics*, (Gdansk, Poland), pp. 1–9, IEEE, May 2007.

[113] A. Ale Ahmd, "A new design procedure for output lc filter of single phase inverters," *International Conference on Power Electronics and Intelligent Transportation System*, 01 2010.

[114] M. Srinivas and L. Patnaik, "Genetic algorithms: a survey," *Computer*, vol. 27, pp. 17–26, June 1994.

[115] P. P. Cruz, *Inteligencia Artificial. Con Aplicaciones a la Ingeniería*. Alfaomega, 2010.

[116] K. Tang, K. Man, S. Kwong, and Q. He, "Genetic algorithms and their applications," *IEEE Signal Processing Magazine*, vol. 13, pp. 22–37, Nov. 1996.

[117] M.-H. Lin, J.-F. Tsai, and C.-S. Yu, "A review of deterministic optimization methods in engineering and management," *Mathematical Problems in Engineering*, vol. 2012, 06 2012.

[118] A. Raghavan, P. Maan, and A. K. B. Shenoy, "Optimization of day-ahead energy storage system scheduling in microgrid using genetic algorithm and particle swarm optimization," *IEEE Access*, vol. 8, pp. 173068–173078, 2020.

[119] A. Askarzadeh, "A memory-based genetic algorithm for optimization of power generation in a microgrid," *IEEE Transactions on Sustainable Energy*, vol. 9, no. 3, pp. 1081–1089, 2018.

[120] A. O. Rousis, I. Konstantelos, and G. Strbac, "A planning model for a hybrid ac–dc microgrid using a novel ga/ac opf algorithm," *IEEE Transactions on Power Systems*, vol. 35, no. 1, pp. 227–237, 2020.

[121] I. Ramirez-Rosado and J. Bernal-Agustin, "Genetic algorithms applied to the design of large power distribution systems," *IEEE Transactions on Power Systems*, vol. 13, no. 2, pp. 696–703, 1998.

[122] IEEE, "IEEE guide for design, operation, and integration of distributed resource island systems with electric power systems," *IEEE Std 1547.4-2011*, pp. 1–54, 2011.

[123] J. Wang, N. C. P. Chang, X. Feng, and A. Monti, "Design of a Generalized Control Algorithm for Parallel Inverters for Smooth Microgrid Transition Operation," *IEEE Transactions on Industrial Electronics*, vol. 62, pp. 4900–4914, Aug. 2015.

[124] W. Bower, "Evaluation of Islanding Detection Methods," *Power systems Programme*, p. 59, 2002.

[125] R. Benato and R. Caldon, "Distribution line carrier: Analysis procedure and applications to dg," *IEEE Transactions on Power Delivery*, vol. 22, no. 1, pp. 575–583, 2007.

[126] W. Wang, J. Kliber, and W. Xu, "A scalable power-line-signaling-based scheme for islanding detection of distributed generators," *IEEE Transactions on Power Delivery*, vol. 24, no. 2, pp. 903–909, 2009.

[127] I. Serban, S. Céspedes, C. Marinescu, C. A. Azurdia-Meza, J. S. Gómez, and D. S. Hueichapan, "Communication requirements in microgrids: A practical survey," *IEEE Access*, vol. 8, pp. 47694–47712, 2020.

[128] S. Ci, J. Qian, D. Wu, and A. Keyhani, "Impact of wireless communication delay on load sharing among distributed generation systems through smart microgrids," *IEEE Wireless Communications*, vol. 19, no. 3, pp. 24–29, 2012.

[129] P. Gupta, R. S. Bhatia, and D. K. Jain, "Active rocof relay for islanding detection," *IEEE Transactions on Power Delivery*, vol. 32, no. 1, pp. 420–429, 2017.

[130] R. Bakhshi-Jafarabadi, J. Sadeh, J. d. J. Chavez, and M. Popov, "Two-level islanding detection method for grid-connected photovoltaic system-based microgrid with small non-detection zone," *IEEE Transactions on Smart Grid*, vol. 12, no. 2, pp. 1063–1072, 2021.

[131] A. G. Abd-Elkader, S. M. Saleh, and M. Magdi Eiteba, "A passive islanding detection strategy for multi-distributed generations," *International Journal of Electrical Power & Energy Systems*, vol. 99, pp. 146–155, 2018.

[132] A. Rostami, H. Abdi, M. Moradi, J. Olamaei, and E. Naderi, "Islanding detection based on rocov and rocorp parameters in the presence of synchronous dg applying the capacitor connection strategy," *Electric Power Components and Systems*, vol. 45, no. 3, pp. 315–330, 2017.

[133] R. Bakhshi-Jafarabadi and J. Sadeh, "New voltage feedback-based islanding detection method for grid-connected photovoltaic systems of microgrid with zero non-detection zone," *IET Renewable Power Generation*, vol. 14, no. 10, pp. 1710–1719, 2020.

[134] S. Murugesan and V. Murali, "Active unintentional islanding detection method for multiple-pmsg-based dgs," *IEEE Transactions on Industry Applications*, vol. 56, no. 5, pp. 4700–4708, 2020.

[135] S. Murugesan and V. Murali, "Decentralized unintentional islanding identification for converter-interfaced multiple dgs," *IEEE Transactions on Industrial Informatics*, vol. 17, no. 7, pp. 4512–4520, 2021.

[136] M. Hamzeh, N. Rashidirad, K. Sheshyekani, and E. Afjei, "A new islanding detection scheme for multiple inverter-based dg systems," *IEEE Transactions on Energy Conversion*, vol. 31, no. 3, pp. 1002–1011, 2016.

[137] IEEE, "IEEE Recommended Practice and Requirements for Harmonic Control in Electric Power Systems," tech. rep., IEEE, 2014. ISBN: 9780738190051.

[138] P. K. Ganivada and P. Jena, "Frequency disturbance triggered d-axis current injection scheme for islanding detection," *IEEE Transactions on Smart Grid*, vol. 11, no. 6, pp. 4587–4603, 2020.

[139] R. Bakhshi-Jafarabadi and M. Popov, "Hybrid Islanding Detection Method of Photovoltaic-Based Microgrid Using Reference Current Disturbance," *Energies*, vol. 14, no. 5, 2021.

[140] "IEEE Standard for Interconnecting Distributed Resources with Electric Power Systems," *IEEE Std 1547-2003*, pp. 1–28, July 2003.

[141] "IEEE Recommended Practice for Utility Interface of Photovoltaic (PV) Systems," *IEEE Std 929-2000*, pp. i–, 2000.

[142] I. J. Balaguer, Q. Lei, S. Yang, U. Supatti, and F. Z. Peng, "Control for grid-connected and intentional islanding operations of distributed power generation," *IEEE Transactions on Industrial Electronics*, vol. 58, no. 1, pp. 147–157, 2011.

[143] S.-I. Jang and K.-H. Kim, "An islanding detection method for distributed generations using voltage unbalance and total harmonic distortion of current," *IEEE Transactions on Power Delivery*, vol. 19, pp. 745–752, Apr. 2004.

[144] M. A. Ebrahim, F. Wadie, and M. A. Abd-Allah, "An Algorithm for Detection of Fault, Islanding, and Power Swings in DG-Equipped Radial Distribution Networks," *IEEE Systems Journal*, vol. 14, pp. 3893–3903, Sept. 2020.

[145] L. Lopes and H. Sun, "Performance assessment of active frequency drifting islanding detection methods," *IEEE Transactions on Energy Conversion*, vol. 21, pp. 171–180, Mar. 2006.

[146] R. Bakhshi-Jafarabadi, J. Sadeh, and M. Popov, "Maximum Power Point Tracking Injection Method for Islanding Detection of Grid-Connected Photovoltaic Systems in Microgrid," *IEEE Transactions on Power Delivery*, vol. 36, pp. 168–179, Feb. 2021.

[147] G. Johns, "IEEE 1547 and Small Photovoltaic- Based Generation Case Studies."

[148] W. K. Sou, W. H. Choi, C. W. Chao, C. S. Lam, C. Gong, C. K. Wong, and M. C. Wong, "A deadbeat current controller of lc-hybrid active power filter for power quality improvement," *IEEE Journal of Emerging and Selected Topics in Power Electronics*, vol. 8, no. 4, pp. 3891–3905, 2020.

[149] S. Golestan, J. M. Guerrero, and A. M. Abusorrah, "Maf-pll with phase-lead compensator," *IEEE Transactions on Industrial Electronics*, vol. 62, no. 6, pp. 3691–3695, 2015.

[150] M. Khodaparastan, H. Vahedi, F. Khazaeli, and H. Oraee, "A Novel Hybrid Islanding Detection Method for Inverter-Based DGs Using SFS and ROCOF," *IEEE Transactions on Power Delivery*, vol. 32, pp. 2162–2170, Oct. 2017.

[151] A. F. Hoke, A. Nelson, S. Chakraborty, F. Bell, and M. McCarty, "An islanding detection test platform for multi-inverter islands using power hil," *IEEE Transactions on Industrial Electronics*, vol. 65, no. 10, pp. 7944–7953, 2018.

[152] "OP5700 - Hardware Products Documentation - Wiki OPAL-RT."

[153] "Rapid prototyping controller for power electronics - B-Box RCP - imperix."